CHALMERS

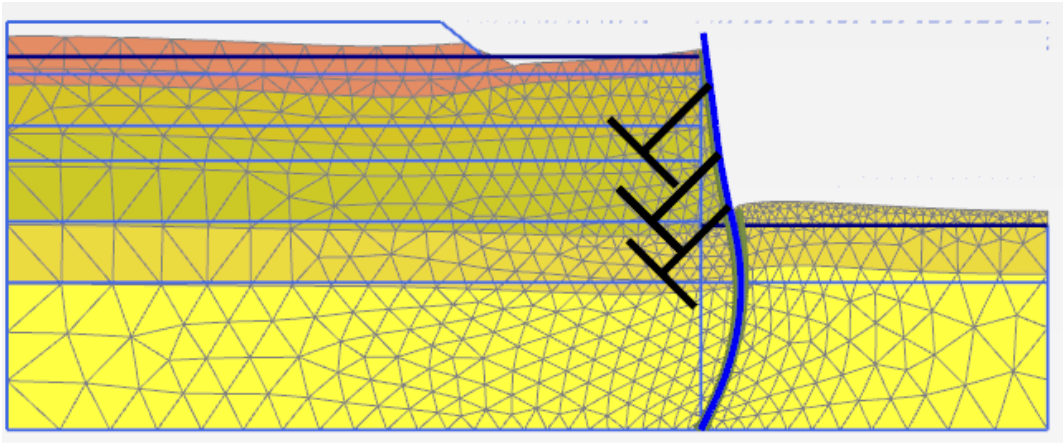

MODELLING OF A DEEP EXCAVATION IN SOFT CLAY

A COMPARISON OF DIFFERENT CALCULATION METHODS TO IN-SITU MEASUREMENTS

Master of Science Thesis in the Master's Programme Infrastructure and Environmental Engineering

EMIL JOHANSSON
EMIL SANDEMAN

Department of Civil and Environmental Engineering
Division of GeoEngineering
CHALMERS UNIVERSITY OF TECHNOLOGY
Gothenburg, Sweden, 2014
Master's Thesis 2014:22

MASTER'S THESIS 2014:22

MODELLING OF A DEEP EXCAVATION IN SOFT CLAY

A COMPARISON OF DIFFERENT CALCULATION METHODS TO IN-SITU MEASUREMENTS

Master of Science Thesis in the Master's Programme Infrastructure and Environmental Engineering

EMIL JOHANSSON

EMIL SANDEMAN

Department of Civil and Environmental Engineering
Division of GeoEngineering
CHALMERS UNIVERSITY OF TECHNOLOGY
Gothenburg, Sweden, 2014

Modelling of a deep excavation in soft clay
A comparison of different calculation methods to in-situ measurement
Master of Science Thesis in the Master's Programme Infrastructure and Environmental Engineering
EMIL JOHANSSON
EMIL SANDEMAN

Examensarbete / Institutionen för bygg- och miljöteknik,
Chalmers tekniska högskola 2014:22

Department of Civil and Environmental Engineering
Chalmers University of Technology
SE-412 96 Göteborg
Sweden
Telephone: + 46 (0)31-772 1000

Sweco Civil AB
Rosenlundsgatan 4
Box 1094
SE-405 23 Göteborg
Sweden
Telephone +46 (0)31-627 500

Cover:
Deformed mesh $|u|$ (scaled up 50.0 times)
Obtained from the Hardening Soil calculation in PLAXIS

Chalmers Reproservice / Institutionen för bygg- och miljöteknik
Göteborg, Sweden 2014

Modelling of a deep excavation in soft clay

A comparison of different calculation methods to in-situ measurements

Master of Science Thesis in the Master's Programme Infrastructure and Environmental Engineering

EMIL JOHANSSON

EMIL SANDEMAN

Department of Civil and Environmental Engineering

Division of GeoEngineering

Chalmers University of Technology

SUMMARY

The largest infrastructure project ever undertaken in Gothenburg, the Västlänken tunnel project, brings new geotechnical challenges when a 6 km long train tunnel is to be built underneath the city. The several deep excavations supported by retaining walls needed in the soft Gothenburg clay raises the question: Which retaining wall design method is the most accurate?

The aim of this thesis is to compare the forces and deformations measured at a multi-anchored sheet pile wall, installed during the construction of Götatunneln with similar conditions, to the results of different calculation methods. The calculation methods are hand calculations, the one-dimensional finite element software Novapoint GS Supported Excavation and the Mohr-Coulomb, Hardening Soil and Hardening Soil with small strain stiffness constitutive models in the two-dimensional finite element software PLAXIS 2D.

The different models were created based on previously conducted investigations of the soil, evaluation of CRS and triaxial tests and blueprints of the sheet pile wall and its anchors. A parametric study was also performed to see how the different models reacted when varying certain parameters and assessing the importance of investigating these parameters.

The results show that the PLAXIS 2D models give the best results, with the Hardening Soil model being the most accurate. Another advantage with the Hardening Soil model is that it provides the possibility of validating the model by comparing the stress paths obtained from triaxial tests to simulated tests in PLAXIS SoilTest.

The parametric study showed that if no triaxial tests are available, the Mohr-Coulomb model can give fairly accurate results as well, using empirical correlations to evaluate the stiffness. It also showed that basing a Hardening Soil with small strain stiffness model on empirical correlations for small strain stiffness should not be done, since there are different methods of correlating these parameters which give different results.

Keywords: Sheet pile wall, Multi-anchored, Deep excavation, Finite element, Novapoint GS Supported Excavation, PLAXIS 2D, PLAXIS SoilTest, Mohr-Coulomb, Hardening Soil, Hardening Soil with small strain stiffness, Geotechnics

TABLE OF CONTENTS

PREFACE

This report is the result of a Master Thesis project conducted at the department of GeoEngineering at Chalmers University of Technology during spring 2014.

We would like to thank Anders Kullingsjö for providing us with raw data as well evaluated parameters obtained during his work on his doctoral thesis. We also want to thank our supervisor at Chalmers, Minna Karstunen, for all the hints and useful information provided when we got lost in the confusing jungle of geotechnical FE analyses.

Above all, we would like to thank Jonas Thelander at SWECO for his help with initiation of the work as well as always being encouraging and supportive throughout the entire process of writing this thesis. Also thanks for putting up with us babbling in your room.

Gothenburg, May, 2014

Emil Johansson
Emil Sandeman

LIST OF NOTATIONS

ROMAN LETTERS

c_{inter}	Shear strength within the interface in PLAXIS	[kPa]
c_{soil}	Shear strength of the soil	[kPa]
c_u	Undrained shear strength	[kPa]
c’	Apparent cohesion	[kPa]
d	Distance from shaft bottom to a point where below, the passive earth pressure is equal to or larger than the active earth pressure	[m]
m	Power for stress-level dependency of stiffness	[-]
p_a	Active earth pressure (GSS)	[kPa]
p_p	Passive earth pressure (GSS)	[kPa]
p_p	Isotropic preconsolidation pressure (PLAXIS)	[kPa]
p_{ref}	Reference pressure (PLAXIS)	[kPa]
p_v	Vertical earth pressure (GSS)	[kPa]
p’	Mean effective stress	[kPa]
q	Deviator stress	[kPa]
q_d	Design load next to shaft for hand calculations	[kPa]
r	Roughness of the SPW (GSS)	[-]
u	Pore pressure	[kPa]
u_{da}	Design pore pressure	[kPa]
v_f	Limit earth strain (GSS)	[-]
w	Weight of SPW	[kN/m^2]
D	Point where beneath that point the total passive pressure is larger than or equal to the total active pressure	[-]
E	Young’s modulus	[kPa]
E_u	Undrained Young’s modulus	[kPa]
E_{50}	Undrained secant stiffness	[kPa]
E_{ur}	Undrained unload-reload stiffness	[kPa]

E'	Effective initial stiffness	[kPa]
E'_{50}	Effective secant stiffness	[kPa]
E'_{oed}	Effective oedometer stiffness	[kPa]
E'_{ur}	Effective unload-reload stiffness	[kPa]
E'^{ref}_{50}	Effective secant stiffness at reference pressure (σ'_3)	[kPa]
E'^{ref}_{oed}	Effective oedometer stiffness at reference pressure (σ'_1)	[kPa]
E'^{ref}_{ur}	Effective unload-reload stiffness at reference pressure (σ'_3)	[kPa]
EA	Normal stiffness	[kN/m]
EI	Flexural rigidity	[kNm^2/m]
G	Undrained shear modulus	[kPa]
G_0	Undrained initial shear modulus	[kPa]
G_0^{ref}	Undrained initial shear modulus at reference pressure (σ'_3)	[kPa]
G'_0	Effective initial shear modulus	[kPa]
G'^{ref}_0	Effective initial shear modulus at reference pressure (σ'_3)	[kPa]
H	Height from shaft bottom to top of the sheet pile wall	[m]
I	Moment of inertia	[m^4]
I_P	Plasticity index	[-]
K_0	Coefficient of lateral earth pressure at rest	[-]
$K_{0,nc}$	Coefficient of lateral earth pressure at rest for normally consolidated soil	[-]
K_A	Coefficient of lateral active earth pressure	[-]
K_P	Coefficient of lateral passive earth pressure	[-]
K_y	Spring stiffness (GSS)	[kPa]
K_{yi}	Initial spring stiffness (GSS)	[kPa]
$\overline{K}_y$	Slope of straight line between initial earth pressure and limit earth pressure (GSS)	[kPa]
M	Slope of line in a p'-q plot	[-]
M_0	Compression modulus, elastic part	[kPa]
M_L	Compression modulus, plastic part	[kPa]

M_{Sd}	Design bending moment	[kNm]
N_{cb}	Bearing capacity factor (hand calculations)	[-]
P	Anchor force	[kN]
P_A	Total active force on the sheet pile wall (hand calculations)	[kN]
P_H	Horizontal anchor force	[kN]
R_f	Scaling factor (GSS)	[-]
R_{inter}	Interface value (PLAXIS)	[-]

GREEK LETTERS

α	Inclination of anchors	[°]
γ	Soil weight	[kN/m^3]
$\gamma_{0.7}$	Shear strain level where $G = 0.722G_0$	[-]
γ_m	Soil weight	[kN/m^3]
γ_s	Shear strain	[-]
γ_{Sda}	Design partial factor (hand calculations)	[-]
ε_1	Axial strain	[-]
κ	Parameter depending on the roughness of the SPW (GSS)	[-]
υ	Poisson's ratio	[-]
υ_u	Undrained Poisson's ratio	[-]
υ_{ur}	Poisson's ratio for unloading-reloading	[-]
υ'	Effective Poisson's ratio	[-]
υ'_{ur}	Effective Poisson's ratio for unloading-reloading	[-]
φ	Friction angle of soil	[°]
φ_d	Design friction angle of soil	[°]
φ_{inter}	Friction angle of interface (PLAXIS)	[°]
φ_{soil}	Friction angle of soil (PLAXIS)	[°]
φ'_{cv}	Critical state friction angle	[°]
σ_1	Major principal stress	[kPa]
σ_3	Minor principal stress	[kPa]

σ_a	Active horizontal earth pressure	[kPa]
σ_f	Limit earth pressure (GSS)	[kPa]
σ_i	Load intensity on SPW (hand calculations)	[kN/m]
σ_{pnetto}	Net earth pressure (hand calculations)	[kPa/m]
σ_v	Vertical stress	[kPa]
$\sigma_{v,as}$	Vertical earth pressure above shaft	[kPa]
σ_{yi}	Initial earth pressure (GSS)	[kPa]
σ'	Effective stress	[kPa]
σ'_1	Effective major principal stress	[kPa]
σ'_3	Effective minor principal stress	[kPa]
σ'_c	Preconsolidation pressure	[kPa]
σ'_r	Confining pressure in triaxial test	[kPa]
σ'_v	Effective vertical stress	[kPa]

ABBREVIATIONS

CRS	Constant Rate of Strain
FE	Finite element
GSS	Novapoint GS Supported Excavation
HS	Hardening Soil
HSs	Hardening Soil with small strain stiffness
MC	Mohr-Coulomb
OCR	Overconsolidation Ratio
PWP	Pore Water Pressure
SPW	Sheet Pile Wall
TSA	Total Stress Automatic

1 INTRODUCTION

The Västlänken tunnel project is the largest infrastructure project undertaken in Gothenburg. The objective is to construct a 6 km train tunnel underneath the city to increase accessibility for commuters from outside the city. In order to construct this tunnel, several deep excavations supported by multi-anchored sheet pile walls (SPW) need to be performed in the soft Gothenburg clay. This raises the question of which sheet pile wall analysis method give the most accurate results. A comparison of different methods and deformation measurements performed on a real sheet pile wall is therefore of interest.

A similar project to Västlänken is Götatunneln, which is a road tunnel constructed in the vicinity completed in 2006. Part of this project was a multi-anchored SPW temporarily installed to support a ten meter deep excavation in soft clay. Forces in anchors and deformations in the SPW and in the area behind it were measured during the excavation and construction of the tunnel. This sheet pile wall would therefore be suited as a reference object for a comparison of different calculation methods.

1.1 AIM

The aim is to compare the forces and deformations measured at a SPW to the results from a hand calculation method, the one-dimensional finite element (FE) software Novapoint GS Supported Excavation (GSS) and three constitutive models in the two-dimensional FE software PLAXIS 2D (PLAXIS). This is done by modelling a multi-anchored SPW and comparing the results from these methods to in-situ measurements to assess which analysis method is the most efficient to use in the design process.

1.2 METHOD

At first, a desk study is performed to obtain the knowledge necessary when designing a SPW, evaluating soil parameters and using the software GSS and PLAXIS.

Soil parameters are either obtained from field and lab tests evaluated by Kullingsjö (2007, p. 136) or evaluated from raw data from triaxial and CRS tests conducted at Chalmers University of Technology during the construction of Götatunneln 2000-2006. No additional tests were performed during the work with this Master's project.

One FE model will be created in GSS and one in PLAXIS. Three different constitutive models will be used in PLAXIS; a Mohr-Coulomb (MC) model, a Hardening Soil (HS) model and a Hardening Soil with small strain stiffness (HSs) model. The models are based on a temporary SPW used during the construction of Götatunneln, Gothenburg.

The input parameters used for the different models, the calculation conditions and the results from all the calculations are presented in section 3. An analysis of the results, where the output from the different models is compared to measurements performed as site, as well as to each other, is conducted to determine which method is the most accurate. The following results are compared and analysed in section 4:

- Horizontal deformations in the SPW
- Anchor forces
- Bending moments and shear forces
- Earth pressures
- Subsidence behind the wall

The comparisons are presented with a short interpretation and discussion. The evaluation of the different calculation methods will focus solely on the accuracy of the methods and the results from these comparisons are then used to assess which software and model is preferable to use in the design process.

Parametric studies are also performed for the PLAXIS models to determine how varying certain parameters affects the results, and if those parameters should be investigated in more detail. In section 6 there is a discussion about the more general issues and discoveries encountered during the work with this project are discussed.

2 LITERATURE STUDY

In this section, studies that are similar to the one performed in this thesis are presented as well as a description of earth pressures and how the different lab tests are performed and evaluated. A description of how the different constitutive models function and what input is required is also found in this section.

2.1 SIMILAR STUDIES

Rankine published a method for analysing earth retaining walls in 1857 in which it is assumed that the lateral earth pressure is fully mobilized and is increased linearly with depth in a homogenous soil. This is a good first assumption but is not the case in reality because it requires quite large movements before full mobilization occurs (Powrie & Simpson, 2001, p. 2).

Since FE analyses have become more and more common due to the rapid development of computer power in recent years, several studies have been conducted and different constitutive models have been developed in order to capture more realistic soil behaviour.

An example of such a study is *Effects of deep excavations in soft clay on the immediate surrounding* by Kullingsjö (2007) where different methods of how to analyse ground deformation when performing deep excavations in soft clay are presented together with how the lateral earth pressures can be estimated. Back calculations are then performed in order to predict and estimate ground deformations adjacent to a multi anchored SPW.

These back calculations are performed using FE analyses with three different constitutive models, namely a linear elastic Mohr-Coulomb model, a total stress based e-ADP model and an effective stress based MIT-S1 model. The results from these different calculations are then compared with in-situ measurements to determine their accuracy, advantages and disadvantages (Kullingsjö, 2007).

The study concludes that there are no additional benefits gained when using the studied FE methods since the results were inaccurate. It also concludes that the collaboration between the contractor and the geotechnical consultancy is important in order to ensure a reliable construction that behaves in an acceptable manner (Kullingsjö, 2007). The study performed in this thesis is similar to Kullingsjö's, using the same raw data and in situ measurements but comparing different constitutive models.

Another similar study was performed by H. F. Schweiger (2009) where calculations with the same constitutive models in PLAXIS as used in this thesis were performed. Schweiger suggests that the MC model is not well suited for this kind of analyses and that a more advanced constitutive model is necessary to obtain reliable results. However, the study focused on comparing the constitutive models to each other and did not compare the results from these models to real measurements.

In Schweiger and Breymann (2005) the HS model has been compared to in-situ measurements performed during deep excavations in soft Salzburg clay. Five individual excavations has been analysed in PLAXIS and compared to the measured deformations and the paper concludes that the agreement between the HS model and reality is overall good and that this constitutive model gives quite accurate results when modeling such problems.

Furthermore, in Kempfert and Gebresellasie (2006, p. 169) it is stated that Schweiger (2000) has compared 14 individual analyses of a 16.8 m deep excavation. The results differ quite a lot between the analyses and the reason for this is, except for differences in modeling in general, that there is a difference in identifying parameters, particularly the stiffnesses. Kempfert and Gebresellasie (2006, p. 170) therefore suggest that a standardization of FE analysis of excavations is necessary.

Simpson and Powrie (2001) present, compare and discuss different design approaches for calculating earth pressures when analysing retaining walls. It highlights some different approaches used in the industry for calculating such problems and what they believe is the most accurate design approach as well as a motivation to why they believe so. They also discuss *Eurocode 7* and describe some problems that can occur when following this design approach if the user is not aware of them.

2.2 EARTH PRESSURE COEFFICIENT

When analysing retaining structures, the change in earth pressure due to movement is taken into account using different earth pressure coefficients. In the initial state, when there is no lateral strain in the soil mass, the soil is at rest and the corresponding coefficient is the earth pressure coefficient at rest, K_0.

If the structure moves, the horizontal stresses on the side it moves away from decreases and this is called the active side. The side it moves towards, where the horizontal stresses increase, is called the passive side, see Figure 1. The new horizontal stresses on the active and passive side are calculated using K_a and K_p respectively.

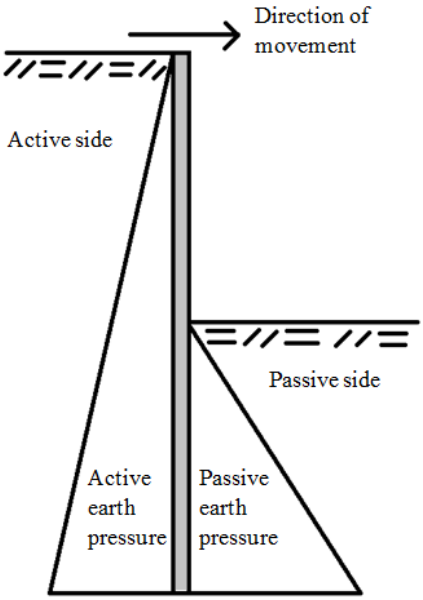

Figure 1 – Illustration of active and passive side for an excavation supported by a retaining wall.

$K_{0,nc}$, which is the lateral earth pressure coefficient at rest for a normally consolidated soil, can be calculated using Jaky's formula (Jaky, 1944), see Equation (1).

$$K_{0,nc} = 1 - \sin\varphi' \tag{1}$$

The K_a and K_p can be calculated according to Rankine's earth pressure theory using Equation (2) and (3).

$$K_a = \frac{1 - \sin\varphi'}{1 + \sin\varphi'} \tag{2}$$

$$K_p = \frac{1 + \sin\varphi'}{1 - \sin\varphi'} \tag{3}$$

The amount of wall movement required to mobilize full active and passive pressure differs, see Figure 2. It only requires small movement in the case of expansion while it takes larger lateral strains to fully mobilize in compression.

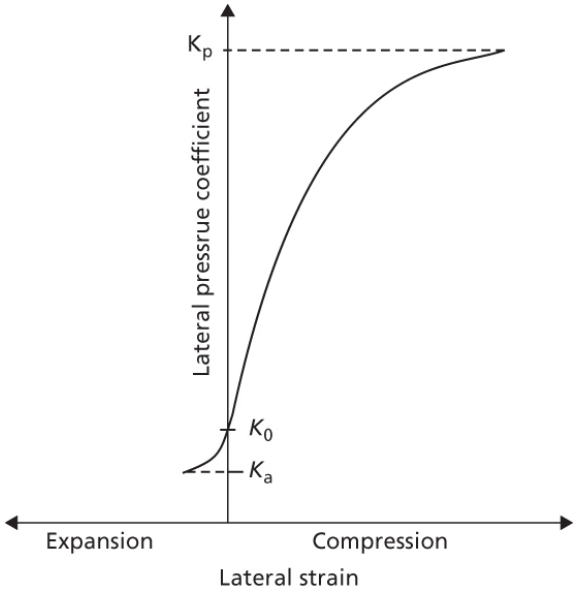

Figure 2 - The relationship between lateral strain and earth pressure coefficients (Craig & Knappett, 2012, p. 417).

If the soil is overconsolidated, it behaves somewhat differently from a normally consolidated soil. The earth pressure at rest is higher in an overconsolidated soil since a stress increase and consolidation has occurred in the past. This increase of K_0 can be taken into account by using a correlation to the overconsolidation ratio (OCR), see Equation (4), suggested in Eurocode 7.

$$K_0 = (1 - \sin\varphi') * \sqrt{OCR} = K_{0,nc} * \sqrt{OCR} \quad (4)$$

2.3 EVALUATION OF LAB TESTS

The lab tests evaluated during this project are CRS tests and triaxial tests and the evaluation process is described below. All other evaluated data from lab and field tests used in this thesis are obtained from Kullingsjö (2007).

2.3.1 *CRS TEST*

The CRS (Constant Rate of Strain) test is a test where a soil specimen is compressed with a constant deformation rate. The deformation rate is usually 0.0025 mm/min which gives approximately 18 % deformation in 24 hours in Gothenburg clay.

The vertical stress, σ_v, the vertical deformation, ε_1 and the pore water pressure (PWP), u, are measured during the test. By plotting the vertical effective stress, σ'_v, against ε_1, the preconsolidation pressure, σ'_c, and the compression moduli, M_0 and M_L, can be evaluated using the method provided in *Kompressionsegenskaper – Geotekniska laboratorieanvisningar, del 10* (Sällfors & Andreasson, 1985), see Figure 3.

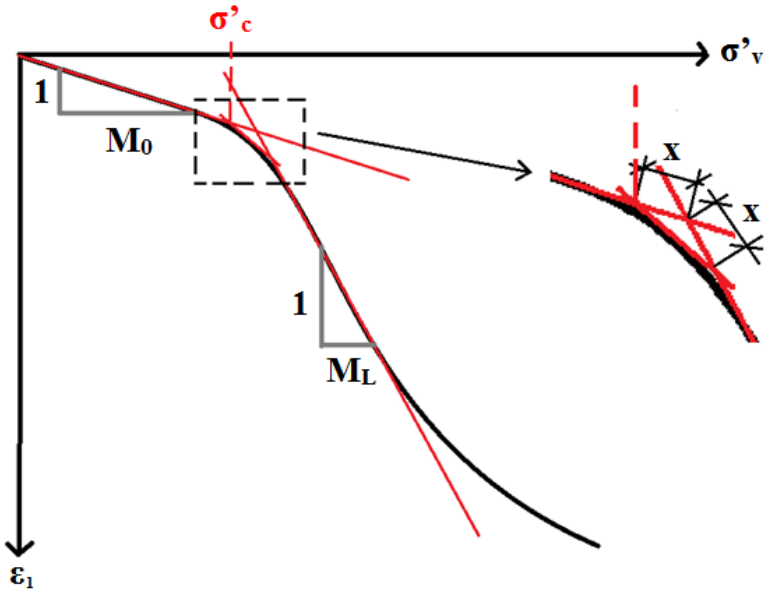

Figure 3 - Evaluation of σ'_c, M_0 and M_L from a CRS-test according to Sällfors method.

2.3.2 *TRIAXIAL TEST*

The triaxial test is performed on an undisturbed piston sample of clay which is inserted into a cell containing liquid (usually water or paraffin oil). The oil is used to control the cell pressure and thus control the horizontal effective stress σ'_3. To allow for drainage, a filter paper is attached to the sample. The clay sample is then enclosed within a rubber membrane to prevent the liquid from penetrating the sample[1].

A triaxial test is performed in two stages. During the first stage the sample is subjected to a pressure corresponding to approximately 85 % of the preconsolidation pressure for both vertical and horizontal stresses. The vertical preconsolidation pressure can be obtained from a CRS test, see section 2.3.1 and the horizontal preconsolidation pressure can be calculated by multiplying the vertical pressure with $K_{0,nc}$.

Since the friction angle is evaluated from this test it is not possible to calculate $K_{0,nc}$ in advance. Instead $K_0 = 0.6$ can be assumed[2]. It is important to avoid exceeding the preconsolidation pressure since the structure of the clay can be affected which would make the evaluation of the effective parameters corresponding to the peak strength impossible (SGF, 2012, p. 42).

During shearing, a vertical strain is applied to the specimen, resulting in a vertical effective stress σ'_1, see Figure 4, which is increased until shear failure occurs. This increase is known as the deviator stress, q, and is calculated as the difference between axial and radial stress, see Equation (5).

$$q = \sigma'_1 - \sigma'_3 \tag{5}$$

[1] Hedborg, Peter; Research Engineer at the Division of Geo Engineering at Chalmers, interview during study visit 2014-02-06.

[2] Ibid.

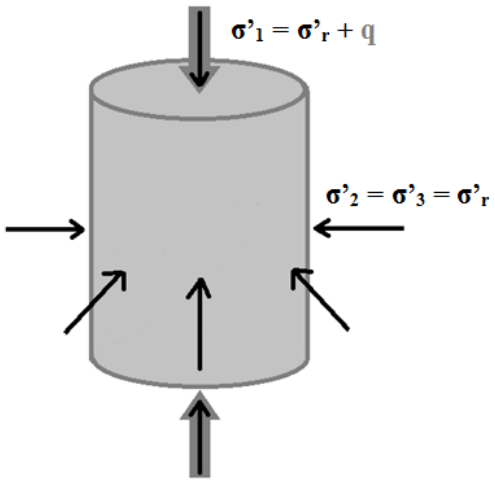

Figure 4 - The axial and radial stresses acting on a triaxial test sample.

The drainage condition in the sample is controlled by a gauge and is either drained, partially drained or undrained. The gauge is open in a drained test which allows water to either enter or leave the sample meaning that the PWP remains constant if the test is run at a sufficiently low rate. The PWP is regulated with a back pressure that often is set equal to the in-situ PWP (SGF, 2012, p. 9). If the gauge is closed, the water conditions are instead undrained and allow an increase in the PWP.

The test can be performed as either a compression test or an extension test. The axial pressure is higher than the radial pressure in the compression test ($\sigma'_1 > \sigma'_3$), while the opposite ($\sigma'_1 < \sigma'_3$) is the case for the extension test. Usually the consolidation stages are identical so that the tests only differ during the shearing stage.

If the PWP is measured throughout the test this information can be used when evaluating the critical state friction angle. Critical state is reached when the undrained peak strength is passed (Larsson, 2008, p. 49), see Figure 5. The height of the undrained peak strength depends on the deformation rate in the test, the slower the rate the lower the peak. The critical state can be explained as the state where the real long term behaviour of the soil is captured.

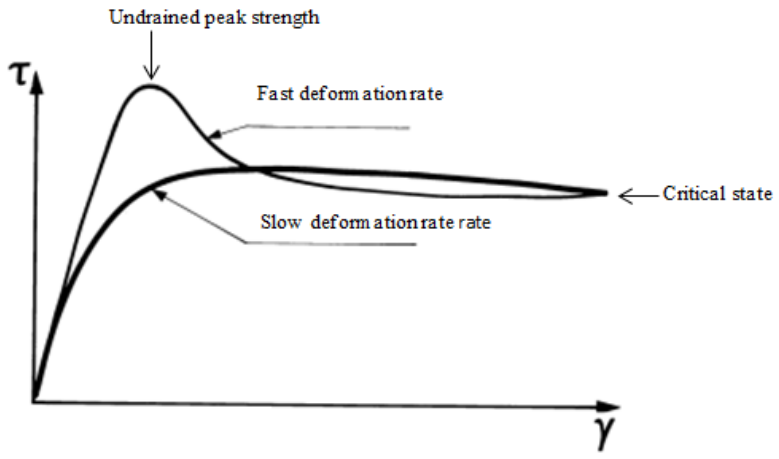

Figure 5 - Shows the different peak shear strengths depending on deformation rate in an undrained triaxial test (Larsson, 2008, p. 49).

The parameters φ'_{cv} and c_u can be evaluated by the following procedures, illustrated in Figure 6:

a) Examine at what strain the PWP has stabilized in a ε_1-σ' plot
b) Examine the deviator stress at the axial strain level obtained.
c) Create a p'-q plot and draw a tangent from the origin to the failure envelope at the deviator stress level obtained.

The parameter p' is the mean effective stress in a triaxial test and is calculated using Equation (6).

$$p' = \frac{\sigma'_1 + 2 * \sigma'_3}{3} \tag{6}$$

The slope of the line produced in the p'-q plot, M, in Figure 6c, is then used to calculate the critical state effective friction angle φ'_{cv} for a compression test with Equation (7). The undrained shear strength c_u is obtained from the ε_1-q, see Figure 6b.

$$\varphi'_{cv} = \arcsin\left(\frac{3 * M}{6 + M}\right) \tag{7}$$

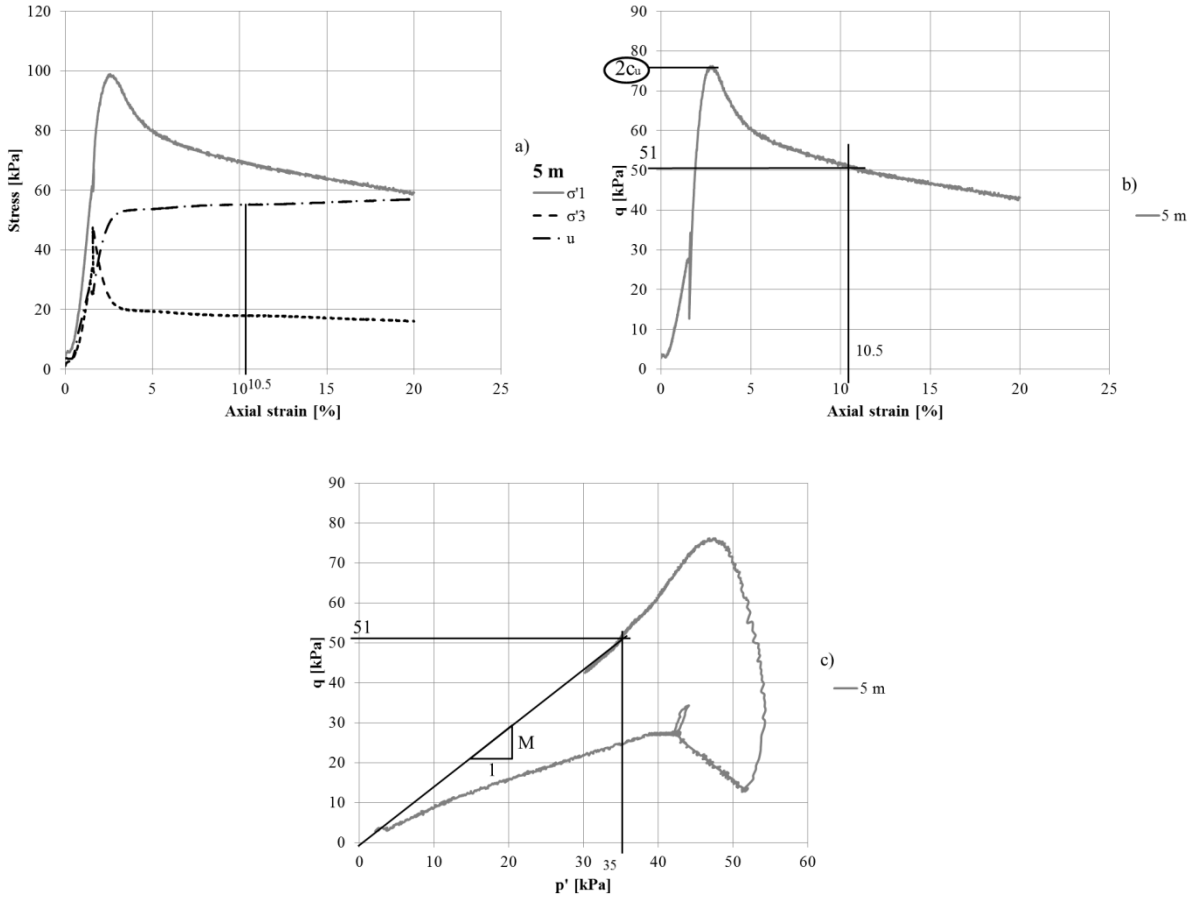

Figure 6 – Procedure for evaluating φ'_{cv} and c_u.

2.4 HAND CALCULATIONS

Simple hand calculations are performed in order to give an estimation of the earth pressures acting on the SPW, the anchor forces and the bending moment in the SPW. For the hand calculations the method provided in *Sponthandboken* (Ryner, et al., 1996) is used. This provides a rough estimation of the anchor forces and design bending moment in the SPW which can be compared to measurements.

The parameter used in this section is:

- Undrained shear strength c_u

The first step is to calculate the active horizontal earth pressure, σ_a, acting on the SPW above the shaft bottom, see Equation (8) for friction material and Equation (9) for cohesion material (Ryner, et al., 1996). These equations are based on Rankine theory but utilize the design values of the soil parameters.

$$\sigma_a = \gamma_{Sda}(\sigma_v - u_{da}) * tan^2\left(45° - \frac{\varphi_d}{2}\right) + u_{da} \quad (8)$$

$$\sigma_a = \gamma_{Sda}(\sigma_v - 2 * c_{ud}) \quad (9)$$

In these equations γ_{Sda} is a design partial factor, σ_v is the vertical soil pressure and u is the pore pressure. The index d signifies a design value.

For this project, where a comparison with actual measured data is performed, the design values are no different than the evaluated values, since all partial factors are set to 1. This gives the Equations (10) - (11).

$$\sigma_a = (\sigma_v - u) * tan^2\left(45 - \frac{\varphi}{2}\right) + u \quad (10)$$

$$\sigma_a = \sigma_v - 2 * c_u \quad (11)$$

Below the shaft bottom, a net earth pressure for clay, σ_{pnetto}, is calculated according to Equation (12) (Ryner, et al., 1996, p. 50).

$$\sigma_{pnetto} = \gamma_{Sd,Ncb} * N_{cb} * c_{ud} - (\gamma * H + q_d) = N_{cb} * c_u - \sigma_{v,as} \quad (12)$$

In this equation $\gamma_{Sd,Ncb}$ is a design partial factor, γ is the soil weight, H is the height of the SPW above shaft bottom, q_d is the load applied behind the SPW and $\sigma_{v,as}$ is the vertical soil pressure above the shaft bottom.

N_{cb} is a bearing capacity factor that depends on the geometry of the shaft. For an anchored SPW with satisfactory vertical support N_{cb} = 5.7 is selected (Ryner, et al., 1996, p. 44). The distance d, which is from the shaft bottom to the point D where beneath that point the total passive pressure, A_P, is larger than or equal to the total active pressure, A_A, can then be found, see Figure 7.

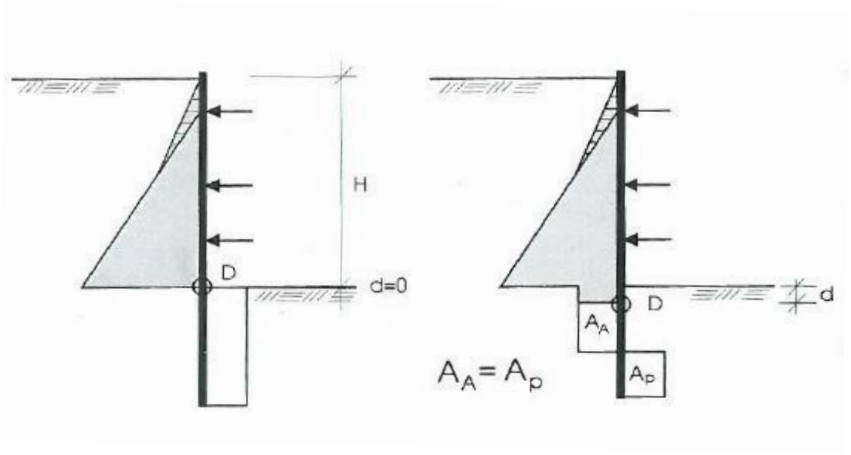

Figure 7 - Earth pressure distribution for different D (Ryner, et al., 1996, p. 54).

The total force, P_A, acting on the SPW is calculated down to the point D, see Equation (13).

$$P_A = \int_0^{(H+d)} \sigma(z)dz \tag{13}$$

The load intensity, σ_i, is then calculated using Equation (14):

$$\sigma_i = \frac{P_A}{(0.9 * H - d)} \tag{14}$$

This load intensity is then distributed between the wales so that the load between two wales is distributed evenly between them, see Figure 8. The force obtained, P_H, is a horizontal force and, if the anchors are inclined, it needs to be transformed before comparing to the measured results. The transformation to a force P with angle α is done by Equation (15).

$$P = \frac{P_H}{\cos \alpha} \tag{15}$$

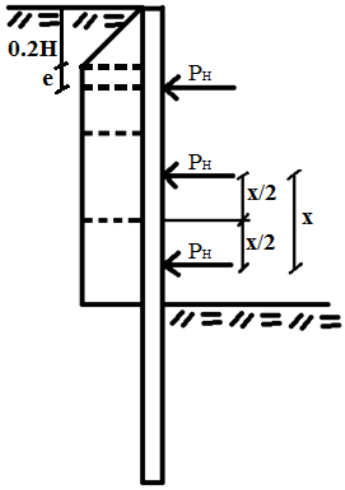

Figure 8 - Load intensity and how it is distributed between wales.

The design moment in the SPW usually occurs by the top wale, and is calculated as described in Equation (16). In between the wales there is usually a lower bending moment, but beneath the bottom wale there is another critical area. The bending moment in that span is calculated as described in Equation (17) according to *Sponthandboken* (Ryner, et al., 1996, p. 55). The design bending moment is given by the equation that gives the largest absolute value.

$$M_{Sd} = 0.1 * H * \sigma_i \left(\frac{0.2 * H}{3} + e\right) \frac{\sigma_i * e^2}{2} \tag{16}$$

$$M_{Sd} = \frac{\sigma_i * l^2}{8} \tag{17}$$

2.5 NOVAPOINT GS SUPPORTED EXCAVATION

Novapoint GS Supported Excavation (GSS) is a one dimensional FE software included in Novapoint GeoSuite Toolbox. In this software, the SPW is modelled as an elastic beam element divided into vertical linear elastic beam elements (Vianova GeoSuite AB, 2010). The surrounding soil is represented by continuous non-linear springs with varying stiffness between the different nodes, see Figure 9. This way of modelling the SPW does not consider vertical deformations and load changes.

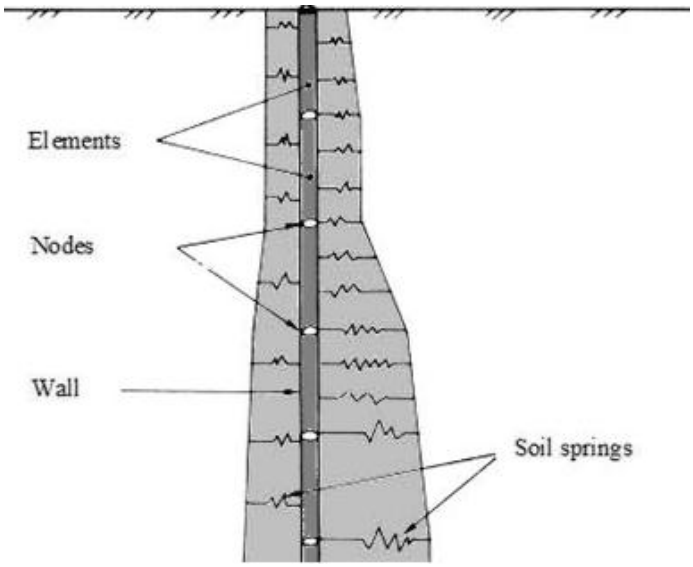

Figure 9 - Elements in the SPW (Vianova GeoSuite AB, 2010).

GSS provides a few different models but the model used in this project is the Total Stress Automatic, TSA, soil model. TSA performs a total stress analysis, which is appropriate for clays with low permeability, and the parameters used are:

- Undrained shear strength c_u
- Shear modulus G

The parameters used to model the SPW are:

- Roughness r
- Young's modulus E
- Moment of inertia I

The roughness, r, defines the amount of friction against the SPW relative to the normal stress (Vianova GeoSuite AB, 2010).The direction in which the friction acts is also defined on both sides of the SPW as either upwards or downwards. For a multi-anchored SPW the friction direction is upwards both behind and in front of the SPW, see Figure 10, and for a SPW installed to bedrock, r = 0 can be considered a conservative value (Vianova GeoSuite AB, 2010).

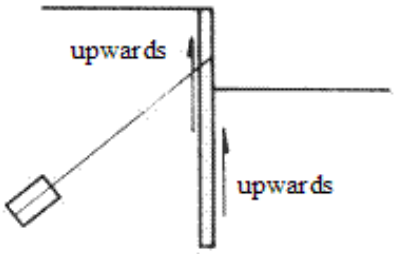

Figure 10 - Friction directions for an anchored SPW (Vianova GeoSuite AB, 2010).

The active and passive limit earth pressures are based on Rankine theory and calculated using Equations (18) - (19).

$$\sigma_{f,a} = p_A = p_v + \kappa * \frac{c_u}{\gamma_m} \tag{18}$$

$$\sigma_{f,p} = p_P = p_v - \kappa * \frac{c_u}{\gamma_m} \tag{19}$$

In these equations, p_v is the vertical earth pressure and κ is a parameter which depends on the roughness of the SPW. For a SPW with r = 0, a passive earth pressure and an upwards friction direction gives the parameter κ = 1, while an active earth pressure and an upwards friction direction gives the parameter κ = 2 (Vianova GeoSuite AB, 2010).

The initial spring stiffness on both sides of the wall is K_{yi} = 4*G (Vianova GeoSuite AB, 2010) and the characteristics of the springs are then generated for each node. The spring stiffness is assumed to be load dependent and is reduced when the earth pressures approach their respective limits, see Figure 11. G can be evaluated from E_u, obtained from triaxial tests, using Equation (20).

$$G = \frac{E_0}{2(1 + \upsilon_u)} \tag{20}$$

In Figure 11, an earth pressure-displacement relationship for a soil spring is shown. This curve shows how the soil stiffness is calculated for each load step and it is generated by adopting a hyperbola between the points of the initial earth pressure, σ_{yi}, and the limit earth pressures, (v_f, σ_f), as seen in Equation (21).

$$\sigma_y = \sigma_{yi} + \frac{v}{\frac{1}{K_{yi}} + \frac{v * R_f}{\sigma_f - \sigma_{yi}}} \tag{21}$$

The term R_f in Equation (22) is a scaling factor which is calculated using Equation (22).

$$R_f = 1 - \frac{\bar{K}_y}{K_{yi}} \tag{22}$$

The secant which intersects the hyperbola at the initial pressure and the limit pressure is called $\overline{K}_y$. The inclination of the curve represents the spring stiffness, K_y, and for the passive case it is calculated for different passive earth pressures as seen in Equation (23).

$$K_y = \frac{d\sigma_y}{dv} = K_{yi}\left(1 - \frac{(\sigma_y - \sigma_{yi}) * R_f}{\sigma_f - \sigma_{yi}}\right)^2 \tag{23}$$

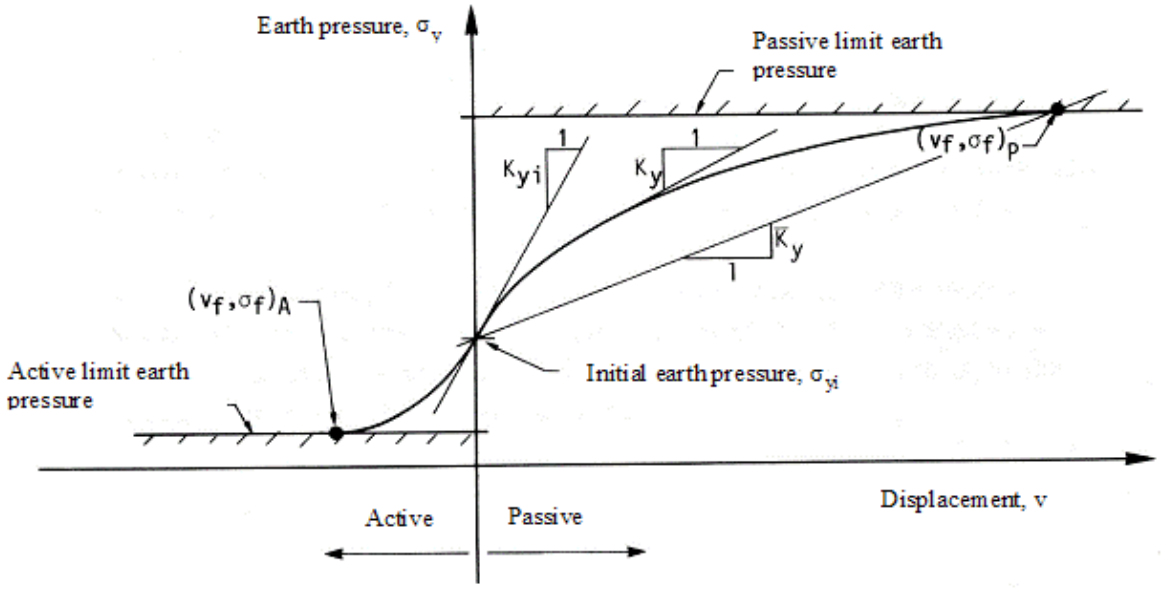

Figure 11 - Earth pressure - displacement relationship for a soil spring (Vianova GeoSuite AB, 2010).

2.6 PLAXIS

The two-dimensional FE software PLAXIS is used to model the SPW with three different constitutive models, Mohr-Coulomb (MC), Hardening Soil (HS) and the Hardening Soil with small strain stiffness (HSs). The MC model have a different stress-strain relationship compared with HS and HSs. MC uses an elastic-perfectly plastic relationship HS and HSs use a strain hardening elasto-plastic model.

There is an input in PLAXIS, which is used in all three models, called interface, R_{inter}. It is used to model the interaction between the soil and a structure, which is done by reducing the shear strength of the soil, see Equations (24) - (25), in a region close to the structure, see Figure 12. It also adds an extra node to the element on the interface to allow different displacements in the soil and the structure and thus allowing them to separate from each other. Using an interface value which is evaluated for the soil-structure interaction improves the accuracy of the model since in reality there is not perfect adhesion between the two and there might be some disturbance of the soil during installation which would lower the soil strength close to the SPW. The interfaces can also be used to make a structure impermeable in PLAXIS (Brinkgreve, et al., 2012c, pp. 96 - 102).

$$c_{inter} = R_{inter} * c_{soil} \tag{24}$$

$$\tan(\varphi_{inter}) = R_{inter} * \tan(\varphi_{soil}) \tag{25}$$

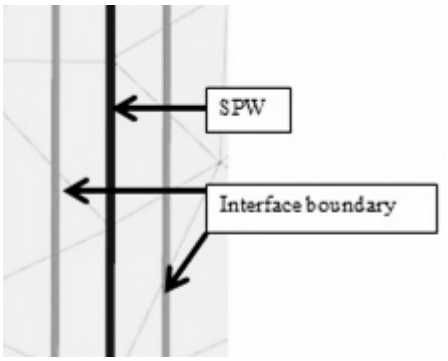

Figure 12 - Interface region close to a structure, from PLAXIS.

2.6.1 *MOHR-COULOMB*

The MC model is a linear elastic perfectly plastic model, which means that when the material is yielding, a perfectly plastic behaviour is assumed.

The parameters used in the MC model are:

- Undrained shear strength c_u
- Undrained Young's modulus E_u
- Coefficient of lateral earth pressure K_0
- Undrained Poisson's ratio υ_u

The user must be aware that the MC model can overestimate the undrained shear strength of a soil if the drainage type *Undrained (A)* is selected for a material in PLAXIS, see Figure 13. The input required for this drainage type are the effective parameters and when PLAXIS calculates the undrained shear strength, c_u, it is increased until the stress path reaches the failure envelope, represented by the inclined line in Figure 13. This gives a c_u which is higher than in reality and thus overestimates the undrained shear strength. However, this overestimation does not occur if the undrained parameters and the drainage type *Undrained (B)* are used since c_u is an input parameter when using this drainage type.

The stress paths for these models do not correspond well with real stress paths. This is a general shortcoming of the MC model and is due to the elastic-perfectly plastic assumption made in the model.

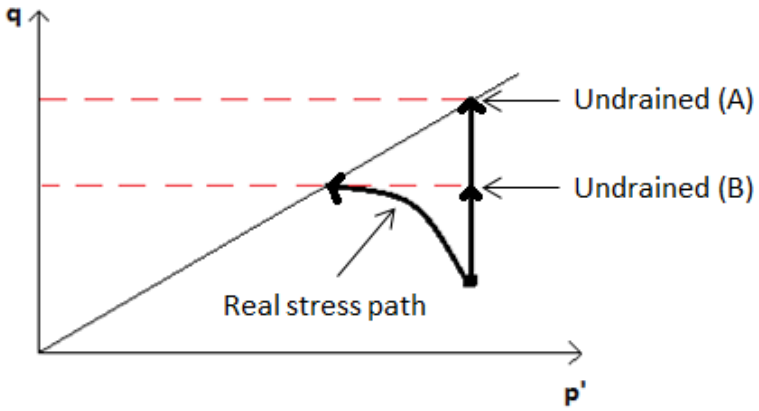

Figure 13 - Stress paths for materials using MC model, with *Undrained (A)* and *(B)* respectively, compared to a real stress path.

2.6.2 *HARDENING SOIL AND HARDENING SOIL WITH SMALL STRAIN STIFFNESS*

HS and HSs are two similar models, both more advanced than the MC model. The main difference between MC and these models is that HS and HSs accounts for the stress dependency of soil stiffness, i.e. changes the moduli depending on the stress state in the soil, see Figure 14.

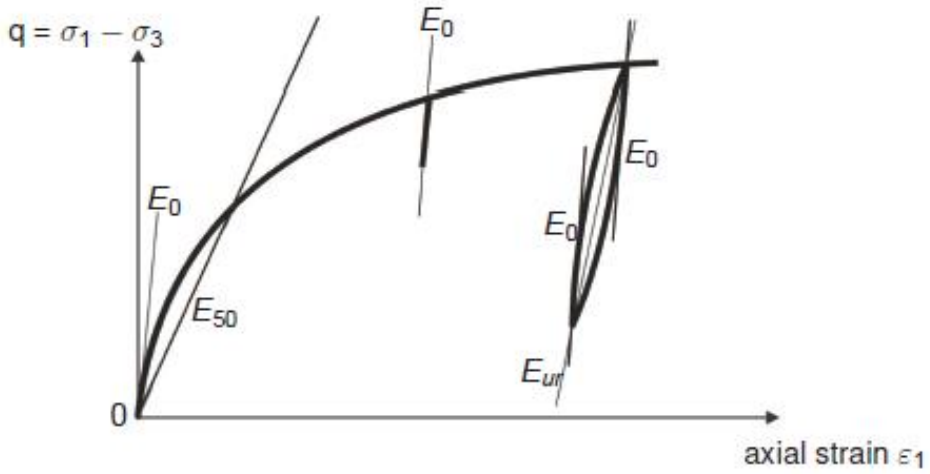

Figure 14 - Stiffness evaluated from triaxial test, which shows how stiffness varies with strain after Brinkgreve et al. (2012b, p. 83).

Since tests on sensitive soft soils are typically performed under undrained conditions, the evaluated stiffnesses are in undrained state and need to be recalculated to effective state. For E_u and E_{ur} this is done using Equation (26) (Muir Wood, 1990, p. 46) with an assumed undrained Poisson's ratio, υ_u, of 0.5 and an effective Poisson's ratio, υ', of 0.2.

$$\frac{E_u}{2(1+\upsilon_u)} = \frac{E'}{2(1+\upsilon')} \tag{26}$$

E_{50} cannot theoretically be recalculated to its effective counterpart, E'_{50}, since E_{50} is not linear elastic, which this relationship requires.

The yield surfaces in HS are shown in Figure 15. The yield cap, or the volumetric yield surface, is formed as an ellipse where the length of the ellipse on the p-axis, p_p, is calculated based on OCR (Brinkgreve, et al., 2012b, pp. 73-74). Where the ellipse intersects the q-axis depends on $K_{0,nc}$. The inclination of the deviatoric yield surface is found by calculating the ratio q/p' when $\sigma'_1 = \sigma'_c$ and $\sigma'_3 = \sigma'_c * K_{0,nc}$. Depending on the calculated stress state, and dependent on which zone that stress state is in, different moduli apply, see Figure 15.

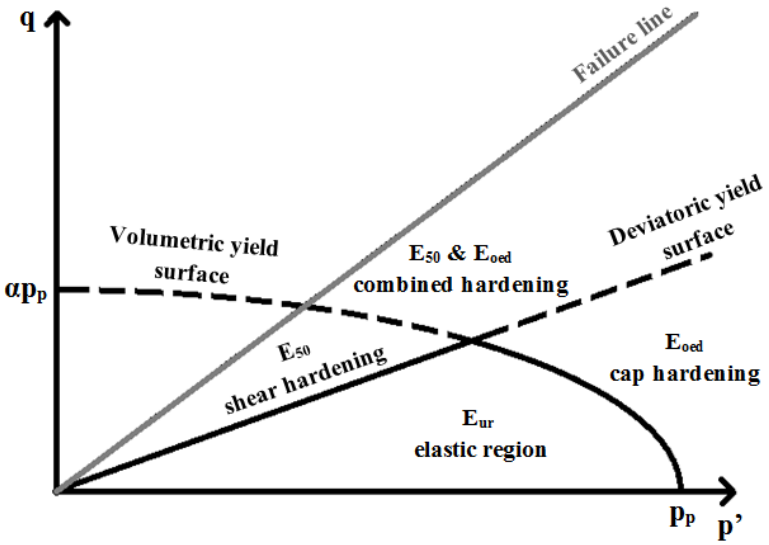

Figure 15 - The yield surfaces and the different stiffnesses in a HS model shown in a p'-q plot.

The difference between HS and HSs is that HSs also provides the possibility of modelling the soil stiffness during very small strains. This stiffness is significantly higher than what can be measured during conventional soil testing, see Figure 16. To measure such small strains would require seismic measurement of shear waves (Larsson & Mulabdic', 1991, p. 24).

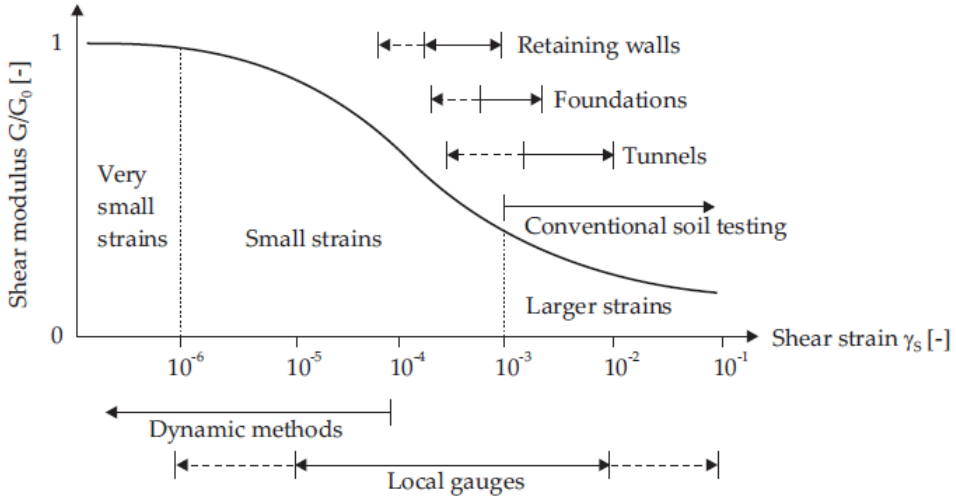

Figure 16 - Typical stiffness-strain behaviour of a soil with strain ranges for different structures and laboratory tests (Sällfors & Atkins, 1991).

The parameters used in HS are:

- Apparent cohesion c'
- Critical state friction angle φ'_{cv}
- Effective secant stiffness ($p_{ref} = \sigma'_3$) E'^{ref}_{50}
- Effective oedometer stiffness ($p_{ref} = \sigma'_1$) E'^{ref}_{oed}
- Effective unload-reload stiffness ($p_{ref} = \sigma'_3$) E'^{ref}_{ur}
- Power for stress-level dependency of stiffness m
- Effective Poisson's ratio for unloading-reloading υ'_{ur}
- Reference pressure p_{ref}
- Coefficient of lateral earth pressure K_0

The additional parameters for HSs are:

- Initial shear modulus at reference pressure (σ'_3) G_0^{ref}
- Shear strain level where $G = 0.722G_0$ $\gamma_{0.7}$

In the both the HS and the HSs models the stiffness varies with stress according to Equations (27)-(30) (Brinkgreve, et al., 2012b, p. 64).

$$E'_{oed} = E'^{ref}_{oed}\left(\frac{c'\cos\varphi - \sigma'_1\sin\varphi}{c'\cos\varphi + p^{ref}\sin\varphi}\right)^m \quad (27)$$

$$E'_{50} = E'^{ref}_{50}\left(\frac{c'\cos\varphi - \sigma'_3\sin\varphi}{c'\cos\varphi + p^{ref}\sin\varphi}\right)^m \quad (28)$$

$$E'_{ur} = E'^{ref}_{ur}\left(\frac{c'\cos\varphi - \sigma'_3\sin\varphi}{c'\cos\varphi + p^{ref}\sin\varphi}\right)^m \quad (29)$$

In these equations, σ'_1 is the major principal stress, σ'_3 is the minor principal stress and p_{ref} is the reference pressure. E'_{50} and E'_{ur} are evaluated as described in section 2.3.2. E'_{oed} can be evaluated from oedometer tests but can also be evaluated through the relationship seen in Equation (30) which is the evaluation method used in this project. Both M_L and σ'_c used in this equation are obtained from CRS tests.

$$E'^{ref}_{oed} = M_L\left(\frac{p_{ref}}{\sigma'_c}\right) \quad (30)$$

The reference stiffness, E'^{ref}_i, is calculated for all evaluated stiffnesses for the same reference pressure to simplify the comparison of them and to use them as input in PLAXIS. For E'_{50} and E'_{ur} this is done by setting σ'_3 in Equations (28) - (29) to the maximum radial stress applied during the triaxial test. With m = 1 for soft soils (Brinkgreve, et al., 2012b, p. 63), the different reference stiffness can be calculated by solving the Equations (27) - (30) for E'^{ref}_i.

The HSs model also implements the use of the initial shear modulus, G_0. Since there are no tests performed which provide such information, G_0 is evaluated using the correlation with undrained shear strength, c_u, and plasticity index, I_P, presented by Larsson and Mulabdic´ (1991, p. 116) seen in Equation (31).

$$G_0 = \left(\frac{208}{I_P} + 250\right) * c_u \quad (31)$$

This undrained shear modulus is then transformed to an effective modulus using Equation (32).

$$G'_0 = G_0 * \frac{(1+\upsilon')}{(1+\upsilon_u)} \quad (32)$$

The shear modulus, G'_0, varies with pressure in the same way as the stiffnesses does, see Equation (33), and thus a G'^{ref}_0 value needs to be calculated as in Equation (34), and as mentioned above, m = 1.

$$G'_0 = G_0'^{ref} \left(\frac{c' \cos\varphi - \sigma'_3 \sin\varphi}{c' \cos\varphi - p^{ref} \sin\varphi} \right)^m \tag{33}$$

$$G_0'^{ref} = G'_0 \frac{c' \cos\varphi + p_{ref} \sin\varphi}{c' \cos\varphi - \sigma'_3 \sin\varphi} \tag{34}$$

The parameter $\gamma_{0.7}$ is the shear strain level at which the shear modulus is 72.2 % of the initial shear modulus, see Figure 17. It can be calculated using Equation (35) (Benz, 2007, p. 23), based on a correlation with I_P.

$$\gamma_{0.7} = 1 * 10^{-4} + I_P * 5 * 10^{-4} \tag{35}$$

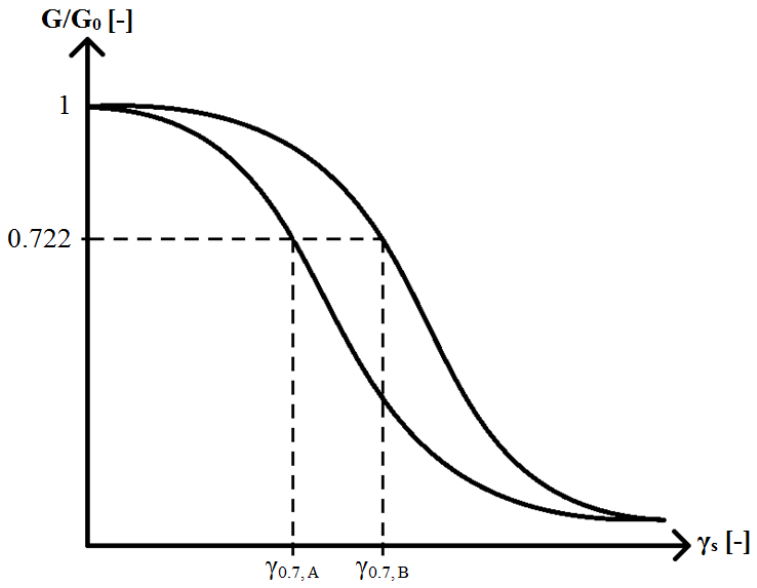

Figure 17 – Shear modulus reduction curve for two different $\gamma_{0.7}$.

3 MODELS, CALCULATIONS AND RESULTS

A description of the general parameters, such as the evaluated soil parameters, pore pressures, the geometry of the excavation and the SPW and anchor characteristics can be found in this section. The input and calculation conditions for the different calculation methods and material models used in this thesis are also described, as well as the results obtained from the different calculations.

3.1 SITE INFORMATION

The SPW was installed during the construction of the southernmost tunnel face of Götatunneln in central Gothenburg; see the area marked by an ellipse in Figure 18.

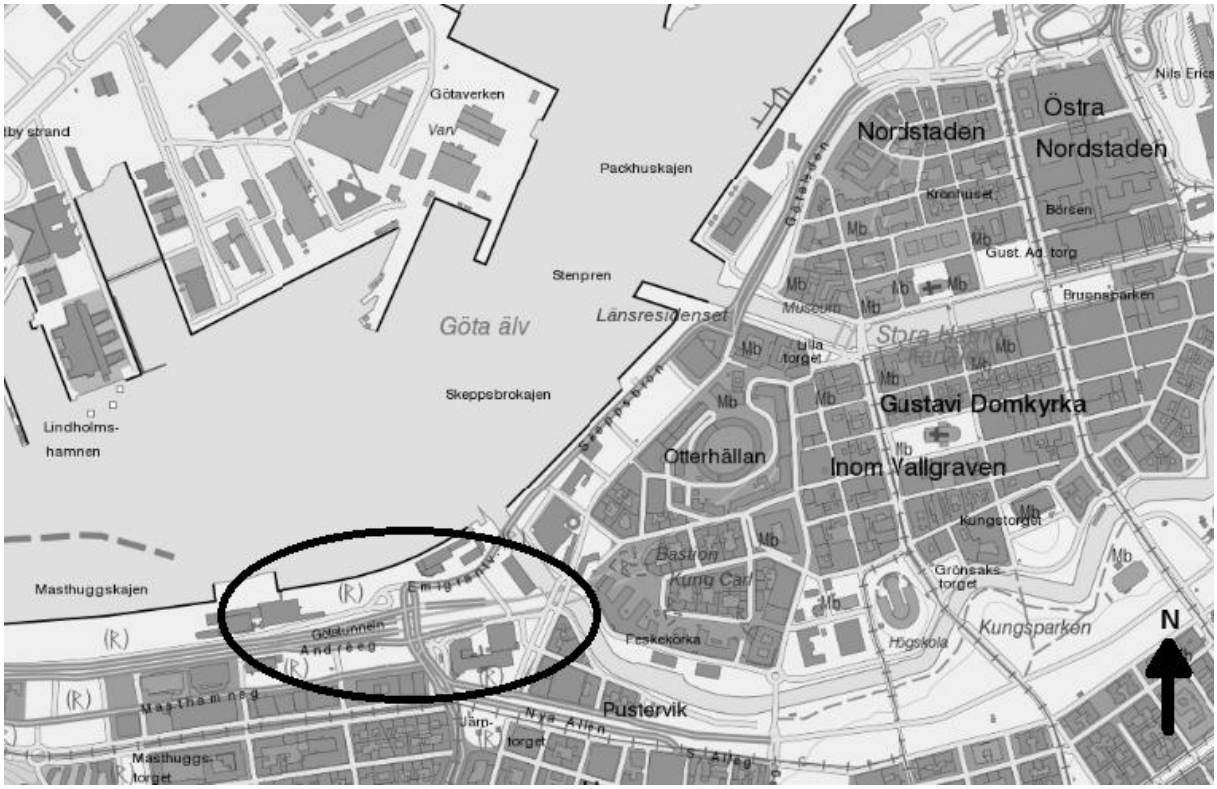

Figure 18 – Location of the excavation shaft (VISS, 2014).

The studied part of the SPW is located between two buildings, see Figure 19. The surrounding buildings are located approximately 20 meters from the studied cross-section and it is therefore assumed that they do not affect the SPW. The excavation might affect the surrounding buildings by causing settlements in the area, but such impacts on the surrounding buildings are not considered in this study.

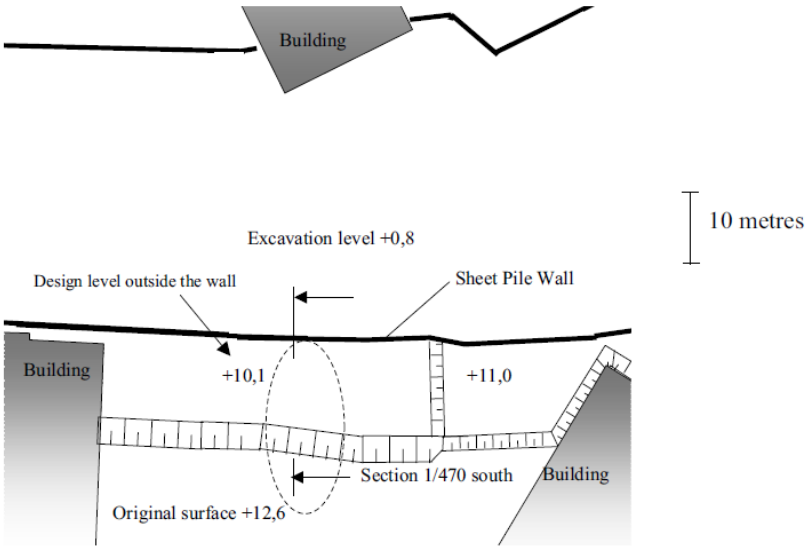

Figure 19 – Plan of the excavation shaft with the studied SPW marked as a section (Kullingsjö, 2007, p. 107).

The geometry used in the calculations is based on Kullingsjö (2007, p. 108). The shaft is approximately 11 meters deep, the SPW is installed down to and attached to the bedrock and has wales and anchors at three different levels, as can be seen in Figure 20.

The installation procedure for the SPW and anchors is illustrated in Figure 20 and is as follows (Kullingsjö, 2007, p. 109):

a) Installation of the SPW.
b) Excavation to a depth of 2 meters on both sides of the SPW.
c) Excavation to a depth of 4 meters in front of the SPW.
d) Installation of wales and anchors at a depth of 3.5 meters.
e) Excavation to a depth of 6.5 meters in front of the SPW and 8.5 meters just beside the SPW.
f) Installation of wales and anchors at a depth of 7.5 meters.
g) Excavation to a depth of 9 meters in front of the SPW and 11.5 meters just beside the SPW.
h) Installation of wales and anchors at a depth of 10.5 meters.
i) Excavation to a depth of 11.7 meters in front of the SPW.

This information is used to model the calculation phases for the different software.

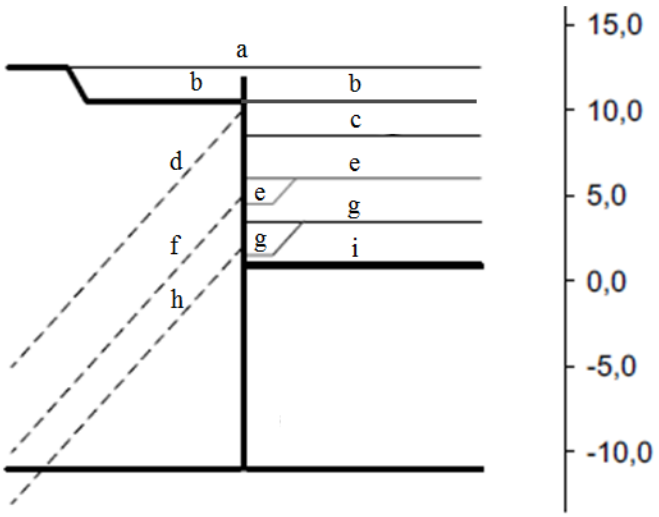

Figure 20 – Schematic figure of the geometry of the excavation shaft (Kullingsjö, 2007, p. 108), modified by authors.

3.1.1 *SOIL*

The soil consists of 3 meters of fill on top of 19 meters of slightly overconsolidated clay. Beneath that there is approximately 1.5 meters of sand and then there is bedrock, see Figure 21. The overconsolidation of the clay is likely due to the fact that the site was used for storing iron arriving at the harbour previously located in the area (Kullingsjö, 2007, p. 135).

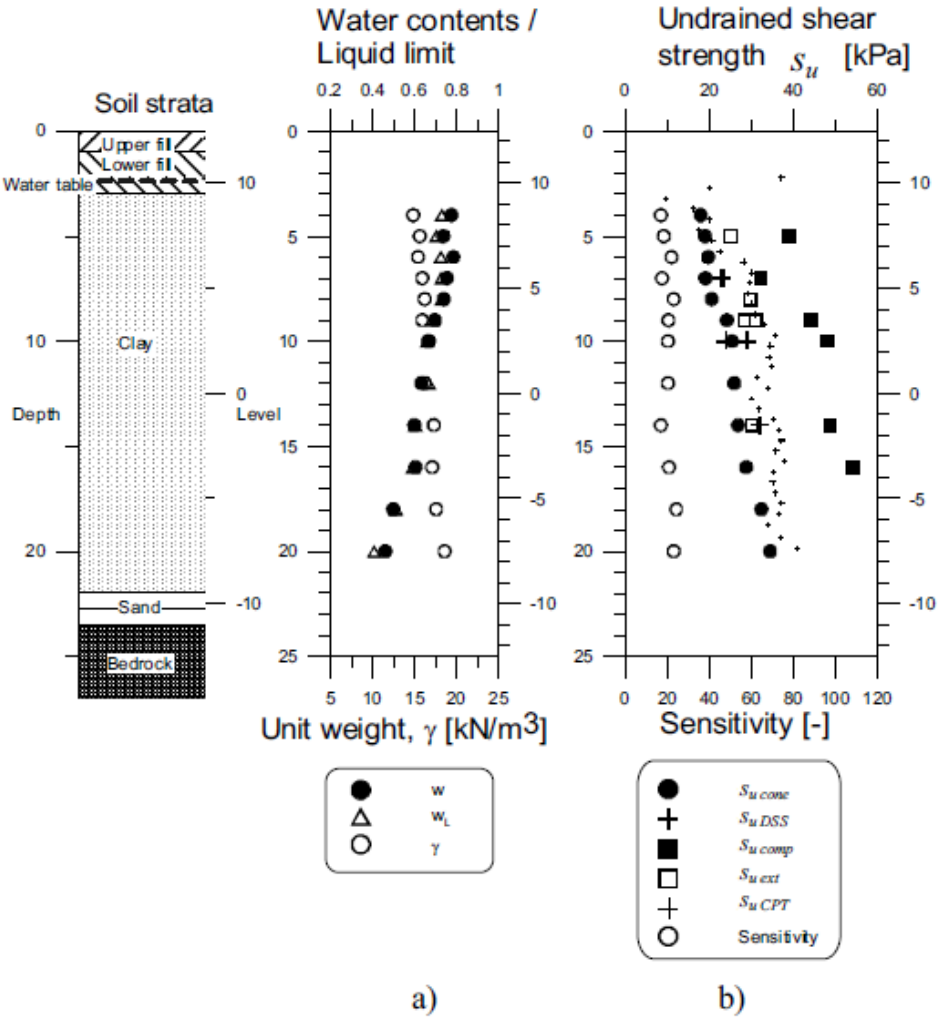

Figure 21 – Soil strata and evaluated soil parameters for the analysed area (Kullingsjö, 2007, p. 136)

A compilation of the in situ conditions and the OCR can be found in Appendix 1:1. The input value for the undrained shear strength used in the hand calculations, GSS and MC model is evaluated from a compilation of several different tests, which can be seen together with the selected distribution in Appendix 1:2

Raw data from CRS and triaxial tests obtained from Kullingsjö are evaluated to determine some input parameters needed for the different models. These tests were performed by Kullingsjö and Hedborg during the work with Kullingsjö's doctoral thesis. The reference pressure used when evaluating all moduli in this project is p_{ref} = 50 kPa. The soil parameters that are not evaluated from CRS or triaxial tests are obtained from Kullingsjö (2007, p. 136), see Figure 21.

The parameter φ'_{cv} which is used for the clay layers in all models is evaluated from triaxial tests. The evaluated values and the selected distribution can be seen in Appendix 1:3. The range of φ'_{cv} is from 33° to 35° which is similar to the values evaluated by Kullingsjö (2007, p. 239).

The undrained Young's modulus, E_u, is also evaluated from triaxial tests, and the evaluated values, as well as the selected distribution, can be found in Appendix 1:4. The chosen distribution is selected by performing SoilTest as described in section 3.1.2.

A similar procedure is used to obtain the effective secant stiffness E'_{50}. A first estimation of the secant stiffness is evaluated for the undrained case which is then recalculated to an effective parameter using Equation (26). In reality there is no such relationship between effective and undrained secant stiffness, but since it is only used as a first estimation before calibrating with SoilTest, it is considered acceptable. The evaluated and the selected E'_{50} used in the HS and HSs models can be seen in Appendix 1:5.

The effective oedometer stiffness E'_{oed} is evaluated using a relationship with M_L and σ'_c, evaluated from CRS tests, as described in section 2.6.2. There is however a limit to how E'_{oed} can vary in relation to other parameters in PLAXIS and since the evaluated parameters are not within this limit they cannot be used as input. The evaluated and selected values can be seen in Appendix 1:6.

Since only one triaxial test with unloading and reloading was performed, this is the only level where there is evaluated effective unload-reload stiffness. Since this also is a parameter that is calibrated using SoilTest it is possible to evaluate a distribution for the entire soil which can be seen, together with the value evaluated from triaxial tests, in Appendix 1:7.

Both G_0 and γ_{07} have been evaluated from correlations as described in section 2.6.2. The evaluated values and selected distribution can be seen in Appendix 1:8-1:9.

The division of the clay into different layers will vary between the different calculation methods and constitutive models due to the variation in input parameters between them. The soil parameters selected for the fill layer are obtained from *TRV Geo* (Trafikverket, 2011, pp. 35-41) since no tests were performed in that layer.

3.1.2 *PLAXIS SOILTEST*

The SoilTest function in PLAXIS can be used to validate the evaluation of field and lab tests. After creating a material in the model, SoilTest can be used to simulate tests in this material, based on the input parameters and constitutive model, which then can be compared to real tests (Brinkgreve, et al., 2012a, p. 10). The simulated tests produce plots, such as the p'-q and the ε_1-q seen in Figure 22, and the parameters in the created material can be varied until adequate fits between these simulated plots and the plots from triaxial tests are found.

The parameters that are varied are the different stiffnesses while φ'_{cv} is kept constant, to get a failure envelope which corresponds well with the triaxial tests. Since SPW are designed to keep deformations small, the focus is on fitting the results for the small deformation intervals rather than the larger ones if a fit cannot be found for the entire plot.

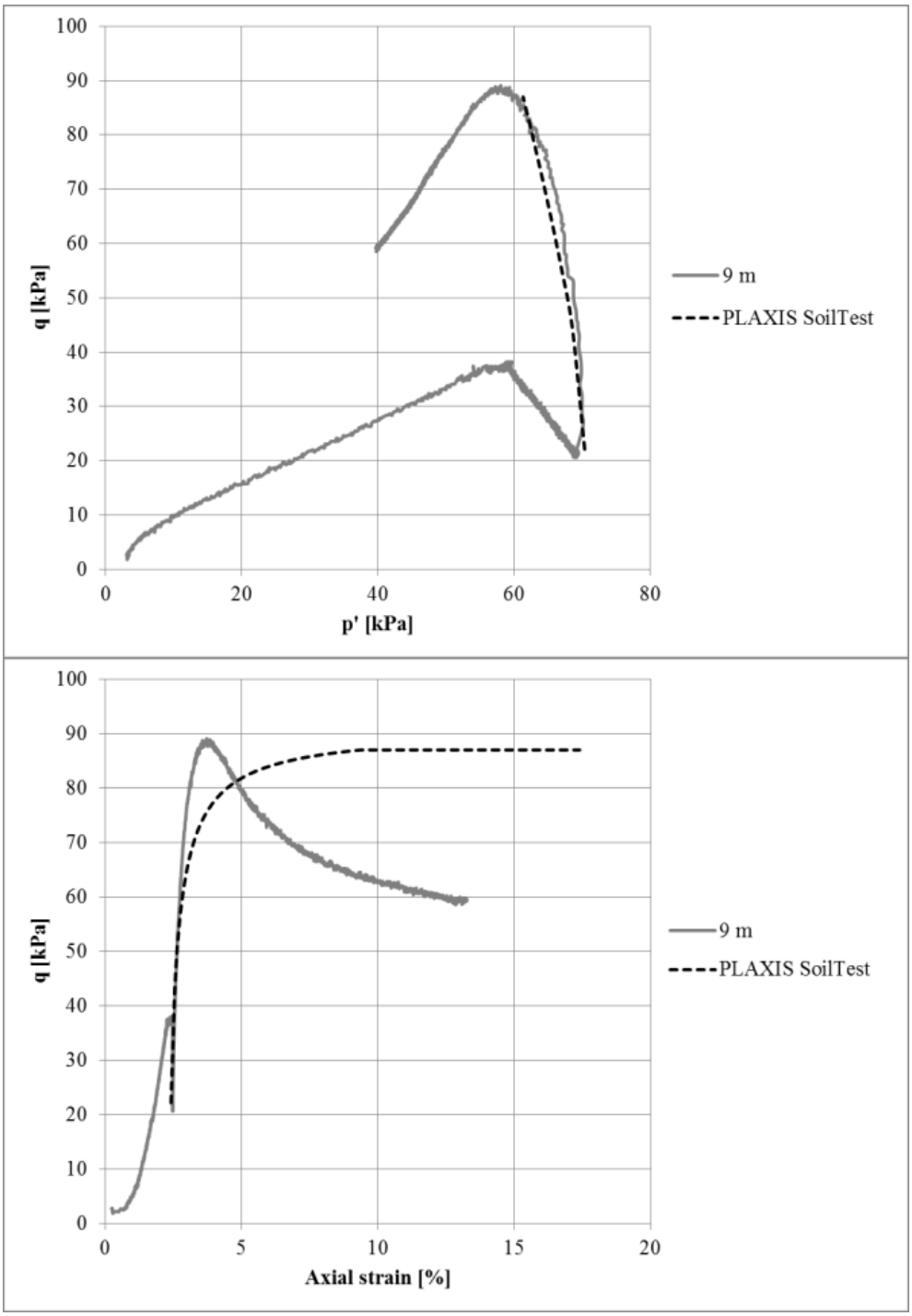

Figure 22 - Comparison between SoilTest and a triaxial test at 9 meter depth.

A comparison between the results from tests simulated using SoilTest and results from the triaxial tests for different depths can be found in Appendix 2:1-2:5.

3.1.3 *PORE WATER PRESSURE*

The PWP is based on measurements performed during the construction of the SPW, which are presented by Kullingsjö (2007). These measurements show that the groundwater surface is at approximately 2 meters below the ground surface and that the hydraulic head measured at different depths vary between approximately 2-2.5 meters beneath the ground surface, see Figure 21.

For simplified use in the models it is assumed that the groundwater surface is 2 meters below the ground surface and that the PWP is hydrostatic.

3.1.4 *SHEET PILE WALL AND ANCHORS*

The SPW is an anchored Z-section AZ36 SPW, see Appendix 3:1-3:3. The characteristics of the SPW are presented in Table 1. The SPW is installed down to and attached to the bedrock, at 23.5 m depth, and the base of the SPW was sealed for groundwater flow to prevent hydraulic uplift (Kullingsjö, 2007, p. 106).

Table 1 - Characteristics of AZ36 SPW (ArcelorMittal, n.d.).

Parameter	Value	Unit
Weight, w	1.90	[kN/m^2]
Young's modulus, E	$2.1 * 10^8$	[kPa]
Moment of inertia, I	$8.28 * 10^{-4}$	[m^4/m]
Normal stiffness, EA	$5.19 * 10^6$	[kN/m]
Flexural rigidity, EI	$1.74 * 10^5$	[kNm^2/m]
Poisson's ratio, υ	0.3	[-]

The anchors used are cable anchors which are installed with an angle of 45° and anchored in bedrock. The anchors are installed in three rows, symbolized by the arrows in Figure 23, at depths 3.5, 7.5 and 10.5 meters (Kullingsjö, 2007, pp. 110-116). The input parameters, c-c distance and the prestress applied to the different anchors can be seen in Table 2.

Table 2 - Characteristics of anchors, see Appendix 3:1-3:3.

Parameter	Row 1	Row 2	Row 3	Unit
Length	28.3	22.6	18.4	[m]
Number of strands	12	12	12	[-]
Young's modulus, E	$1.95 * 10^8$	$1.95 * 10^8$	$1.95 * 10^8$	[kPa]
Normal stiffness, EA	$4.88 * 10^5$	$4.88 * 10^5$	$4.88 * 10^5$	[kN/m]
c-c distance	5.9	2.2	2.1	[m]
Prestress	170	523	548	[kN/m]

The deformation figure and anchor forces obtained from measurements performed on the SPW during the final excavation stage (Kullingsjö, 2007) are shown in Figure 23.

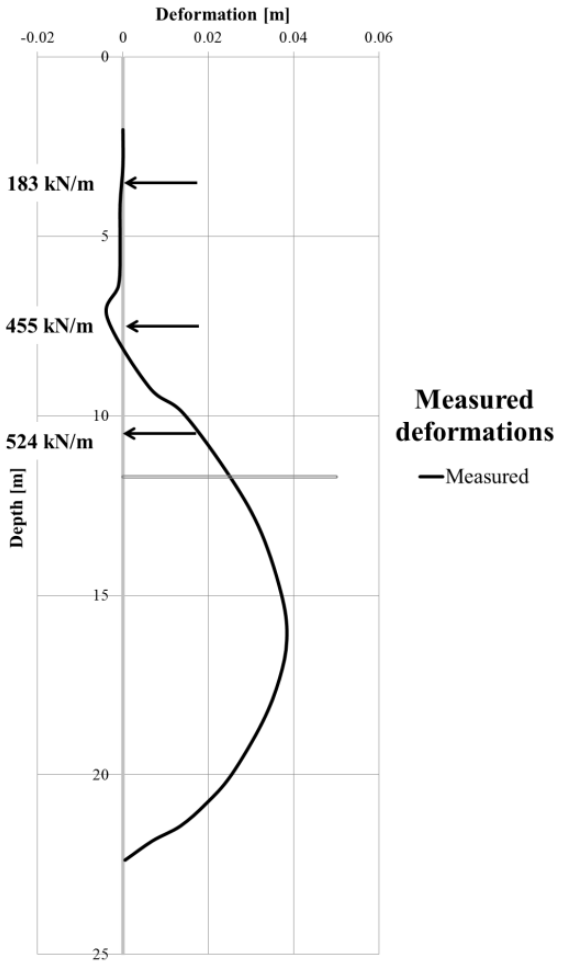

Figure 23 – Measured deformations and anchor forces in the SPW during the final excavation stage.

3.2 HAND CALCULATIONS

The hand calculations are performed in Excel using the method provided in *Sponthandboken* (Ryner, et al., 1996), see section 2.4. It is not possible to obtain a deformation figure with values on horizontal deformations when using this method. Instead, the calculated anchor forces and the design bending moment are used when comparing with measured results and other models.

3.2.1 *INPUT*

The soil layer division and the parameters assigned to each layer are presented in Table 3. The groundwater table is set two meters below the surface and the PWP is assumed to increase hydrostatically.

Table 3 - Soil layer division and parameters used for hand calculations.

Layer	Depth [m]	Soil weight, γ [kN/m^3]	Undrained shear strength, c_u [kPa]	Increase in undrained shear strength with depth, $c_{u,inc}$ [kPa/m]	Friction angle, φ[°]
Fill	0-3	18	0	0	30
Clay	3-23.5	16	29	1	0

The parameters used for the fill layers are taken from Kullingsjö's doctoral thesis (2007, p. 290) and these are the design parameters stated in a contract between the Swedish Road Administration and the contractor for this section of the SPW.

3.2.2 *CALCULATION*

Excel is used to calculate the earth pressure distribution acting on the SPW. The results from this calculation are then used to calculate the resulting anchor forces and design bending moment. The calculations and the results can be seen in Appendix 4:1-4:6.

3.2.3 *RESULTS*

The resulting anchor forces are presented in Table 4. The design bending moment acting on the SPW is calculated to 154 kNm/m.

Table 4 - Forces obtained from hand calculations.

Anchor row	Anchor force, P [kN/m]
Row 1	417
Row 2	343
Row 3	294

3.3 NOVAPOINT GS SUPPORTED EXCAVATION

Since GSS is performing one-dimensional FE calculations, it is only possible to obtain the horizontal deformations along the SPW. The vertical deformations and how the excavation is affecting the surrounding area are not possible to obtain from the software.

3.3.1 *INPUT*

The model created in GSS, seen in Figure 24, has the soil layer division and parameters presented in Table 5.

Table 5 - Soil layer division and parameters used for calculations in GSS.

Layer	Depth [m]	Soil weight, γ [kN/m^3]	Undrained shear strength, c_u [kPa]	Coefficient of lateral earth pressure at rest, K_0 [-]	Undrained initial shear modulus, G_0 [MPa]
Clay 1	3-10	15-16.5	29-36	0.56-0.52	4.3-5.7
Clay 2	10-18	16.5-18	36-44	0.52-0.48	5.7-7
Clay 3	18-23.5	18-19.8	44-49.5	0.48-0.47	7-8

The constitutive model used for the clay is TSA, see section 2.5, since the clay is considered impermeable enough to prevent pore pressures from dissipating. The reason that K_0 varies is due to OCR-correction, see section 2.2.

The fill layer is modelled using effective parameters in the model Effective Stress Simplified (Vianova GeoSuite AB, 2010) since it is a drained layer. The parameters used for the fill layer are the same as for the hand calculations except for c', which is set to 1 kPa since it has to be a positive number in the

software, and E', which is assumed to be the same as the Young's modulus found in *TRV Geo* (Trafikverket, 2011, p. 41). The value selected is for a firmly packed layer since the area has previously been used as storage for iron coming in from the harbour (Kullingsjö, 2007, p. 135).

The properties of the SPW and the anchors used are described in section 3.1.4.

3.3.2 *CALCULATION*

The calculation phases are based on the installation sequence described in section 3.1. It is however not possible to model local excavations within the shaft in the software. Instead, when there is an excavation just beside the wall, the excavations in the software are modelled to the depth of the local excavation.

Since the software only allows modelling an excavation in front of the SPW, the excavation to 2 meters depth on both sides of the wall could not be modelled. This was considered by setting the ground surface 2 meters beneath the original surface, giving a fill layer 1 meter thick instead of 3 meters. The effects from not being able to include this excavation are assumed to be small.

3.3.3 *RESULTS*

The results from the GSS calculation can be seen in Figure 24, which shows the geometry of the open shaft and the displacement curve.

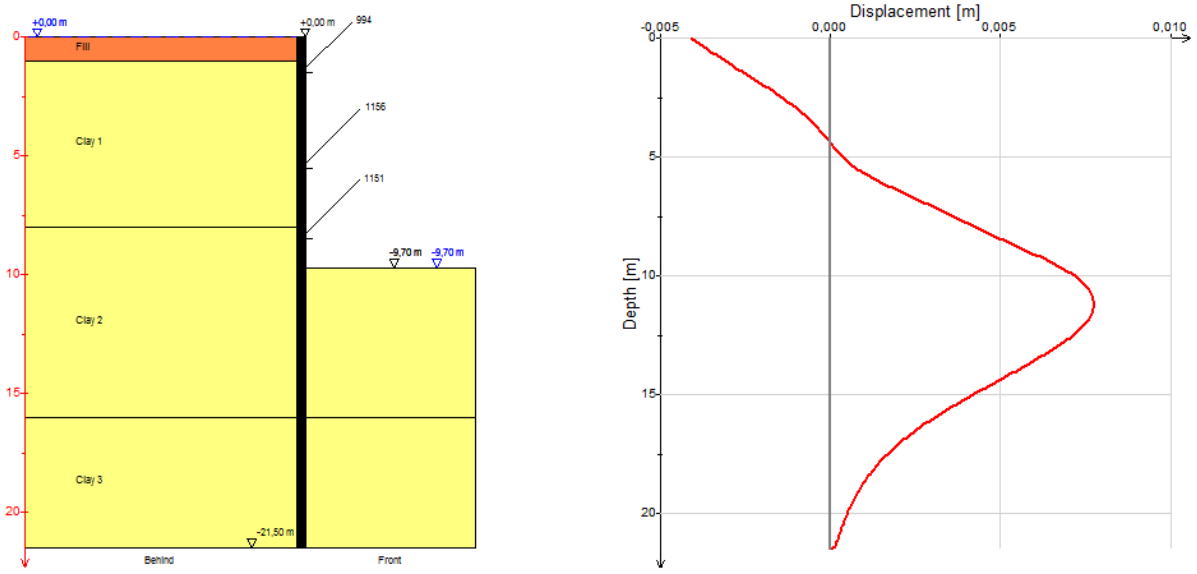

Figure 24 – Geometry of final excavation stage and the corresponding displacement curve.

The maximum displacement is approximately 8 mm and occurs 1.5-2 m below shaft bottom. The anchor forces are presented in Table 6.

Table 6 – Anchor forces from GSS calculation.

Anchor row	Anchor force [kN]	Anchor force per meter [kN/m]
Row 1	994	168
Row 2	1156	525
Row 3	1151	548

3.4 PLAXIS – GENERAL MODEL SETUP

The calculation setup is identical for all the PLAXIS models, except for constitutive models and drainage conditions. The calculations are performed using plane strain conditions with 15 node elements and medium mesh coarseness, see Figure 25. The mesh is gradually refined until the difference in output between the finer mesh and the previous mesh is negligible.

The calculation type is plastic and the loading input is staged construction. The water table is reduced to the bottom of the shaft and the excavated clusters are set to dry in each step. The phases are modelled based on the information in section 3.1.

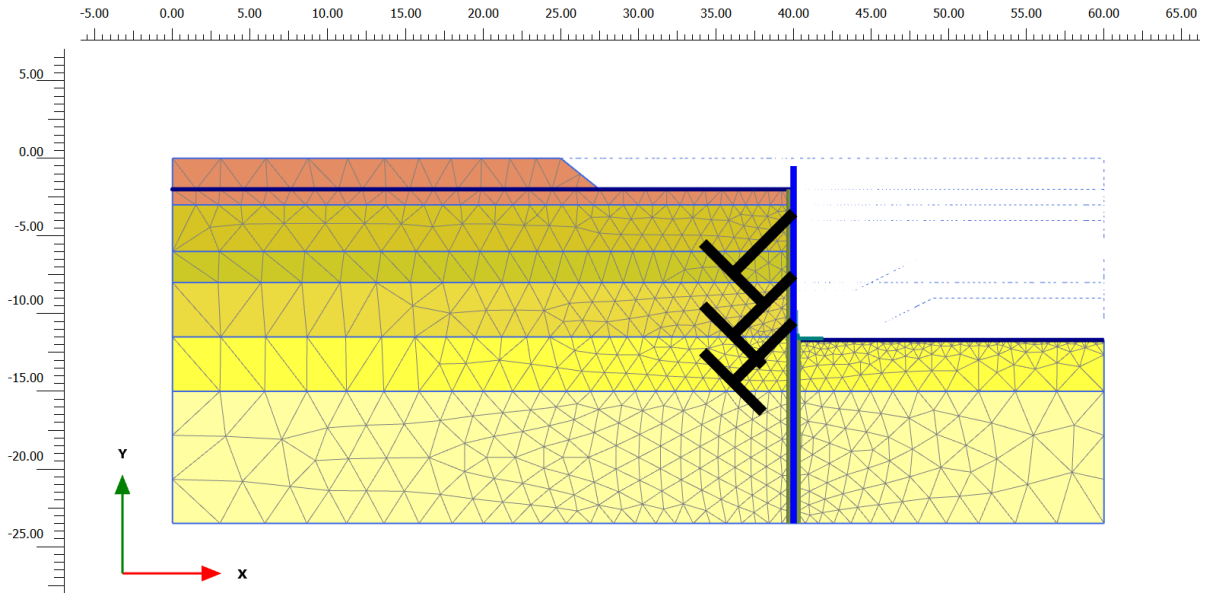

Figure 25 - The mesh during the final excavation stage in the MC model, with a global medium coarseness.

3.5 PLAXIS – MOHR-COULOMB

3.5.1 *INPUT*

The soil layer division and the input parameters used in PLAXIS are presented in Table 7 below. The drainage conditions are set to *Undrained (B)* to avoid overestimation of the shear strength in the soil, see section 2.6.1. The interface is set to 0.67 in the fill layer and to 0.5 for all the clay layers (Karstunen, 2013b, p. 43).

Table 7 – Soil layer division and parameters used for the MC model in PLAXIS.

Layer	Depth [m]	Soil weight, γ [kN/m^3]	Undrained shear strength, c_u [kPa]	Initial stiffness, E_u [MPa]	Critical state friction angle, φ'_{cv} [°]	OCR [-]	Coefficient of lateral earth pressure at rest, K_0 [-]
Fill	0-3	18	0	50	30	-	0.47
Clay 1	3-6	16	29-32	12.4	35	1.8	0.57
Clay 2	6-8	16	32-34	7	35	1.65	0.55
Clay 3	8-11.5	16	34-37.5	20	35	1.55	0.53
Clay 4	11.5-15	17	37.5-41	16	33	1.32	0.52
Clay 5	15-23.5	18	41-49.5	22	35	1.29	0.48

3.5.2 *RESULTS*

Figure 26 shows the deformation figure with 27 mm as the maximum horizontal displacement. The total principal strains span from -4.1*10^{-3} to 6.5*10^{-3}, which proves that the assumption made in section 3.1.2 that small strains occur is valid and thus the calibration of the soil parameters in SoilTest is performed for the right strain levels.

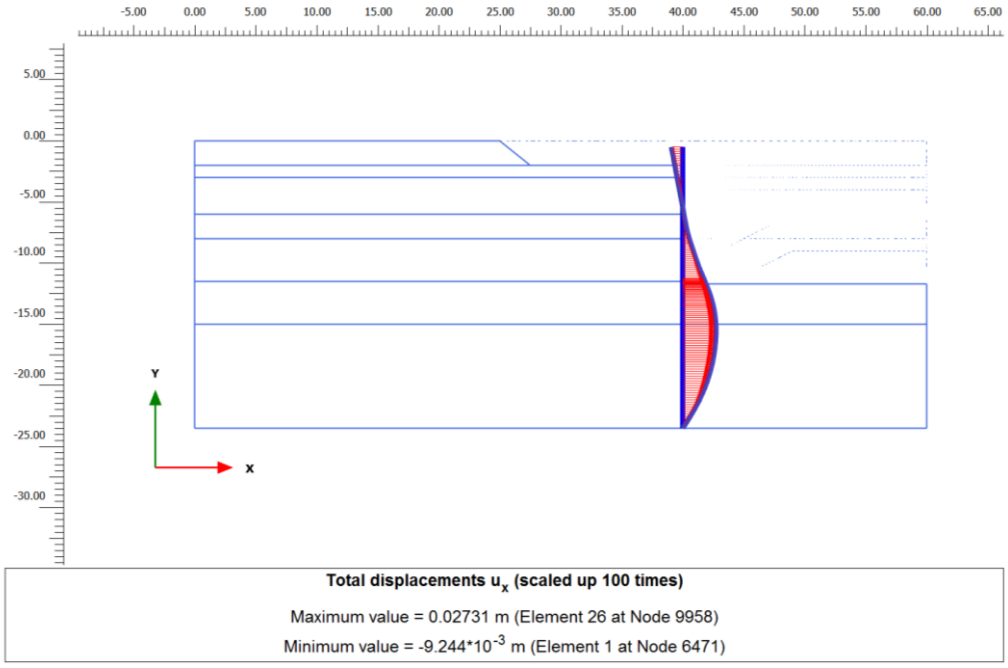

Figure 26 – Total horizontal displacements in the SPW calculated in the MC model, scaled up 100 times.

The shear force and the bending moment in the SPW is also obtained from PLAXIS, see Table 8, as well as the anchor forces after the final excavation stage, which can be found in Table 9.

Table 8 – Shear force and bending moment in the SPW calculated in the MC model.

Type	Maximum	Minimum	Unit
Shear force	260	-212	[kN/m]
Bending moment	237	-198	[kNm/m]

Table 9 – Anchor forces calculated in the MC model.

Anchor row	Anchor force per meter [kN/m]
Row 1	152
Row 2	498
Row 3	569

3.6 PLAXIS – HARDENING SOIL

3.6.1 *INPUT*

The soil layer division and the input parameters used in PLAXIS are presented in Table 10 below. The drainage conditions are set to *Undrained (A)* since effective parameters are required for the soil stiffness stress dependency, described in section 2.6.2. The input parameters are obtained using SoilTest, see section 3.1.2.

Table 10 - Soil layer division and parameters used for the HS model in PLAXIS.

Layer	Depth [m]	Soil weight, γ [kN/m^3]	Effective secant stiffness, E'_{50} [MPa]	Effective oedometer stiffness, E'_{oed} [MPa]	Unload-reload stiffness, E'_{ur} [MPa]	Critical state friction angle, φ'_{cv} [°]	OCR [-]	Coefficient of lateral earth pressure at rest, K_0 [-]
Clay 1	3-6	16	8	5.8	16	35	1.8	0.57
Clay 2	6-11.5	16	8	4.7	16	35	1.6	0.54
Clay 3	11.5-15	17	10	5	20	33	1.32	0.52
Clay 4	15-23.5	18	5	1.65	12	35	1.29	0.48

The interface is set to 0.67 in the fill layers and to 0.5 for all the clay layers (Karstunen, 2013b, p. 43). The fill layer is modelled the same as in the MC model since there are no tests to provide additional information for the HS model.

3.6.2 *RESULTS*

Figure 27 shows the deformation figure with 46 mm as the maximum horizontal displacement. The total principal strains span from $-6.3*10^{-3}$ to $9.8*10^{-3}$, which proves that the assumption made in section 3.1.2 that small strains occur is valid and thus the calibration of the soil parameters in SoilTest is performed for the right strain levels.

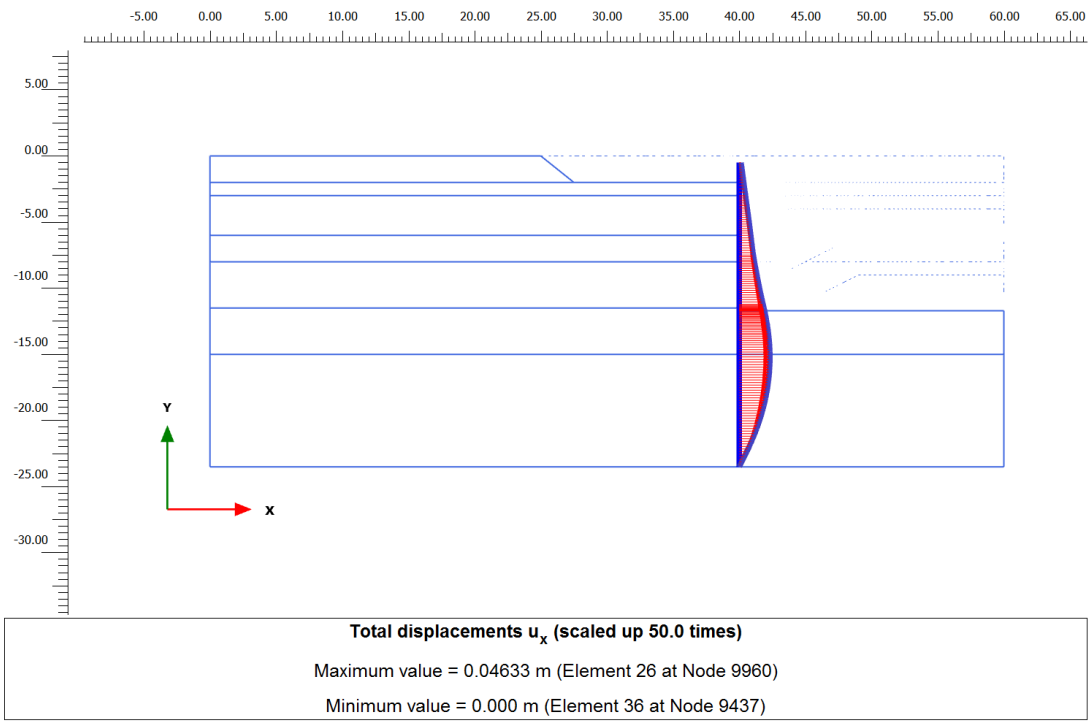

Figure 27 – Total horizontal displacement in the SPW calculated in the HS model, scaled up 50 times.

The shear force and the bending moment in the SPW is also obtained from PLAXIS, see Table 11, as well as the anchor forces after the final excavation stage, which can be found in Table 12.

Table 11 – Shear force and bending moment in the SPW calculated in the HS model.

Type	Maximum	Minimum	Unit
Shear force	277	-225	[kN/m]
Bending moment	265	-189	[kNm/m]

Table 12 – Anchor forces calculated in the HS model.

Anchor row	Anchor force per meter [kN/m]
Row 1	159
Row 2	511
Row 3	580

3.7 PLAXIS – HARDENING SOIL WITH SMALL STRAIN

3.7.1 *INPUT*

The input for the HSs model is the same as for the HS model, except for the additional parameters presented in Table 13. The interface is set to 0.67 in the fill layers and to 0.5 for all the clay layers (Karstunen, 2013b, p. 43).

Table 13 - Soil layer division and additional parameters used for the HSs model in PLAXIS.

Layer	Depth [m]	Effective initial shear modulus, G'_0 [MPa]	Shear strain level where $G'/G'_0 \approx 0.7$, $\gamma_{0.7}$ [-]
Clay 1	3-6	20	$3 * 10^{-4}$
Clay 2	6-11.5	20	$3 * 10^{-4}$
Clay 3	11.5-15	23	$3 * 10^{-4}$
Clay 4	15-23.5	28	$2.2 * 10^{-4}$

3.7.2 *RESULTS*

Figure 28 shows the deformation figure with 28 mm as the maximum horizontal displacement. The total principal strains span from $-4.4*10^{-3}$ to $9.1*10^{-3}$, which proves that the assumption made in section 3.1.2 that small strains occur is valid and thus the calibration of the soil parameters in SoilTest is performed for the right strain levels.

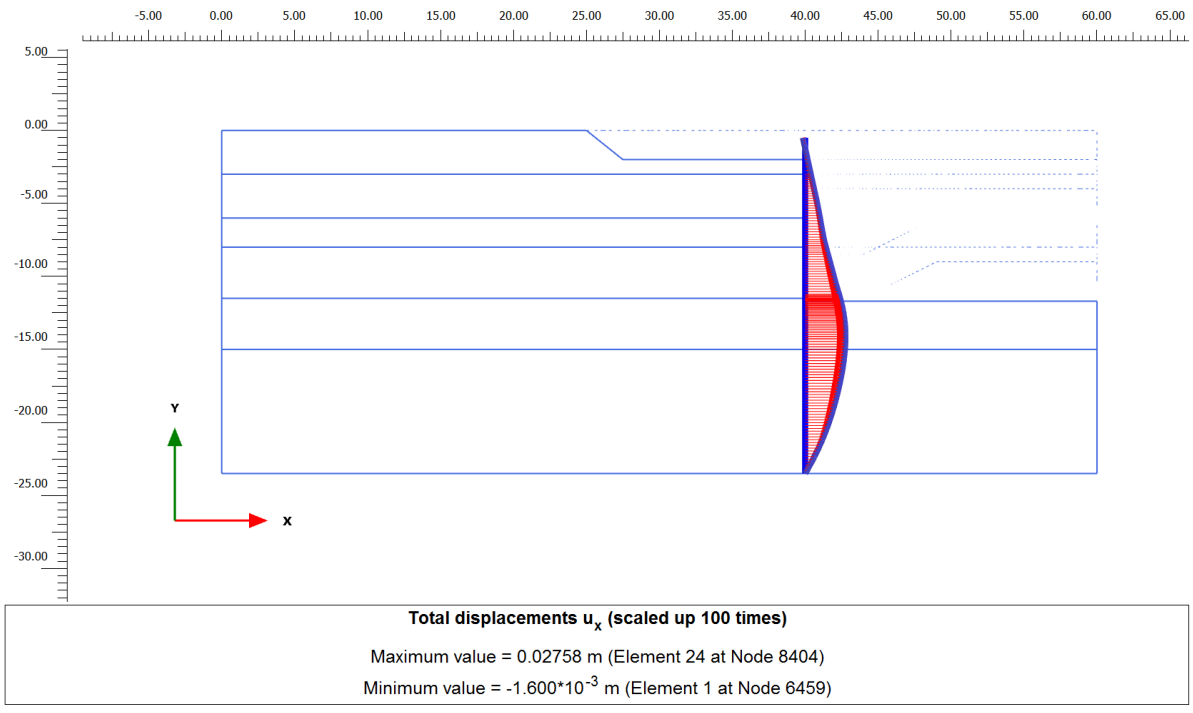

Figure 28 – Total horizontal displacement in the SPW calculated in the HSs model, scaled up 100 times.

The shear force and the bending moment in the SPW is also obtained from PLAXIS, see Table 14, as well as the anchor forces after the final excavation stage, which can be found in Table 15.

Table 14 – Shear force and bending moment in the SPW calculated in the HSs model.

Type	Maximum	Minimum	Unit
Shear force	253	-180	[kN/m]
Bending moment	214	-160	[kNm/m]

Table 15 – Anchor forces calculated in the HSs model.

Anchor row	Anchor force per meter [kN/m]
Row 1	162
Row 2	515
Row 3	548

4 ANALYSIS OF RESULTS

The results from the different calculations described in section 3 are compared to each other and to in-situ measurements in this section. The different comparisons are performed to assess the accuracy of the different methods and to illustrate their differences. Interpretations of the different results are also included here.

4.1 SHEET PILE WALL DEFORMATIONS

When comparing the resulting deformations from the different models it is clear that they all give results of the same magnitude, varying between approximately 7-46 mm, see Figure 29. The model that gives the most different results compared to the measured deformations is the GSS model. The maximum deformation differs approximately 80 % from the measured one and the model also fails to capture the shape of the real deformation curve.

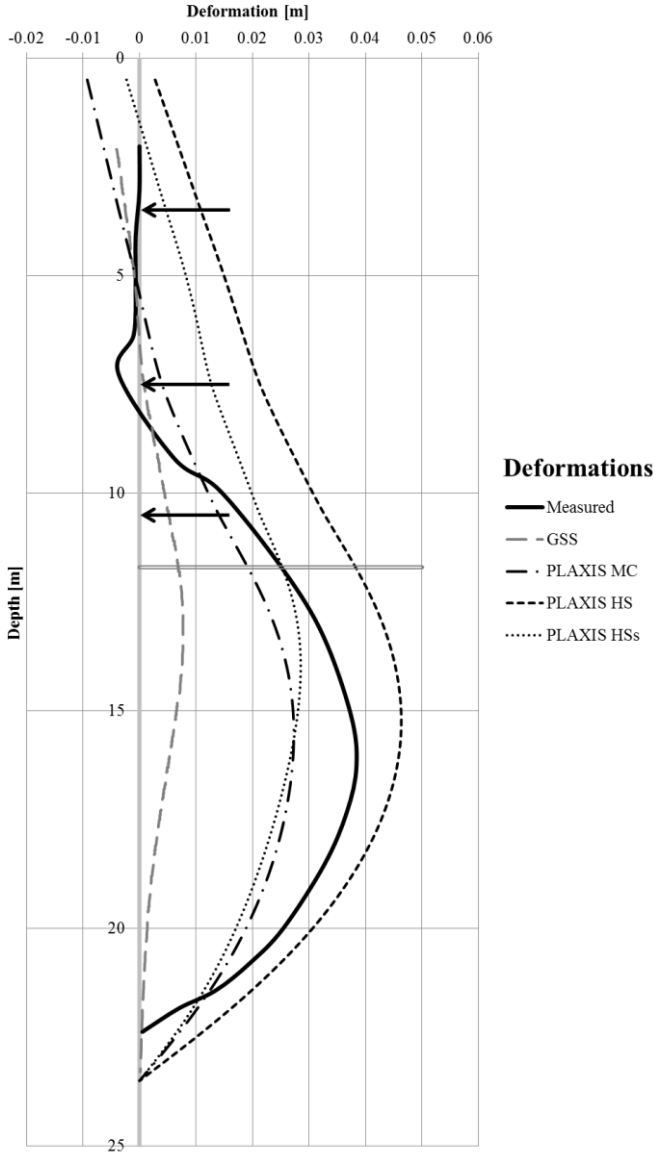

Figure 29 - Comparison of calculated deformations in the SPW from different models to measured deformations.

The results from the PLAXIS models correspond fairly well to the size of the deformation, 71-121 % of measured maximum deformation. Above the middle anchor however, the measured deformations suggest that there are almost no deformations in the SPW.

4.1.1 *DISCUSSION*

The reason for the SPW deforming above the middle anchor in the PLAXIS models might be that the idealized characteristics of the SPW and anchors used in the model might differ from reality, since these are based on specifications from the manufacturer. When comparing the deformation curves below the shaft bottom, a better compliance is obtained. Another reason might be that problems occurred during installation of the measuring instruments or that these were damaged during the construction period.

The HS model gives both the most accurate maximum deformation and a deformation curve which matches the measured one most accurately. Another advantage is that it is the only model that overestimates the deformations at all depths, which indicates that the results are just on the safe side.

4.2 ANCHOR FORCES

A comparison of the anchor forces show that they generally correspond very well to the measured values and to each other, see Figure 30. There is also not much difference between the prestress and the stress during the final excavation stage, when the shaft is completely open, for any of the models.

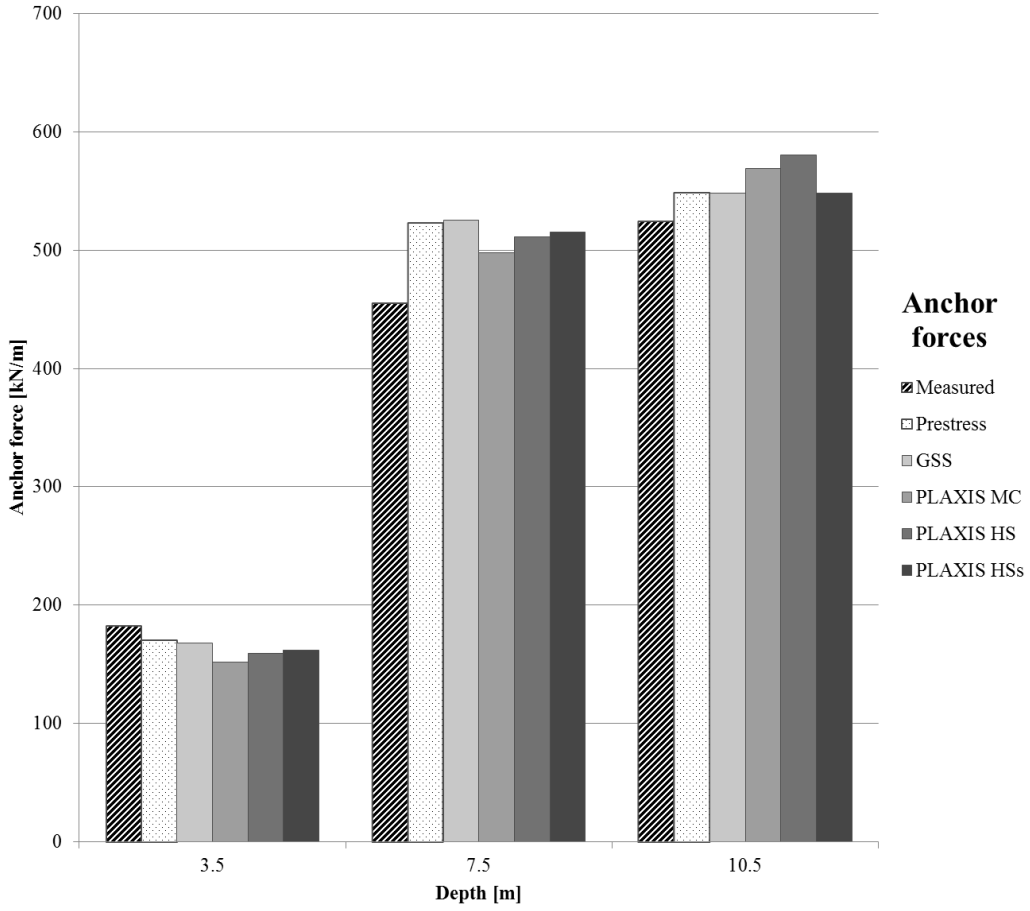

Figure 30 - Comparison of anchor forces calculated with different models and measured anchor forces.

When comparing the results from hand calculations it is clear that they do not correspond very well, see Figure 31. This is because the prestress is not considered in this method. The result instead shows what anchor forces would be necessary to reach force equilibrium between the earth pressures and the anchor forces.

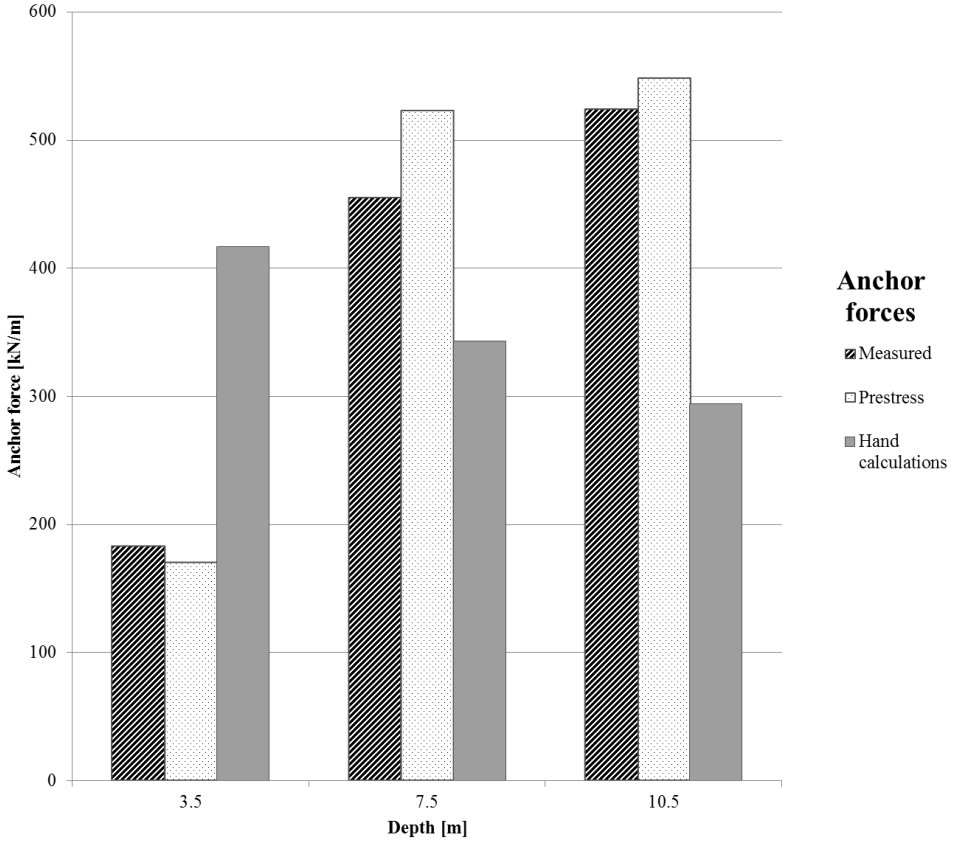

Figure 31 - Comparison of hand calculated anchor forces to measured forces and prestress.

4.2.1 *DISCUSSION*

The measured values are lower than the calculated ones at 7.5 m and 10.5 m depth. This might be due to time effects in the clay or relaxation in the anchors (Kullingsjö, 2007, p. 126), which is not possible to consider in the models used.

4.3 BENDING MOMENT AND SHEAR FORCE

The bending moments calculated in the different models are very similar down to 10.5 m depth, where the lowest anchor row is, see Figure 32. Below that, the difference is large and the shapes of the different distributions are varying. This trend of the bending moments being similar above the anchors and differing below is also something observed by Schweiger (2009, p. 7) when comparing the same constitutive models used in PLAXIS.

There are however some differences to Schweiger's comparison, one of which being the fact that the MC model gives the lowest bending moments in that comparison while in this comparison the HSs model gives the lowest bending moments of the PLAXIS models. The largest difference though is the distribution of the bending moments. The PLAXIS calculations performed in this study shows different shapes for the different models, while they are uniform in Schweiger's comparison (2009, p. 7).

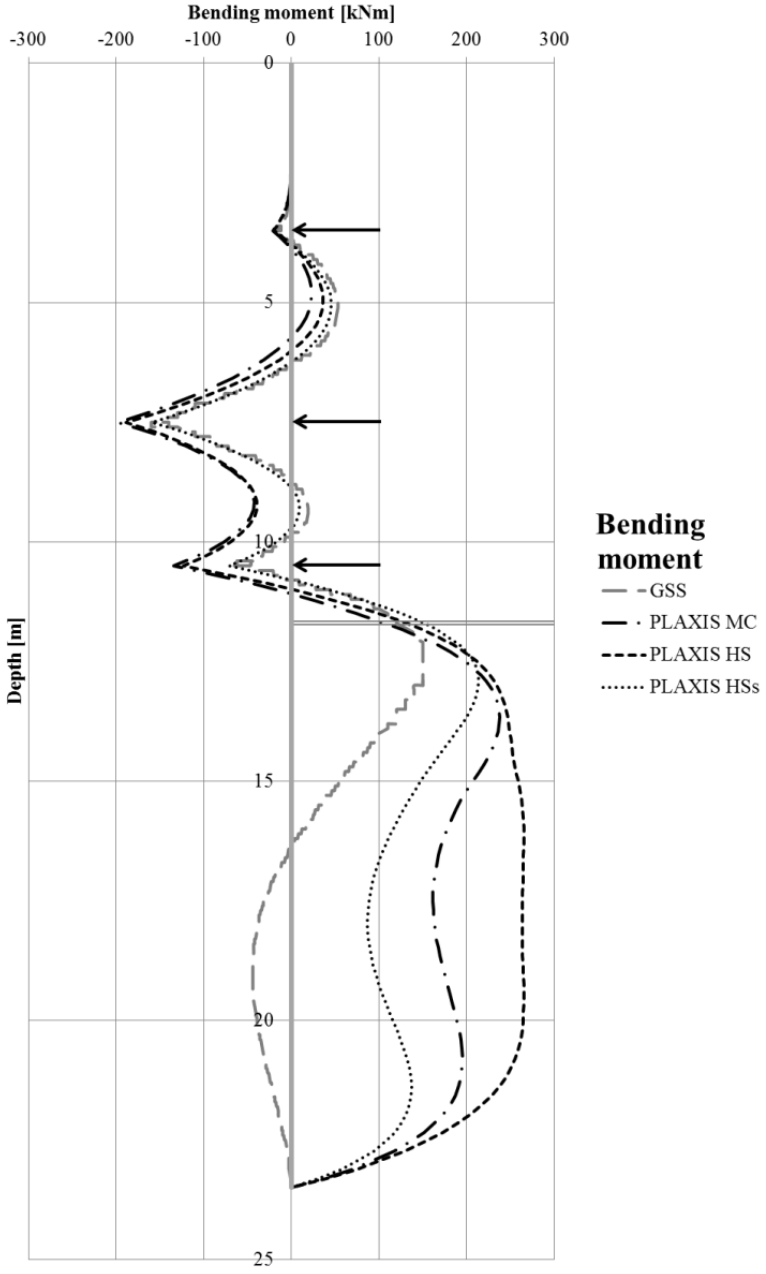

Figure 32 - Comparison of calculated bending moments in the SPW from different models.

The maximum bending moment is rather similar for all PLAXIS models, while it is a bit lower in the GSS model. The hand calculations do not give similar results at all, with a design bending moment of approximately 154 kNm/m.

The shear forces calculated in the different models are, much like the bending moments, very similar down to where the lowest anchor row is, see Figure 33, due to the high prestresses. Below that, the models still produce quite similar distribution shapes with the magnitude varying somewhat. However, all calculations give similar values for the maximum shear force.

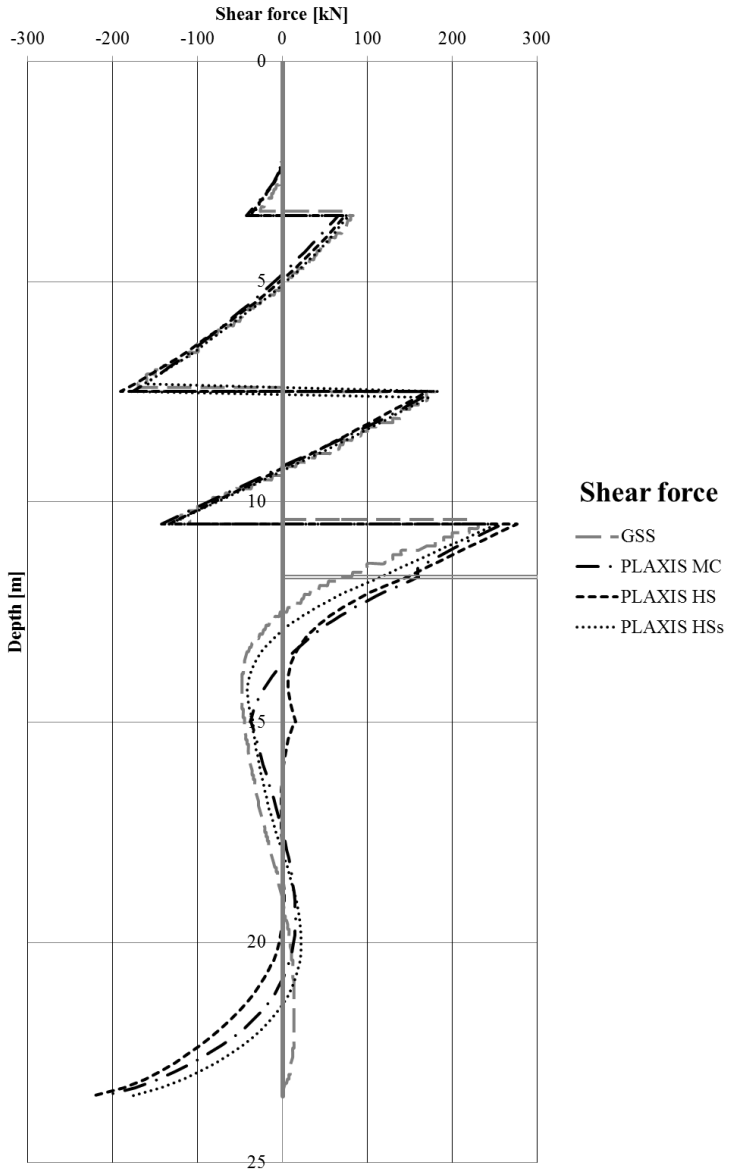

Figure 33 - Comparison of calculated shear forces in the SPW from different models.

The results from the HS model indicate that there is no shear force at all from 16-20 m depth. This explains why the bending moment calculated in the HS model is virtually constant in this span.

4.3.1 *DISCUSSION*

The reason for the HSs model giving lower bending moments than the MC model in this comparison and not in the one performed by Schweiger is probably due to the results of the HSs model being very sensitive to the choice of parameters G_0 and $\gamma_{0.7}$, see sections 5.4 and 5.5 respectively.

The differences in bending moment distribution between Schweiger's comparison and this one are probably due to the SPW analysed by Schweiger being installed in a much stiffer soil than the Gothenburg clay modelled in this project. Another reason might be the difference in length of the SPW in the two studies.

The reason for the design bending moments obtained in the hand calculations being different is most likely due to not being able to consider the effect of the prestressed anchors.

4.4 EARTH PRESSURES

The earth pressure distribution comparison also shows that the results from the PLAXIS models are more similar to each other than to other models, see Figure 34. The pressure distributions behind the SPW are very similar to each other down to 9 m depth, except for the hand calculations. Below that, the results from the PLAXIS models are fairly similar to each other, with the MC model giving slightly lower earth pressures than the other two, and the GSS model and hand calculations giving higher pressures.

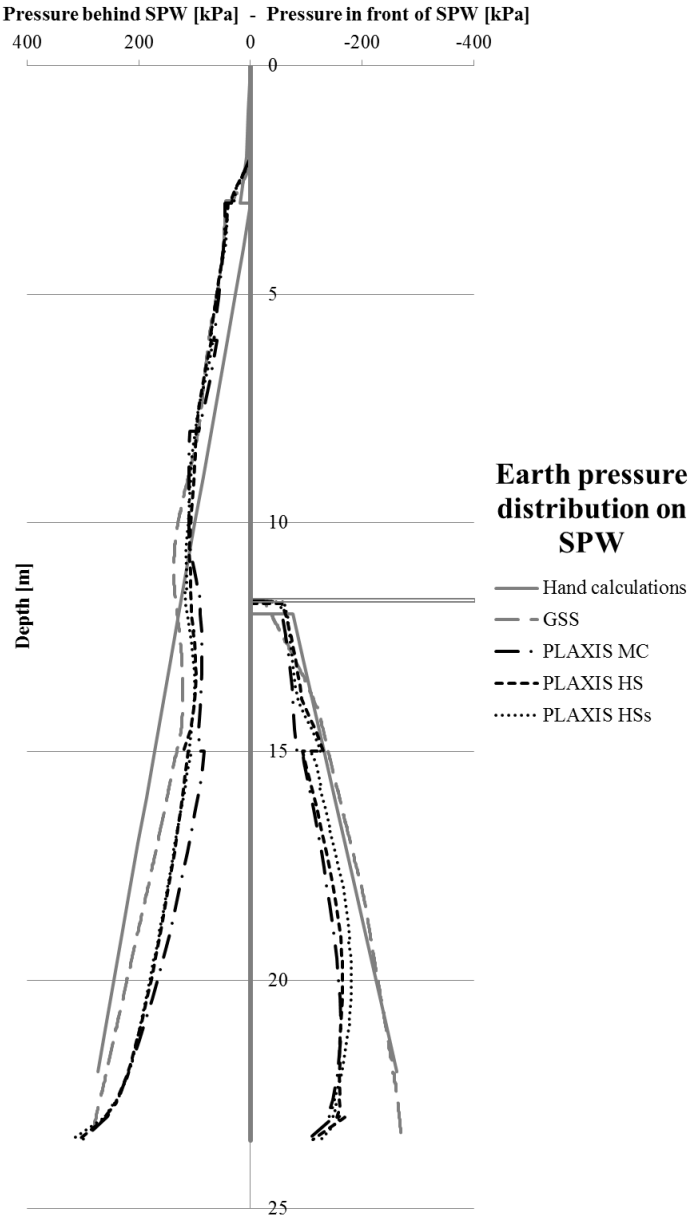

Figure 34 - Comparison of earth pressures acting on the SPW calculated using different models.

In front of the SPW the GSS model and the hand calculations give very similar results while the PLAXIS models generally give lower pressures. At 15 m depth, the earth pressures from the HS and HSs models decrease instantly. Below that the results from the PLAXIS models are quite similar, with HSs giving slightly higher earth pressures than the other two.

4.4.1 *DISCUSSION*

The hand calculation method assumes full mobilization of the earth pressures which does not apply in this case since the SPW is anchored in bedrock, which prevents the movement required for full mobilization. In the GSS model, the earth pressures are very similar to the hand calculations in front of the SPW, and are thus nearly fully mobilized. This might be an explanation to why the resulting deformations in GSS are smaller than the other FE models. The instant decrease in earth pressure for the HS and HSs models at 15 m depth is probably due to there being a soil layer boundary there over which the friction angle changes.

4.5 SUBSIDENCE BEHIND THE SHEET PILE WALL

The measured subsidence that eventually occur behind the SPW after the final excavation stage can be seen in Figure 35, together with the resulting subsidence calculated using the different PLAXIS models. Neither GSS nor the hand calculations are sophisticated enough to provide such information and are thus not included.

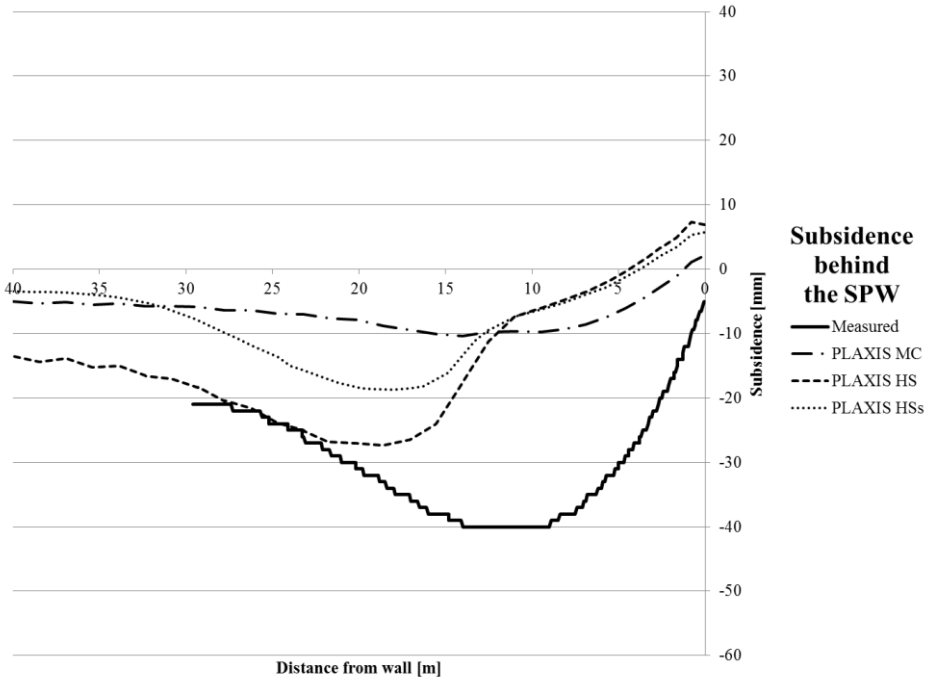

Figure 35 - Comparison of subsidence behind the SPW calculated from the PLAXIS models and measured results.

The comparison shows that all three constitutive models underestimate the maximum measured subsidence. None of the models capture the shape of the deformation curve for the first 20 meters behind the wall, but after that the HS model seems to give quite realistic results. All three models also show that heave occurs just behind the SPW, which is not something that has been measured. The prediction of heave instead of subsidence was also something that was observed by Schweiger (2009) when comparing the same models.

4.5.1 *DISCUSSION*

The reasons for heave occurring in the models and not in reality might be due to a number of things. For example, the soil might have been disturbed during installation, causing subsidence just around the SPW, which is not considered in the models. Another explanation might be that the models show that the SPW bends inwards at the top which could result in a heave.

Furthermore, the calculations were performed with undrained conditions, which is most likely not the real case. There might be partial drainage occurring in the area, which could cause consolidation settlements in the soil. The parameter E_{oed} might also affect the subsidence behind the SPW. Since it is much higher in the model than what was evaluated from CRS-tests, it might lead to an underestimation of the settlements.

5 PARAMETRIC STUDIES

The models used for the parametric study are identical to the original models, except for certain parameters being changed in order to determine the impact of these specific parameters. The parameters are varied as described below and the results are then compared to the results from the original models as well as to the measured results. Interpretations and discussion of these comparisons are also included in this section.

5.1 E FROM EMPIRICAL EVALUATION IN PLAXIS MC

Triaxial tests are the basis for the evaluation of E_u, which is used in the original MC model. However, the relatively high cost of triaxial tests combined with the limited knowledge about how to evaluate them makes the use of these tests uncommon[3].

If no triaxial tests are available, another procedure where the undrained Young's modulus is evaluated empirically as E_{50} can be used, see Equation (36) (Trafikverket, 2011, p. 41). Two scenarios are calculated, one with the Young's modulus set to E_{50} for the entire soil, case A, and one where the Young's modulus is set to $3*E_{50}$ in front of the SPW[4] to account for unload-reload stiffness, case B, see Figure 36.

$$E_{50} = 250 * c_u \tag{36}$$

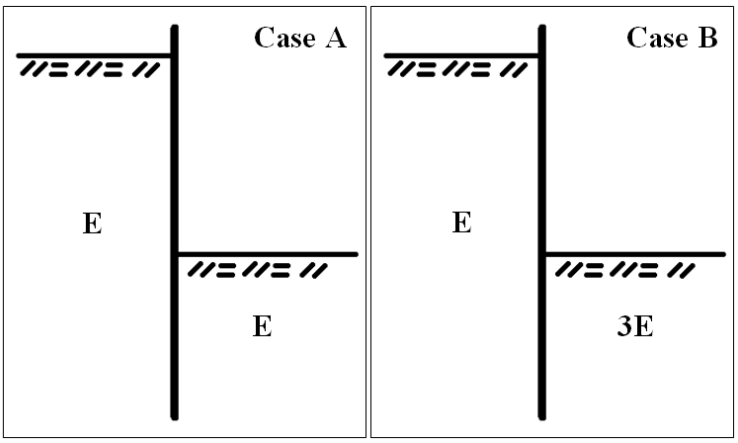

Figure 36 – Two different calculation scenarios with E evaluated from an empirical correlation to c_u.

The undrained shear strength distribution used in this parametric study differs from the one used in the original MC model. This is due to not considering the undrained shear strengths evaluated from triaxial tests, which generally give higher undrained shear strength values than conventional soil tests. The new shear strength distribution and the empirically evaluated parameters together with the parameters evaluated from lab tests are shown in Appendix 5:1-5:2.

A comparison between the results from a MC model with E_{50} evaluated using this correlation and one with E_u evaluated from triaxial tests might provide information about the necessity of triaxial tests and is therefore of interest. The resulting deformations in the SPW from the different calculations are shown in Figure 37.

[3] Thelander, Jonas; geotechnical engineer at Sweco, interview 2014-03-31.

[4] Johansson, Pia; geotechnical engineer at Sweco, interview 2014-03-31.

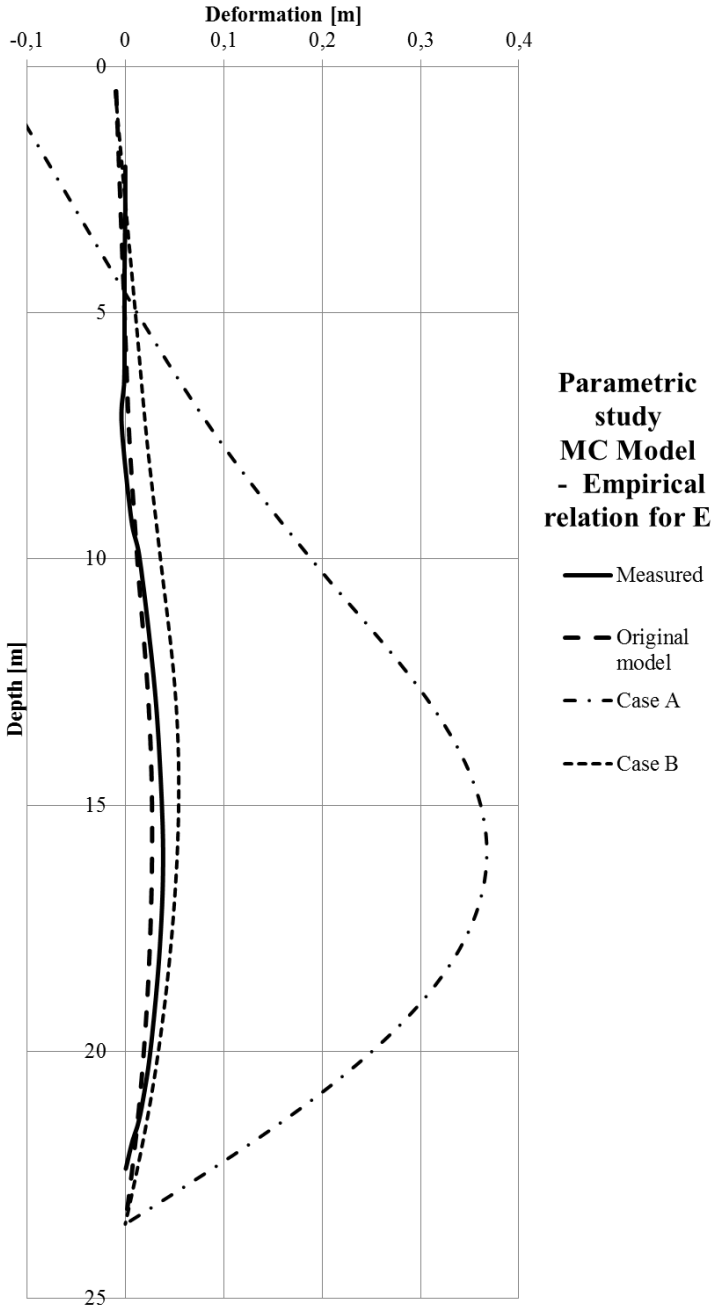

Figure 37 - Comparison of resulting deformations in SPW from calculations with varying E in the MC model and measured deformations.

This comparison shows that when using the empirical values, dividing the soil into two zones (case B), gives more accurate results than using the same distribution of undrained Young's modulus for the entire soil (case A). This indicates that using empirically evaluated stiffness parameters in the MC model might be a good option if no triaxial tests are performed.

5.2 φ'_{CV} AND C' IN PLAXIS HS

When evaluating drained strength parameters according to Swedish practice, φ'_{cv} is usually assumed to be 30°. This would when evaluating triaxial tests give a line which does not pass through the origin but instead intersect the q-axis; half the value at which it does so is called apparent cohesion, c'.

According to *TRV Geo* (Trafikverket, 2011, p. 44) c' can be estimated using either Equation (37), using a correlation to the undrained shear strength, or Equation (38), using a correlation to the preconsolidation pressure. Since *TRV Geo* (Trafikverket, 2011) is widely used as a reference in Sweden, it is of interest to compare the methods presented there to the method used in the original HS model.

$$c' = 0.1 * c_u \tag{37}$$

$$c' = 0.03 * \sigma'_c \tag{38}$$

The results from this comparison show that the calculations where φ'_{cv} is lowered to 30º give smaller deformations and that c' had an insignificant impact on the result. Therefore, another calculation is performed where φ'_{cv} is lowered to 25º and c' = 1 kPa, also shown in Figure 38. This further lowered the deformations obtained. A comparison between these calculations and the original model, with φ'_{cv} = 35º and c' = 1 kPa, see Figure 38.

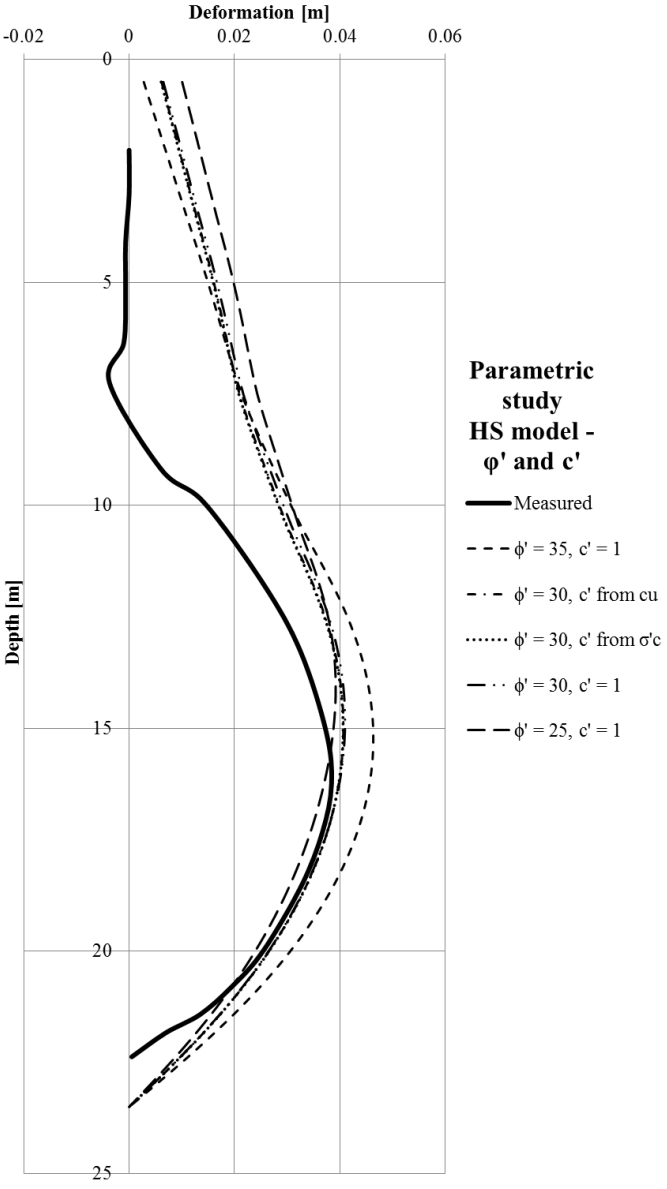

Figure 38 – Comparison of different input values for φ' and c'.

The explanation for smaller deformations when decreasing φ'_{cv} might be due to a number of things. One explanation can be found in Figure 39 and Figure 40, where the stress paths for two calculations at depth 11.57 m with different φ'_{cv} are plotted together with schematic yield and failure lines. It can be seen that the yield surfaces differ for different φ'_{cv} and that the stress paths thus are in different areas. A large part of the stress path for the original model is within the cap hardening zone, where the stiffness is based on E_{oed}. Since E_{oed} is generally lower than the other moduli, larger deformations are to be expected.

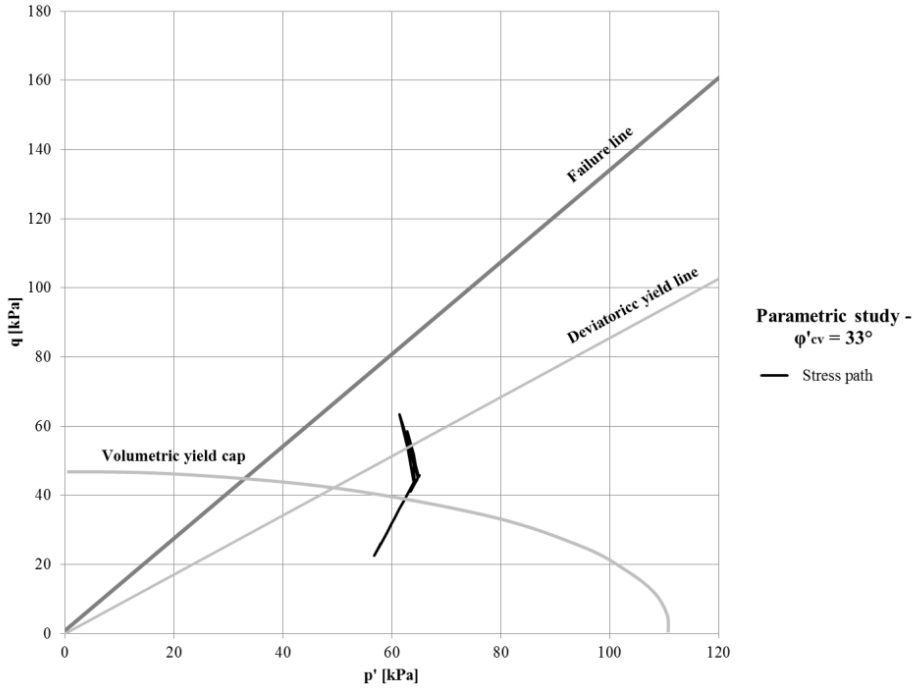

Figure 39 - Stress path for a point in the soil, 11.57 m deep behind the SPW, for a calculations with the original model.

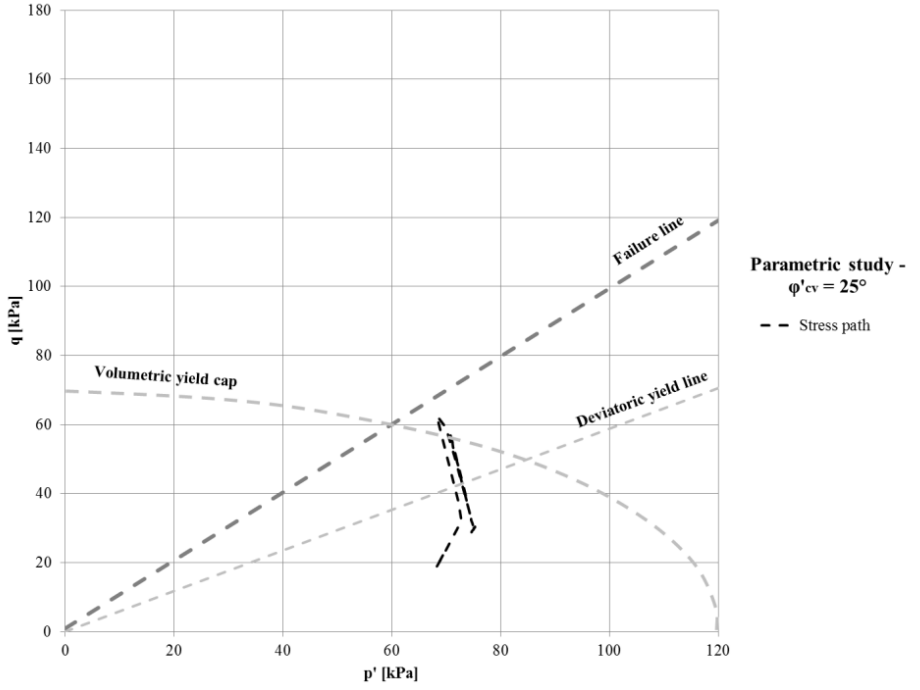

Figure 40 - Stress path for a point in the soil, 11.5 m deep behind the SPW, for a calculations with φ'_{cv} = 25°

Another reason might be that when lowering φ'_{cv}, $K_{0,nc}$ is increased which changes the initial conditions for the soil in the model. This leads to the stress state in the soil increasing which in turn leads to higher moduli, due to them being stress dependent. This change of initial conditions is also what causes the volumetric yield cap to start at different p'.

The stress paths both yield seemingly independent of both the volumetric yield cap and the deviatoric yield line. This is probably due to not being able to consider three-dimensional effects properly using these plots. This phenomenon and the variations in deformations are probably due to how the HS model functions.

5.3 INTERFACE IN PLAXIS HS

The interface value is not measured but instead taken from a table of suggested values (Karstunen, 2013b, p. 43) and it would therefore be interesting to see how the calculation results vary when changing this value. Calculations for interface values between 0.1 and 1 are thus carried out in the HS model. The resulting deformations in the SPW for the different calculations can be seen in Figure 41.

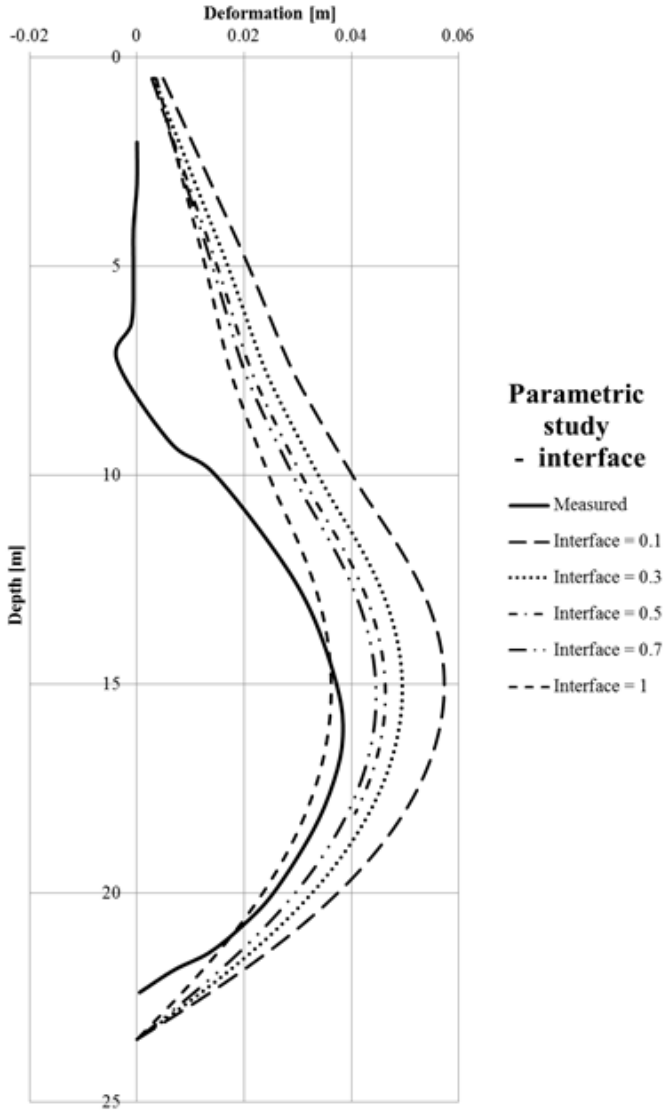

Figure 41 – Comparison of different values for the interface in the PLAXIS HS model.

This comparison shows that the input values for the interface has low impact on the resulting deformations; it only differs 5 mm between the calculations performed with interface value 0.3 and 0.7. When using the minimum and maximum values, 0.1 and 1, in the calculations the results differ more, approximately 20 mm, but such values are should be used with care. This suggests that when selecting interface values within the range 0.3-0.7, they have little impact on problems where small deformations occur and focus should not be on evaluating this parameter further for such cases.

This might be due to the fact that the SPW is anchored in bedrock, which prevents it from moving in the bottom. If this would not have been the case and the SPW would be able to fail through rotation, the interface value might have a greater influence.

5.4 INITIAL SHEAR MODULUS G_0 IN HSS

Since G_0 is based on empirical correlations, see section 2.6.2, it is of interest to see how much changing this parameter affects the results of the calculations. Two additional calculations are performed where G_0 is varied with 20 %, see Appendix 5:3. The resulting deformations in the SPW from these two calculations are then compared to the results of the original HSs model and the measured deformations.

The resulting deformations in the SPW from the different calculations are shown in Figure 42.

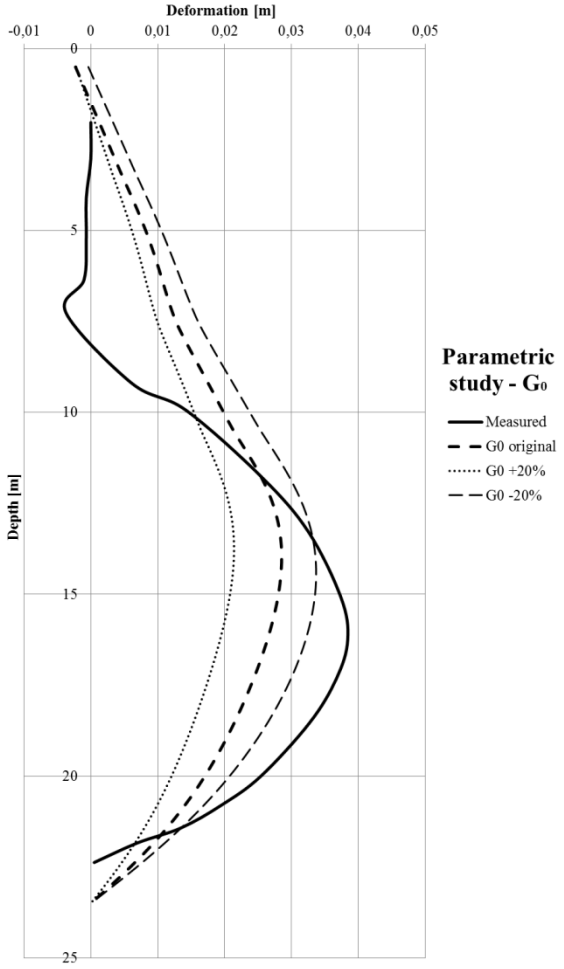

Figure 42 - Comparison of resulting deformations in SPW from calculations with varying G_0 and measured deformations.

These results show that increasing G_0 results in smaller deformations while increasing this parameter results in larger deformations. Since there are no obvious advantages to using the HSs model for this case compared to other models and since there is an uncertainty when selecting the parameter G_0, which affects the result, the HSs model should not be used without properly measuring G_0.

5.5 $\gamma_{0.7}$ IN HSs

Since there are different empirical correlations for $\gamma_{0.7}$ (Benz, 2007) it would be interesting to see how the values that these correlations give differ and how this difference affects the result in the HSs model. To calculate $\gamma_{0.7}$ in this parametric study Equation (39), which is based on a correlation to $G_0'^{ref}$, c', φ'_{cv} and K_0, is used instead of Equation (35).

$$\gamma_{0.7} = \frac{0.385}{4G_0'^{ref}}\left(2c'(1+\cos 2\varphi'_{cv}) + \sigma'_1(1+K_0)\sin 2\varphi'_{cv}\right) \tag{39}$$

The values evaluated using this correlation, $\gamma_{0.7,b}$, can be seen together with the ones described in section 2.6.2, $\gamma_{0.7,a}$, and their respective selected distributions in Appendix 5:4. The deformation in the SPW obtained from the calculations with varying $\gamma_{0.7}$ is presented in Figure 43.

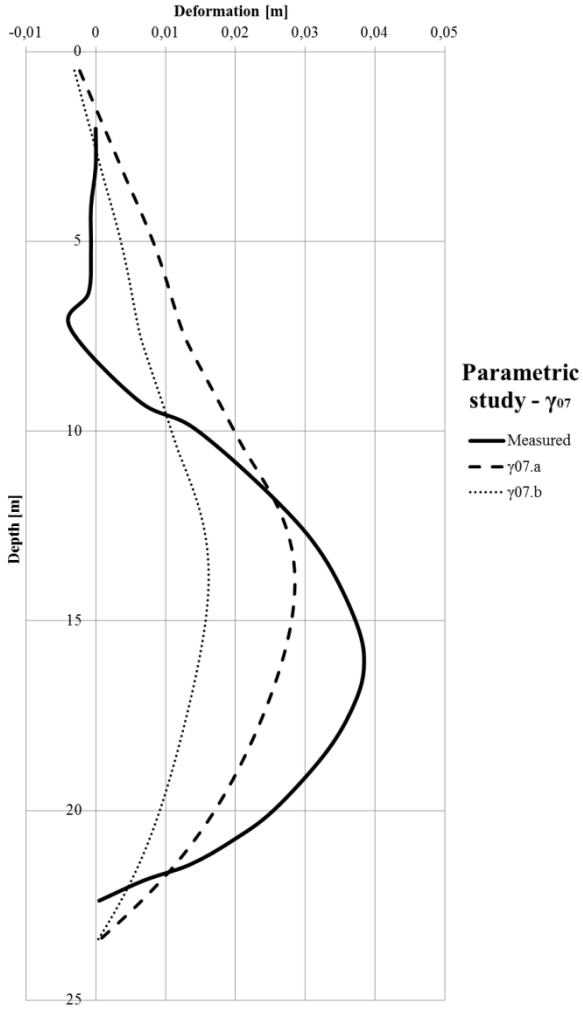

Figure 43 - Comparison of resulting deformations in SPW from calculations with varying $\gamma_{0.7}$ and measured deformations.

This comparison that there is quite the difference between the calculation with the original $\gamma_{0.7,a}$ and the calculation with $\gamma_{0.7,b}$, described above, which are both based on empirical correlations. This indicates the same thing as the results in section 5.4, i.e. that there is no advantage to using the HSs model compared to other constitutive models if the input parameters G_0 and $\gamma_{0.7}$ are not accurately measured.

6 GENERAL DISCUSSION

A general discussion about issues and discoveries encountered during the work with this master's project is found in this section. Some general sources of error are also discussed here, as well as some suggestions for further investigations. The specific discussions and analyses of the comparisons of the results and the parametric studies can be found in section 4 and 5.

6.1 TRIAXIAL TESTS

Something that was discovered during the work with this project is that there is a surprising lack of Swedish guidelines and standards on how to evaluate triaxial tests for clay soils. Most guides tend to focus on evaluation of s-t plots rather than p'-q plots, and it is usually recommended to evaluate φ' to 30° together with an apparent cohesion.

There also seems to be some differences between Swedish and international practice when it comes to notation. For example, in Swedish literature, compression and extension triaxial tests are commonly referred to as active and passive triaxial tests, probably due to the use of triaxial tests for evaluating shear strength in active and passive zones during slope stability analysis.

The Swedish standard practice of evaluating φ' to 30° together with the apparent cohesion in clays might be due to the geotechnical problems in Sweden consisting largely of infrastructure projects where embankments are common. Embankments increase the stresses in the soil and for such high stress intervals this Swedish method of evaluating effective shear strength parameters gives a good representation of the soil behaviour.

If, however, the case is a deep excavation with a SPW, such as in this thesis, these high stress increases do not occur. For such cases, evaluating the critical state friction angle gives a better representation of the soil since it includes these small stress intervals.

When creating soil models in GSS and PLAXIS, information about different soil stiffness parameters is necessary. These can be obtained from a triaxial test or from empirical correlations to undrained shear strength. Even though the triaxial test is more expensive than conventional soil tests, the information obtained can be used to either improve the accuracy of the created model or to create a more sophisticated model which would provide more accurate results. This could help avoid over-dimensioning e.g. a SPW and thus save money in the construction stage, which would justify use of the triaxial tests.

6.2 HAND CALCULATIONS

Hand calculations are often used as a first step in a SPW design to determine the installation depth, a first assumption of the properties of the SPW and the number of anchors needed. These first assumptions are then refined using more sophisticated calculation method.

However, since the SPW was already designed in this project, a back calculation was performed to check the accuracy of the different constitutive models used. The hand calculations gave very poor results when doing this, since there is no way of considering the prestressing of the anchors. Therefore no conclusions about the accuracy of the hand calculations can be drawn.

6.3 NOVAPOINT GS SUPPORTED EXCAVATION

When comparing the deformation figure obtained in GSS it is somewhat similar in shape to the measured one but it is inaccurate regarding the magnitude of the deformations. The anchor forces are close to the measured ones which is probably due to the high prestress levels. The same applies to the shear forces obtained in GSS; it is also probably due to the prestress. When comparing bending moment obtained GSS with the ones obtained from the other models it differs significantly, and this could be an explanation to the large difference in the deformations. The fact that modeling excavations behind the SPW as well as modeling local excavations within the shaft is not possible, might affect the accuracy of the calculations.

It is difficult to assess what makes the bending moment differ since the user manual for GSS seems incomplete, with poor descriptions of the input parameters needed for the different calculation models, in comparison to the quite detailed PLAXIS manuals. There were some instances where the only solution to determine which parameter to use was to ask the support staff at Novapoint. An upgrade of the user manual would make this software easier to understand and use in the future.

6.4 PLAXIS SOILTEST AND EVALUATED PARAMETERS

The stiffness parameters were changed when simulating tests in SoilTest in order to find an accurate match between the stress paths of the simulated tests and the real ones, and the results were still not ideal. However, it is most important to get a good match in the early stages of the test, before shear failure, since this is how the soil behaves when small deformations are occurring. The stress paths correspond fairly well to each other for the early stages of the tests but tend to differ further on.

When examining the ε_1-q plot, the simulated test and the real test also have a good compliance in the early stages of the test, when the strains are still small. During shear failure and after, the curves differ more from each other. This is due to the fact that the models used do not consider strain softening, which occurs in the triaxial tests on soft natural soils.

In PLAXIS there is a limit to how E'^{ref}_{oed} can vary with regards to E'^{ref}_{50} and K_0. Therefore, PLAXIS cannot handle E'^{ref}_{oed} which are as low as the ones evaluated from the CRS-tests, and they thus need to be increased. This is probably due to the fact that the models were not developed for Scandinavian soils. These parameters were adjusted using the suggestions from PLAXIS when trying to achieve the best possible stress path fit in SoilTest. It was not considered a problem to change this parameter since it is not very important when considering the small horizontal deformations that occur during deep excavations. However, such changes might produce unrealistic results when analysing subsidence behind the SPW.

The standard value used in PLAXIS for the reference pressure, p_{ref}, is 100 kPa. The depth at which such an in-situ horizontal effective pressure is reached is larger than the depth of the SPW studied in this project. Using p_{ref} = 50 kPa for the models in this project is considered more realistic.

6.5 MOHR-COULOMB AND HARDENING SOIL MODEL

The MC model might be easily perceived as a simpler model to use than other models since it needs fewer input parameters. This might be the case if a model is to be created without using triaxial tests, since there are fewer parameters to base on empirical correlations, and if done properly it produces fairly accurate results, see section 5.1.

The empirical correlations used in this thesis to estimate E_{50} differ in magnitude if the soil has high or low plasticity. This means that evaluation of stiffness in soils with plasticity close to the limits of high

or low plasticity give different values depending on which side of the limit it is on, making the evaluation quite arbitrary.

Another disadvantage of evaluating stiffness parameters using empirical correlations over triaxial tests is that the soil's behaviour in the model cannot be validated using SoilTest, since there are no triaxial tests to compare with. If triaxial tests are performed however, there are no benefits to using the MC model rather than the more sophisticated HS model.

6.6 HARDENING SOIL WITH SMALL STRAIN STIFFNESS MODEL

Regarding the HSs model it is very difficult to see any advantages of using it rather than the other models, since there were no in-situ measurements of G_0 and $\gamma_{0.7}$ performed during this project. Using a model with an increased level of sophistication only improves the result if the input data is evaluated properly.

6.7 PARAMETRIC STUDIES

The parametric studies were only performed for the PLAXIS models since the results from these models were the most accurate. Another reason for this was to increase the knowledge of how PLAXIS functions in general, but also about how the different constitutive models function.

6.8 FURTHER INVESTIGATIONS

It is difficult to say how general the results and conclusions drawn from this study are, since only one area with a SPW has been studied. It would have been interesting to study another SPW with similar measurements and see how the models behaved in comparison to that, and if the conclusions are valid for other cases as well.

Comparing hand calculations according to *Sponthandboken* to the other methods analysed is difficult since it is supposed to be used in the design process and not for back calculations. It is therefore difficult to draw any conclusions about the accuracy of this method when used to design a SPW. A comparison between different design methods could be performed to better assess the quality of this calculation method.

7 CONCLUSIONS

The preferred method to use in the design process is the Hardening Soil constitutive model in PLAXIS. This model produces accurate results for horizontal deformations in the sheet pile wall and anchor forces when compared to in-situ measurements performed on a real sheet pile wall.

It is also possible to calibrate the input parameters for the Hardening Soil model by comparing simulated triaxial tests in SoilTest with results from real triaxial tests, and thus check that the soil behaviour is realistic. When calibrating the parameters like this it is important to validate that the strain interval for which they were calibrated is not exceeded in the calculations, since this would give an incorrect representation of the soil.

The accuracy of the Hardening Soil with small strain stiffness model is difficult to assess since no in-situ measurements of the small strain stiffness were available. There are some uncertainties when using empirical correlations for the small strain stiffness parameters, and therefore this model should not be used without accurately measuring these parameters.

If no triaxial tests are available, the Mohr-Coulomb constitutive model in PLAXIS is the preferred alternative. This is due to the model producing fairly accurate results when using empirical correlations for evaluating stiffness parameters instead of evaluating these from triaxial tests. However, validation of the model by comparing the behaviour of the soil in the model to true soil behaviour is not possible. There are no advantages to using a more sophisticated model when basing the stiffnesses on empirical correlations since it only increases the level of uncertainty in the model.

REFERENCES

ArcelorMittal, n.d. *Profile: AZ 36.* [Online]
Available at:
https://www.arcelormittal.com/projects/europe/foundationsolutions/EN/sheet_piling/AZ_sections/AZ36.htm
[Accessed 02 04 2014].

Benz, T., 2007. *Small-Strain Stiffness of Soils and its Numerical Consequences.* Stuttgart: Institut für Geotechnik der Universität Stuttgart.

Breymann, H. & Schweiger, H. F., 2005. *Chapter 123. FE-analysis of five deep excavations in lacustrine clay and comparison with in-situ measurements.* Amsterdam, Taylor & Francis.

Brinkgreve, R., Engin, E. & Swolfs, W., 2012a. *PLAXIS 2D 2012l - General Information.* Delft, Netherlands: Plaxis bv.

Brinkgreve, R., Engin, E. & Swolfs, W., 2012b. *PLAXIS 2D 2012 Materials Manual.* Delft, Netherlands: Plaxis bv.

Brinkgreve, R., Engin, E. & Swolfs, W., 2012c. *PLAXIS 2D 2012 Reference Manual.* Delft: Plaxis bv.

Craig, R. F. & Knappett, J. A., 2012. *Craig's Soil Mechanics.* Eight Edition ed. Abingdon: Spon Press.

Jaky, J., 1944. The coefficient of earth pressure at rest. *Journal of the Society of Hungarian Architects and Engineers,* 78(22), pp. 355-358.

Karstunen, M., 2013a. *Lecture 7: Soil modelling in the course BMT041 Infrastructure Geo-engineering.* Gothenburg: Chalmers University of Technology.

Karstunen, M., 2013b. *Lecture 8: Earth retaining structures in the course BMT041 Infrastructure Geo-engineering.* Gothenburg: Chalmers University of Technology.

Kempfert, H.-G. & Gebreselassie, B., 2006. *Excavations and Foundations in Soft Soils.* Berlin: Springer-Verlag.

Kullingsjö, A., 2007. *Effects of deep excavations in soft clay on the immediate surroundings.* Diss. Göteborg: Chalmers University of Technology.

Larsson, R., 2008. *Jords egenskaper,* Linköping: Swedish geotechnical institute.

Larsson, R. & Mulabdic', M., 1991. *Shear moduli in Scandinavian clays.* Linköping: Swedish Geotechnical Institute.

Muir Wood, D., 1990. *Soil behaviour and critical state mechanics.* Cambridge: Cambridge University Press.

Powrie, W. & Simpson, B., 2001. *Embedded retaining walls: theory, practise and understanding.* Istanbul, 15th International Conference on Soil Mechanics and Geotechnical Engineering.

Ryner, A., Fredriksson, A. & Stille, H., 1996. *Sponthandboken.* Stockholm: Byggforskningsrådet.

Schweiger, H., 2000. Ergebnisse des Berechnungsbeispieles Nr. 3 “3 - fach verankerte Baugrube": Gegenüberstellung der eingesandten Berechnungsergebnisse. i: *Verformungsprognose für tiefe Baugruben: AK 1.6 “Numerik in der Geotechnik“.* u.o.:u.n., pp. 7-67.

Schweiger, H. F., 2009. Influence of constitutive model and EC7 design approach in FE analysis of deep excavations. *Proceeding of ISSMGE International Seminar on Deep Excavations and Retaining Structures, Budapest,* pp. 99-114.

SGF, 2012. *Triaxialförsök - En vägledning,* Linköping: SGF - Svenska Geotekniska Föreningen.

Sällfors, G. & Andreasson, L., 1985. *Kompressionsegenskaper - Geotekniska laboratorieanvisningar, del 10.* Stockholm: Statens råd för byggnadsforskning.

Sällfors, G. & Atkins, J., 1991. Experimental determination of soil properties. *Proceedings of the 10th European Conference on Soil Mechanics and Foundation Engineering,* Volume 3, pp. 915-954.

Trafikverket, 2011. *TRV Geo, Trafikverkets tekniska krav för geokonstruktioner.* u.o.:Trafikverket.

Vianova GeoSuite AB, 2010. *GS Supported Excavation Help,* Solna: Vianova GeoSuite AB.

VISS, 2014. *Vattenkartan.* [Online]
Available at: http://www.viss.lansstyrelsen.se/MapPage.aspx
[Accessed 12 03 2014].

Appendix 1:1

Compilation of soil parameters

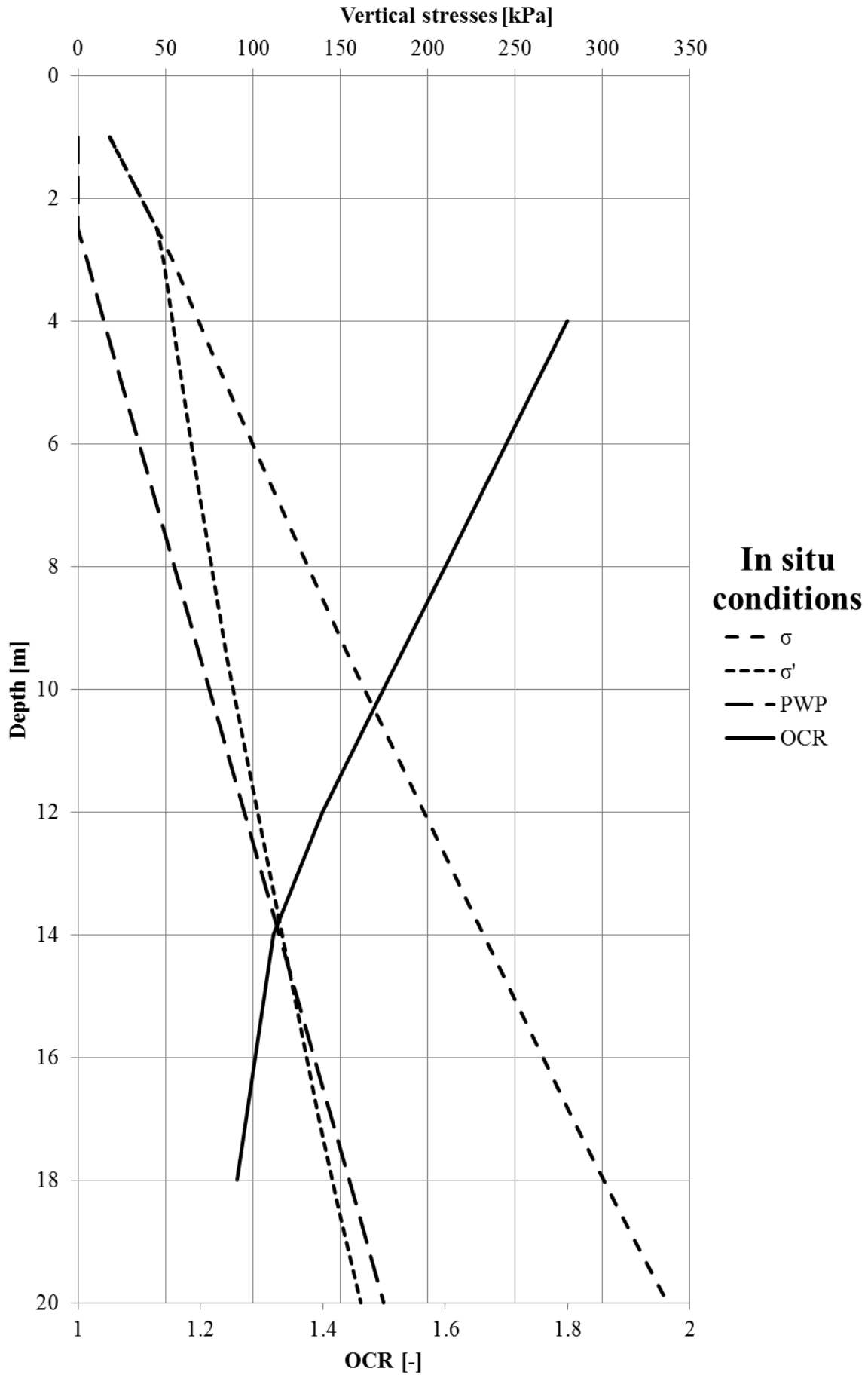

Appendix 1:2

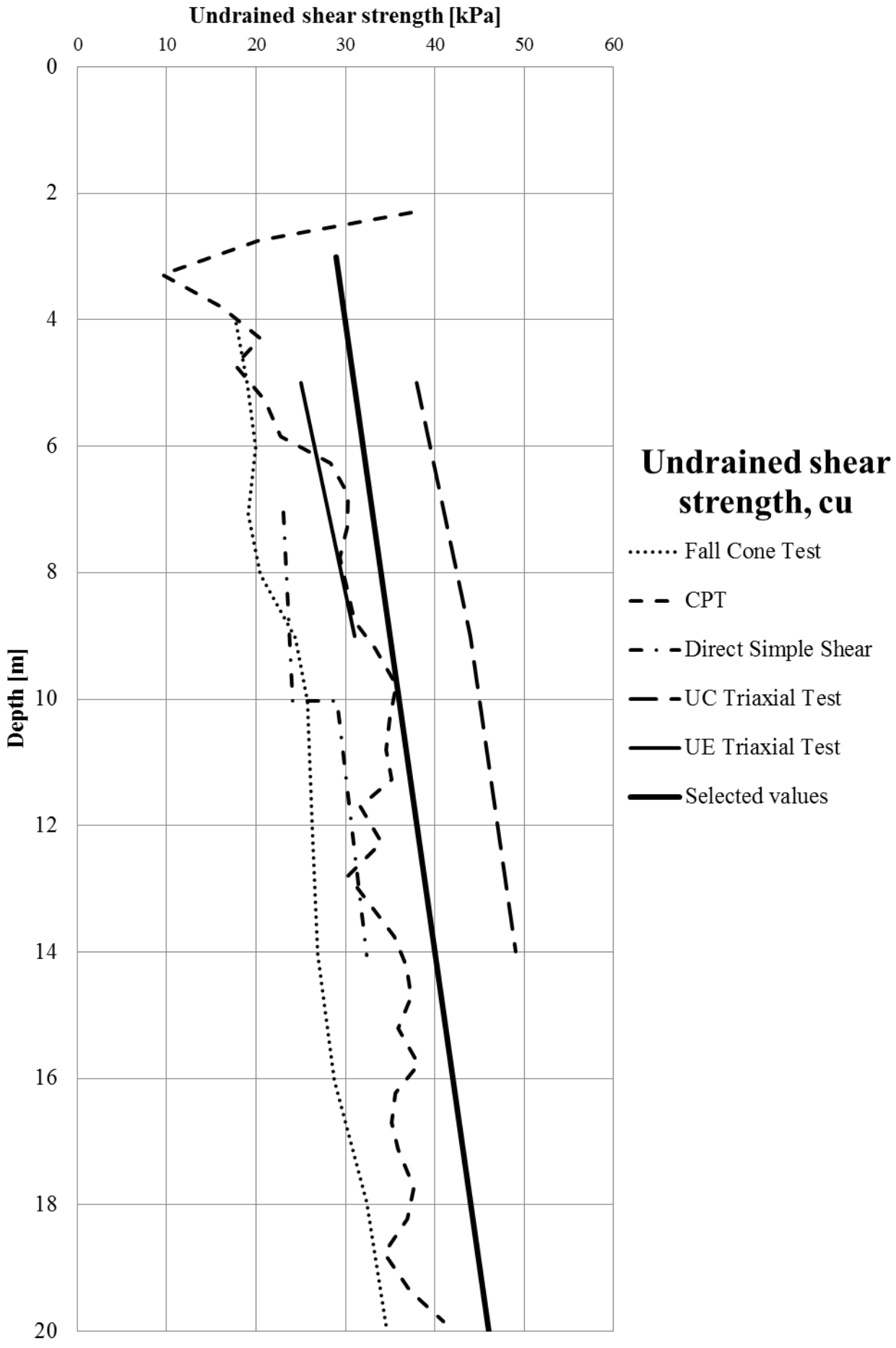
Undrained shear strength [kPa]
0
10
20
30
40
50
60
Depth [m]
0
2
4
6
8
10
12
14
16
18
20
Undrained shear strength, cu
Fall Cone Test
CPT
Direct Simple Shear
UC Triaxial Test
UE Triaxial Test
Selected values

Appendix 1:3

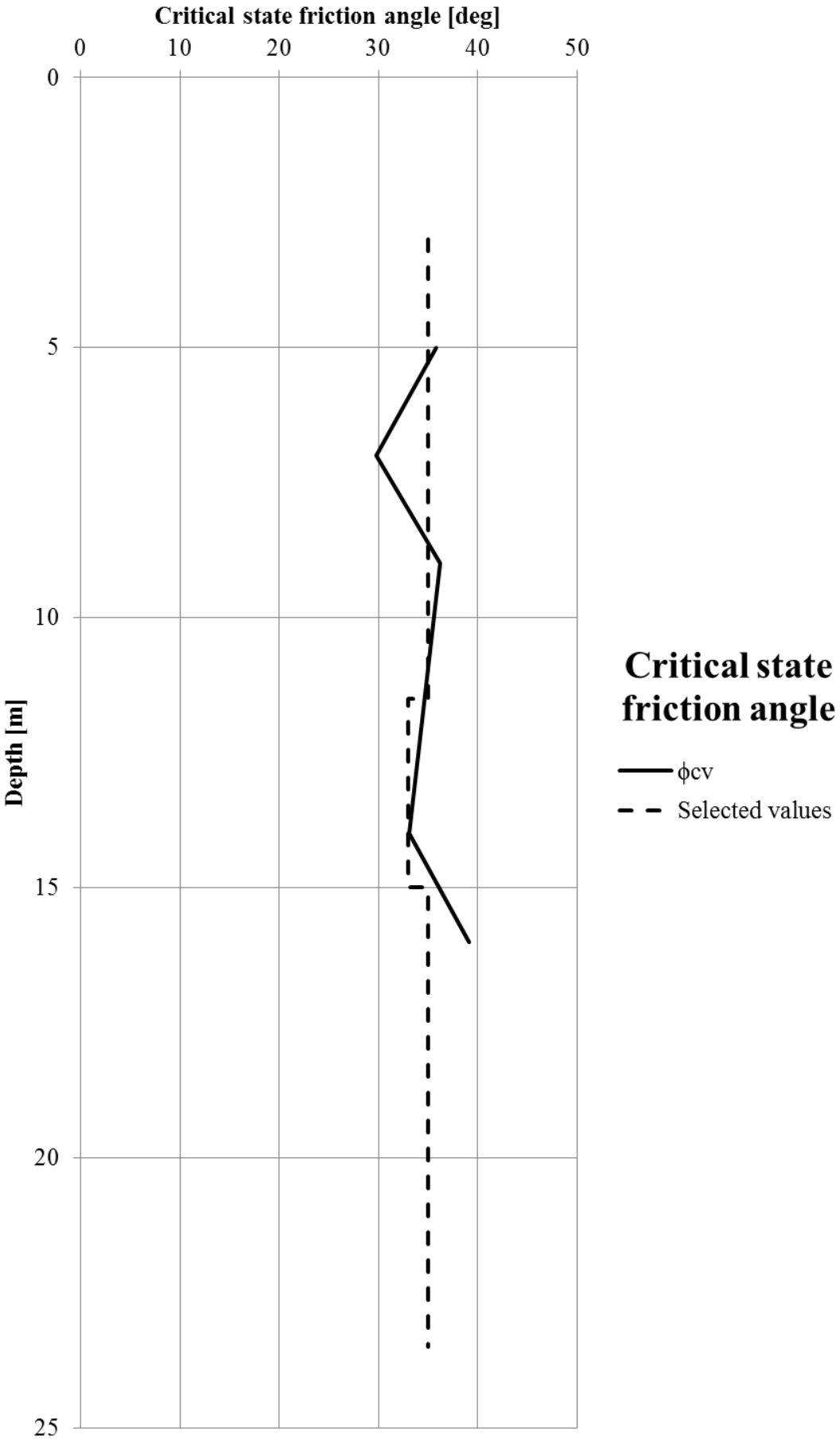
Critical state friction angle [deg]
0
10
20
30
40
50
0
5
10
15
20
25
Depth [m]
Critical state friction angle
ϕcv
Selected values

Appendix 1:4

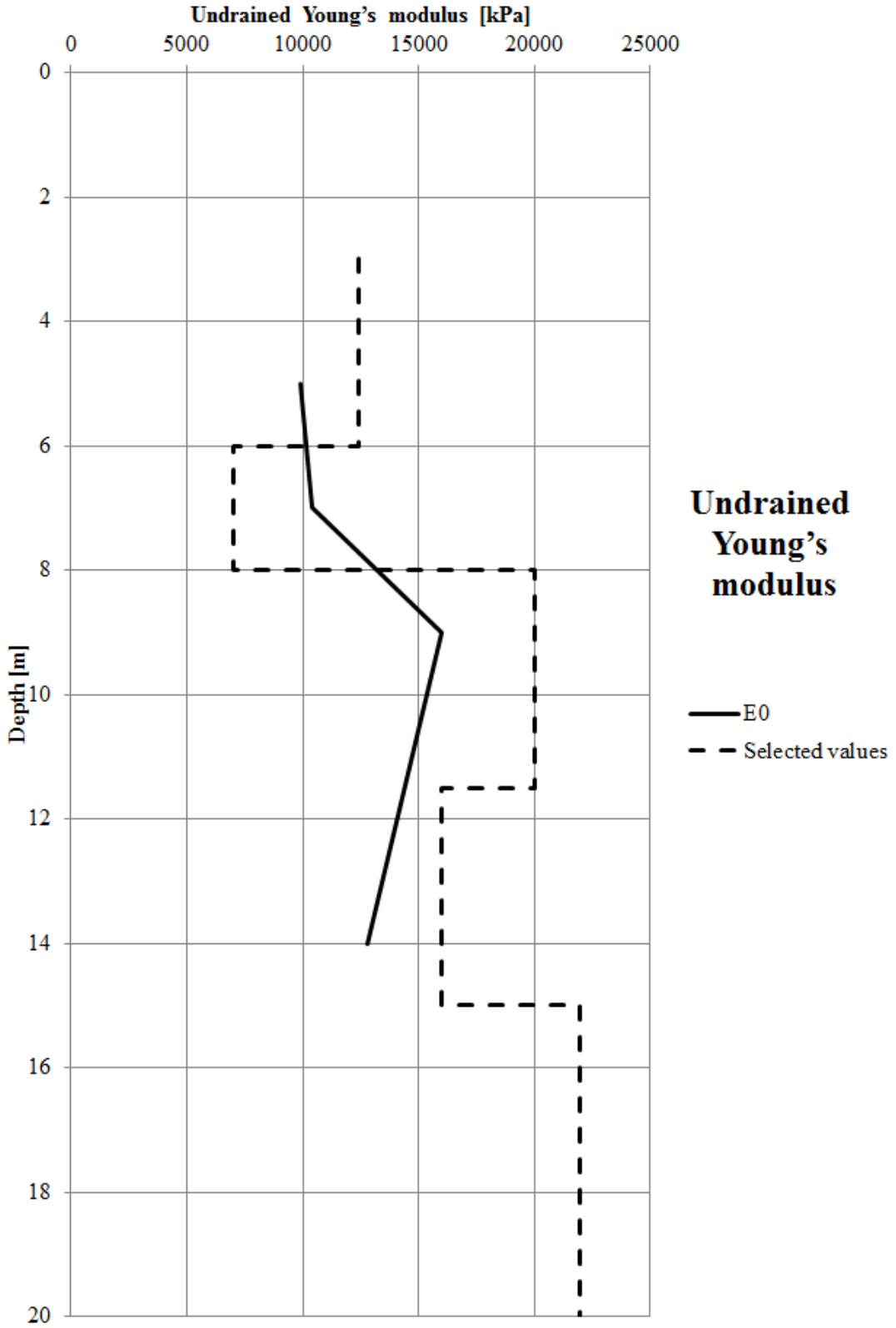
Undrained Young's modulus [kPa]
0
5000
10000
15000
20000
25000
Depth [m]
0
2
4
6
8
10
12
14
16
18
20
Undrained Young's modulus
E0
Selected values

Appendix 1:5

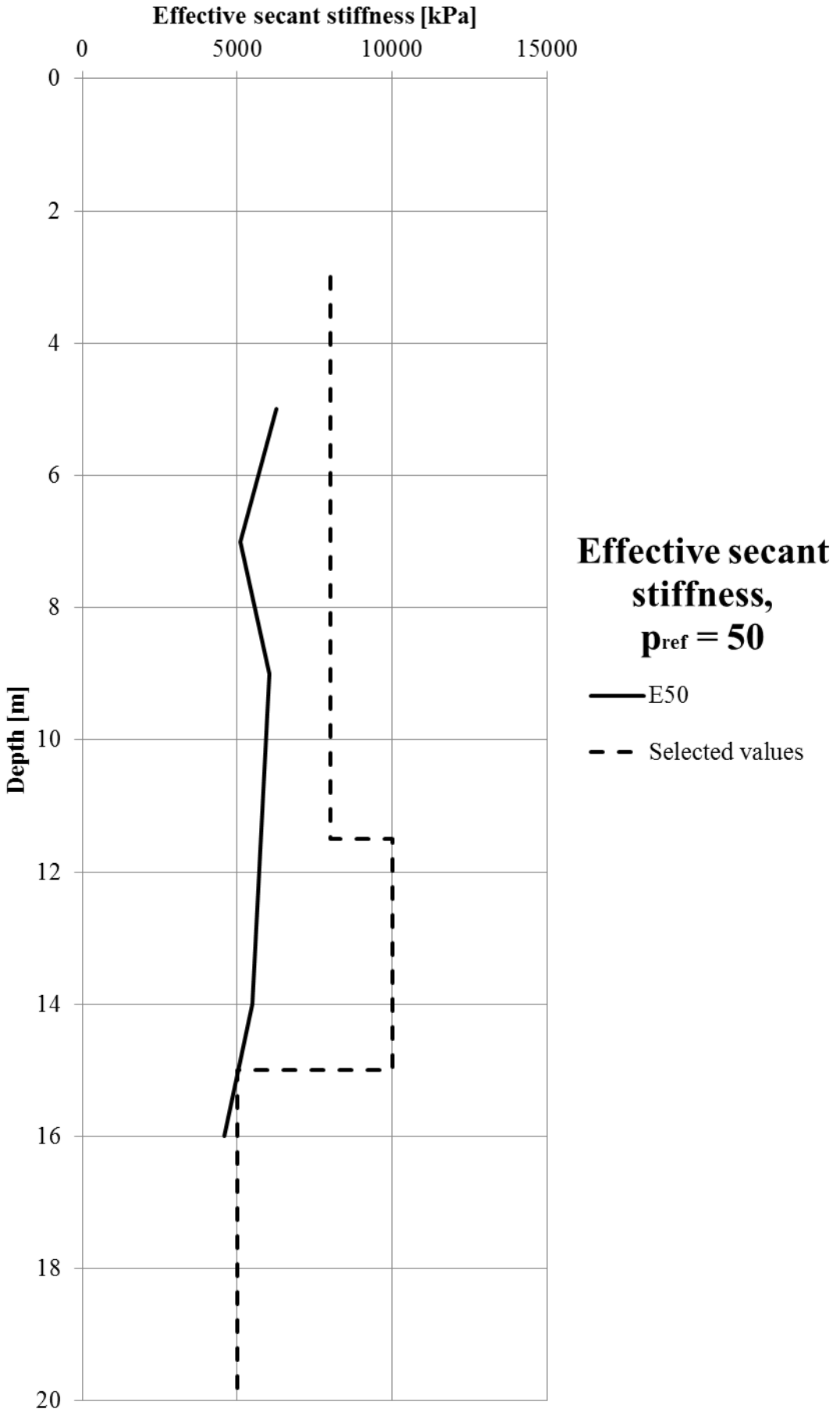
Effective secant stiffness [kPa]
0
5000
10000
15000
Depth [m]
0
2
4
6
8
10
12
14
16
18
20
Effective secant stiffness, pref = 50
E50
Selected values

Appendix 1:6

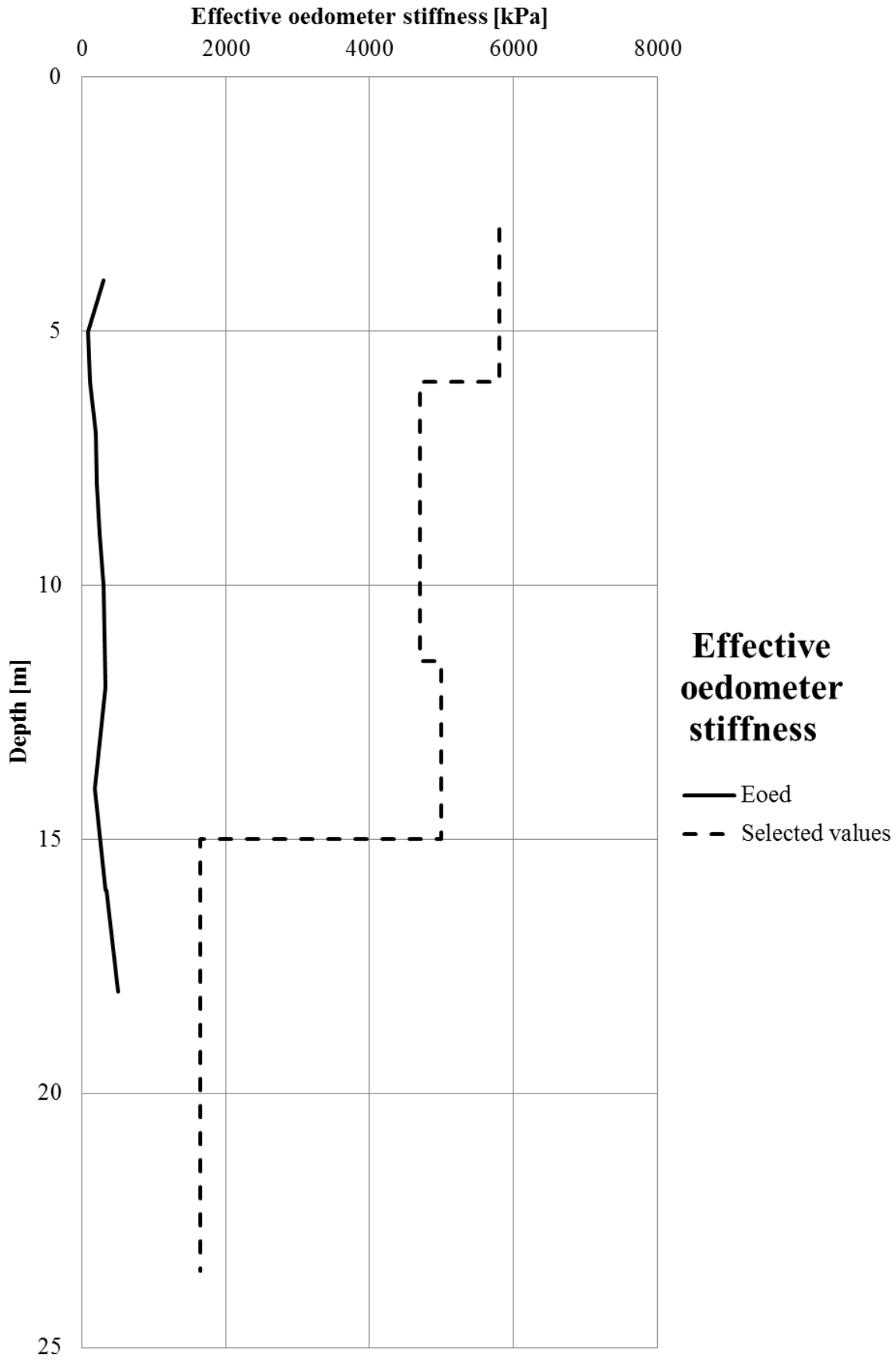
Effective oedometer stiffness [kPa]
0
2000
4000
6000
8000
0
5
10
15
20
25
Depth [m]
Effective oedometer stiffness
Eoed
Selected values

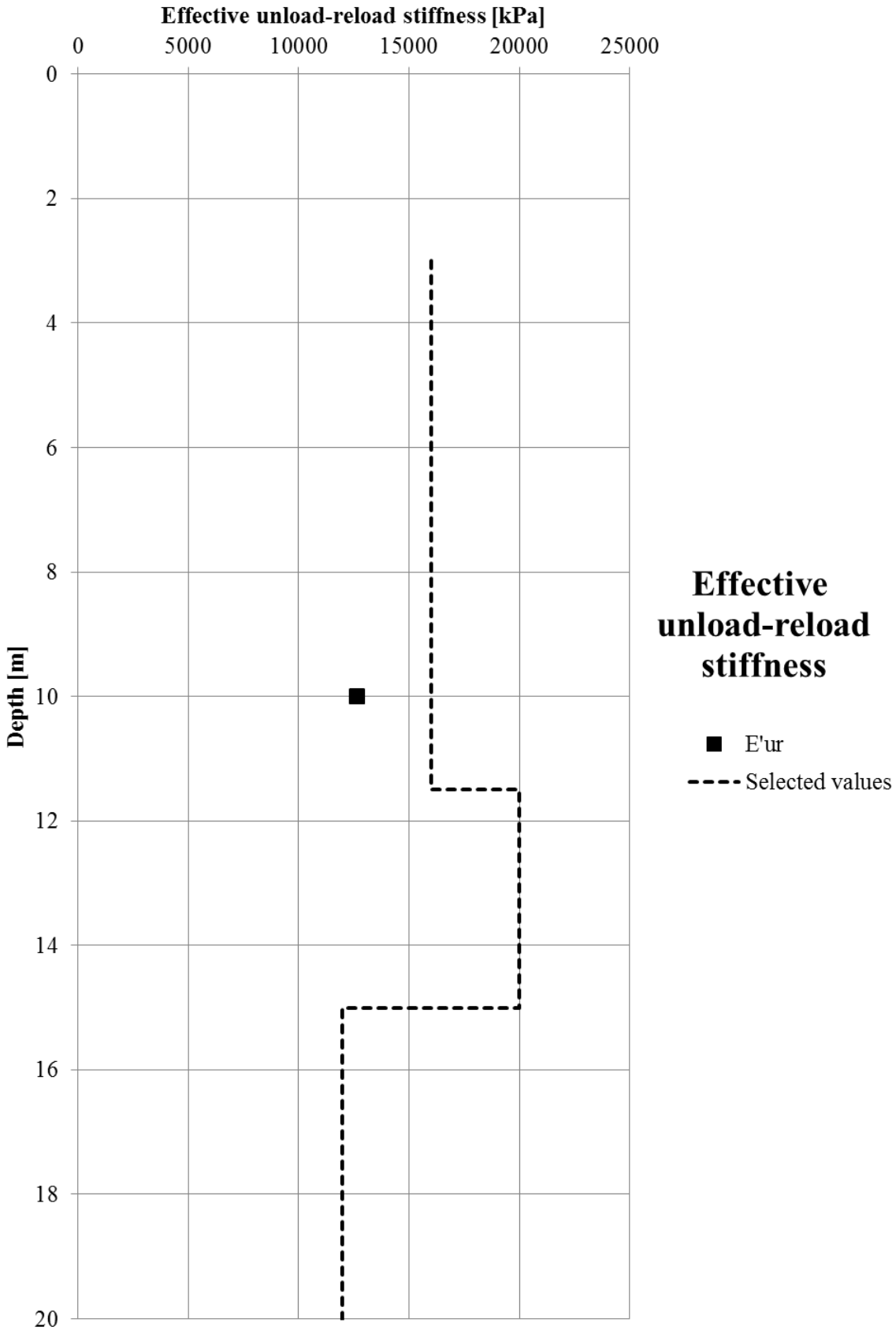
Effective unload-reload stiffness [kPa]
0
5000
10000
15000
20000
25000
Depth [m]
0
2
4
6
8
10
12
14
16
18
20
Effective unload-reload stiffness
E'ur
Selected values

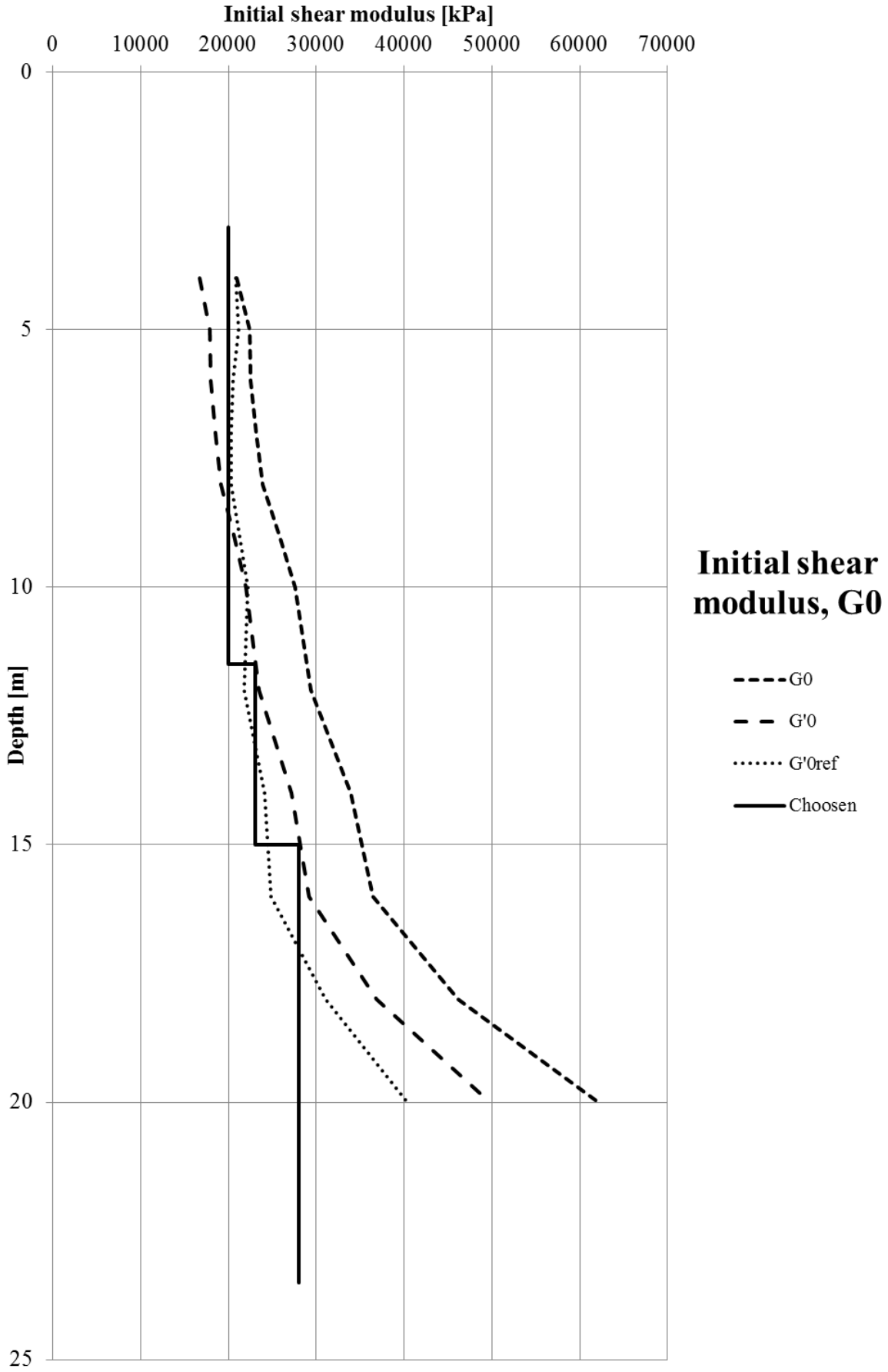
Initial shear modulus [kPa]
0
10000
20000
30000
40000
50000
60000
70000
Depth [m]
0
5
10
15
20
25
Initial shear modulus, G0
G0
G'0
G'0ref
Choosen

Appendix 1:9

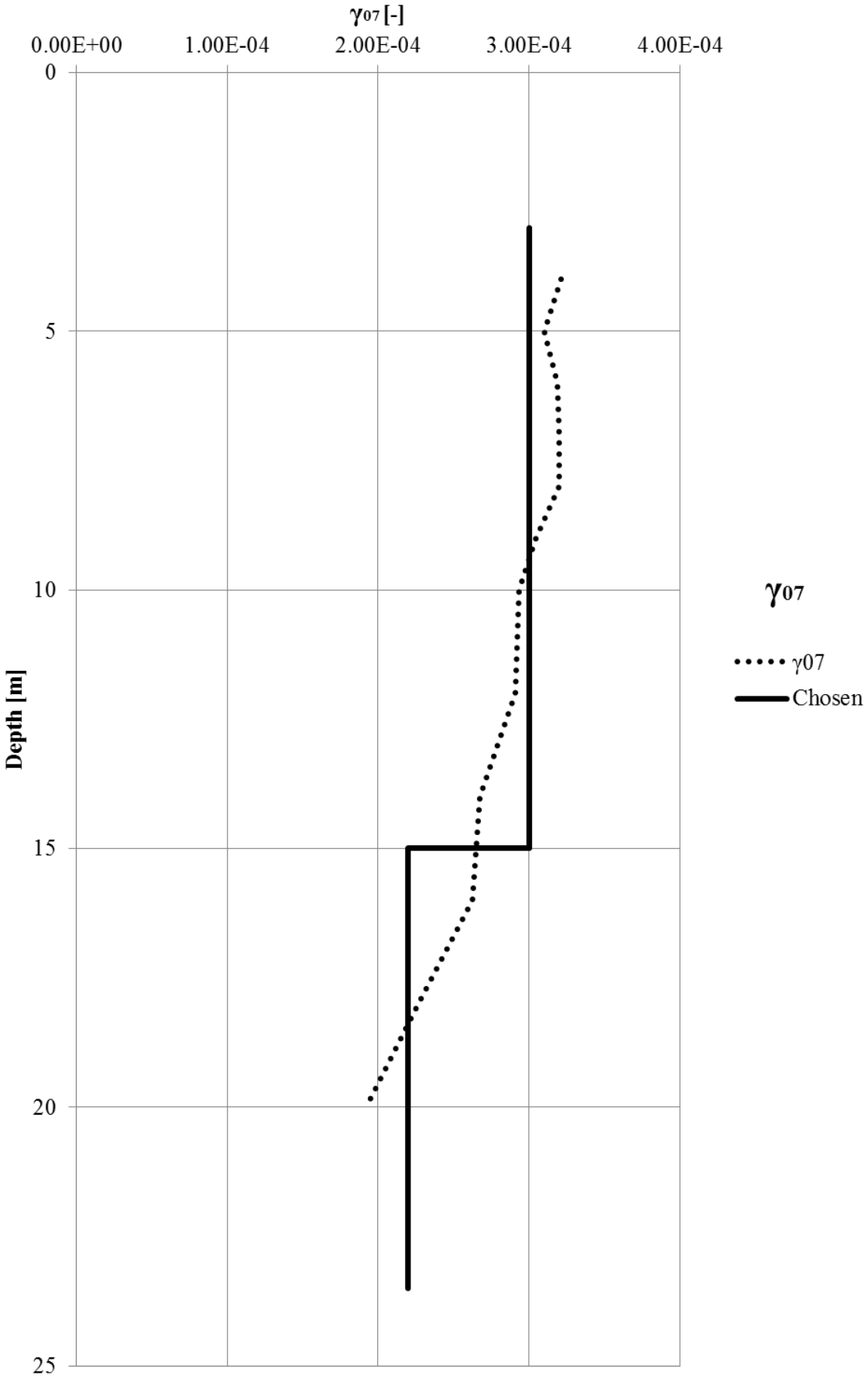
γ07 [-]
0.00E+00
1.00E-04
2.00E-04
3.00E-04
4.00E-04
0
5
10
15
20
25
Depth [m]
γ07
γ07
Chosen

Appendix 2:1

Comparison between PLAXIS SoilTest and a real triaxial test at 5 meter depth.

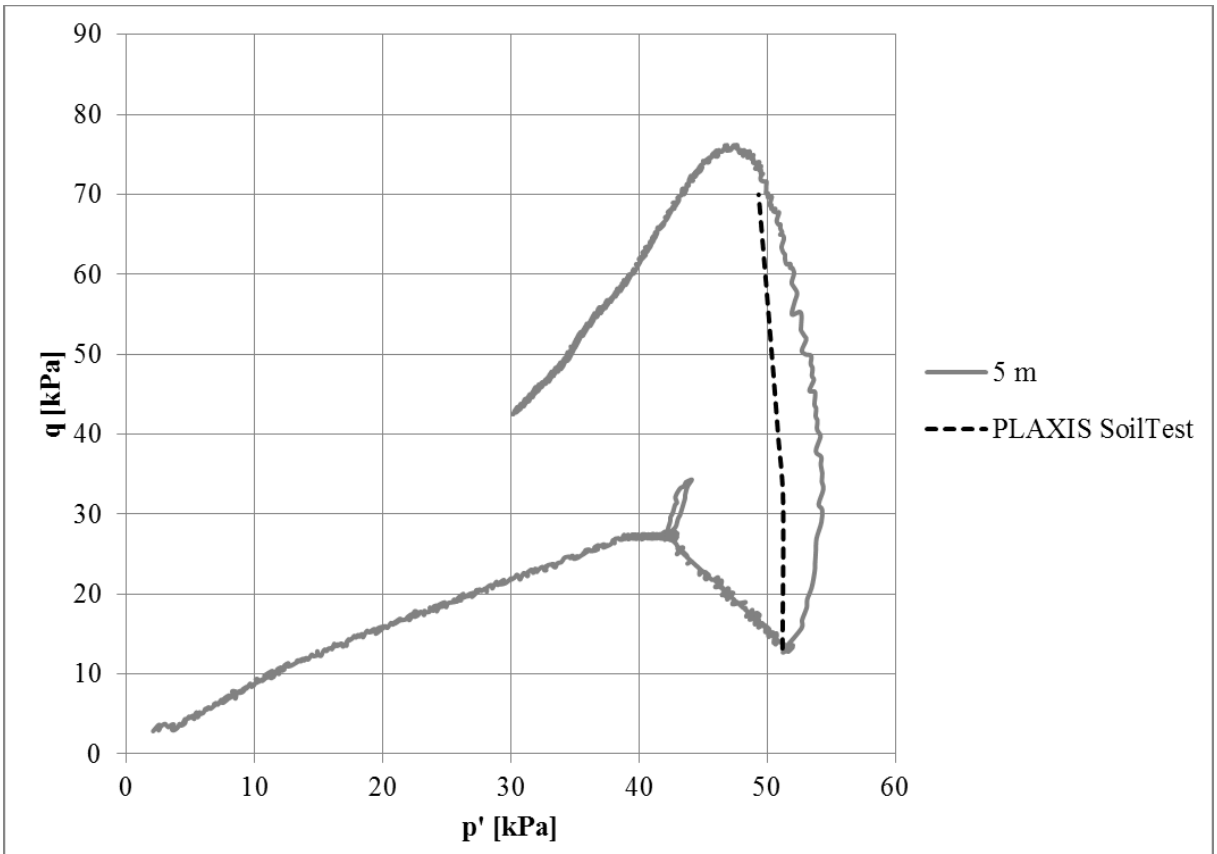

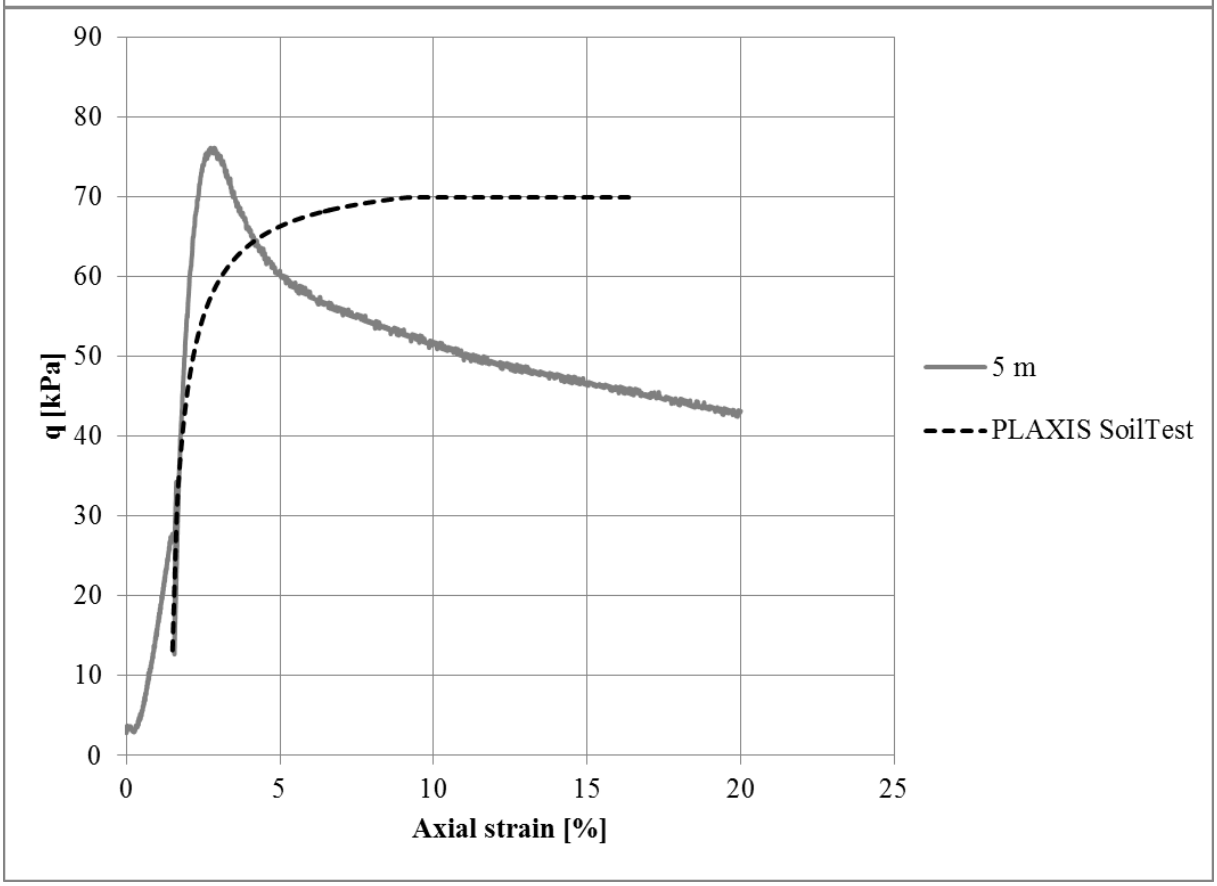

Appendix 2:2

Comparison between PLAXIS SoilTest and a real triaxial test at 7 meter depth.

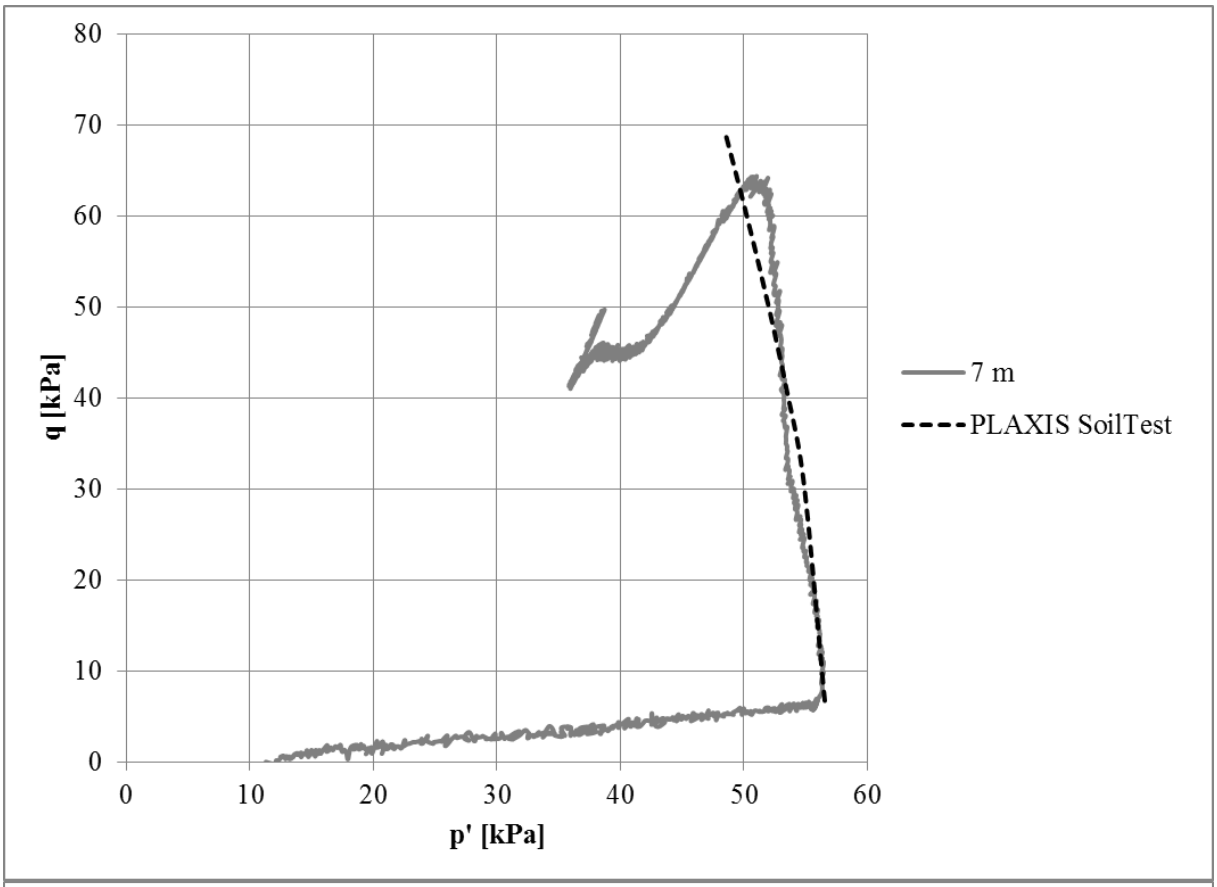

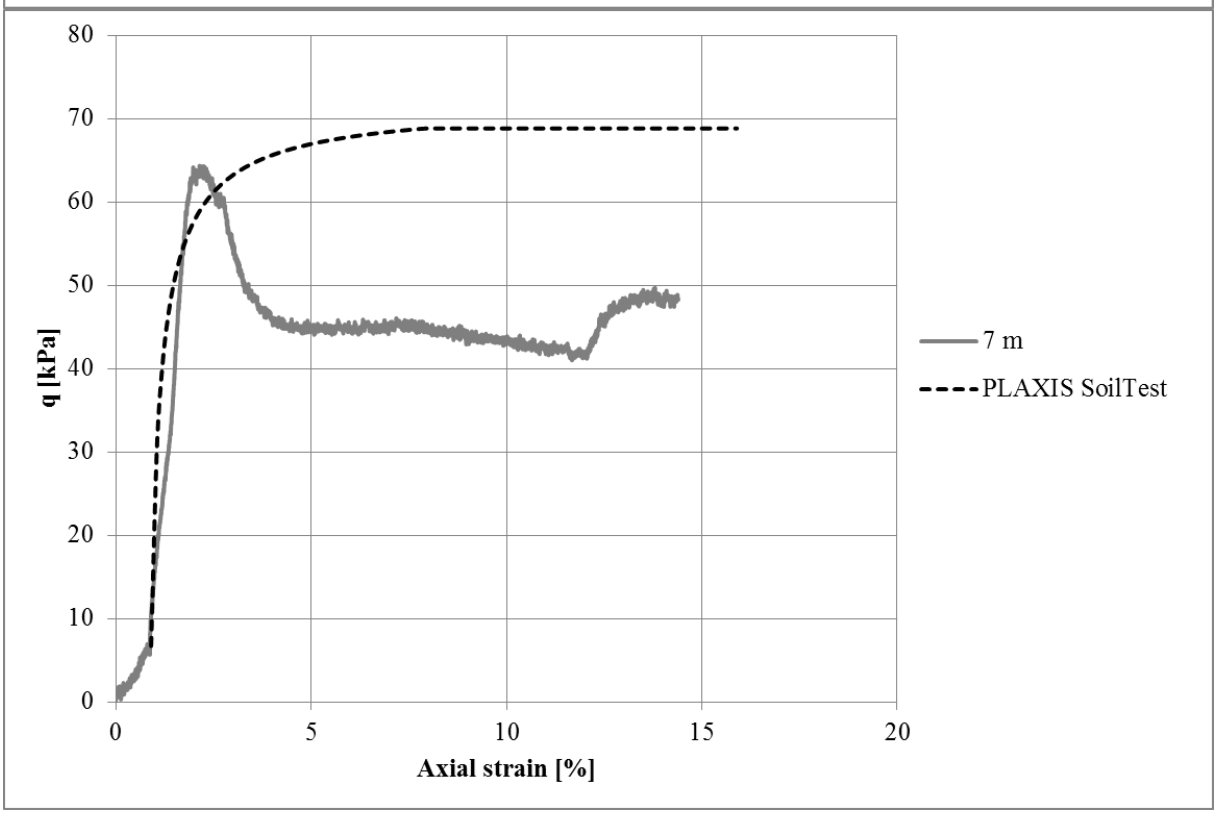

Appendix 2:3

Comparison between PLAXIS SoilTest and a real triaxial test at 9 meter depth.

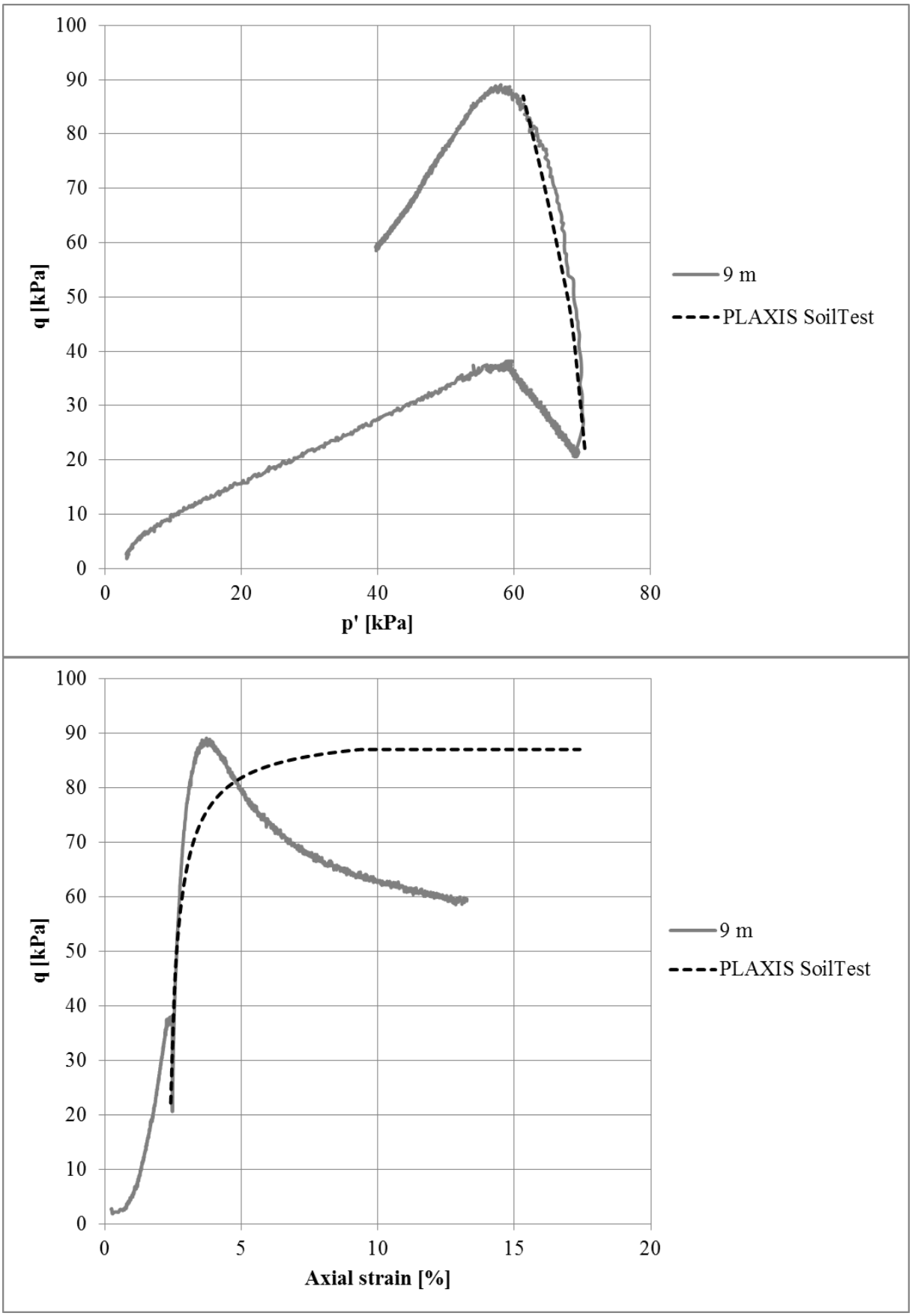

Appendix 2:4

Comparison between PLAXIS SoilTest and a real triaxial test at 14 meter depth.

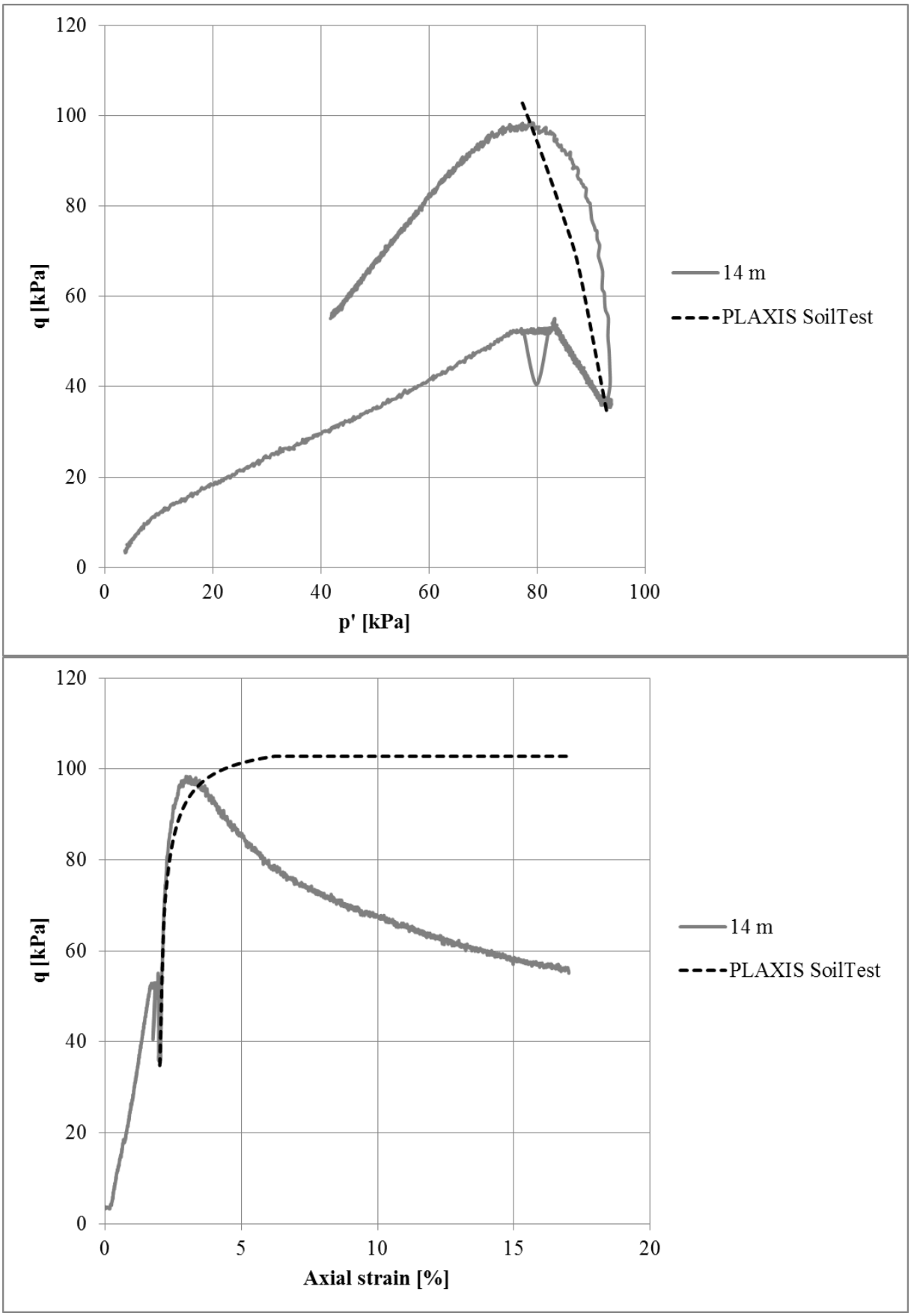

Appendix 2:5

Comparison between PLAXIS SoilTest and a real triaxial test at 16 meter depth.

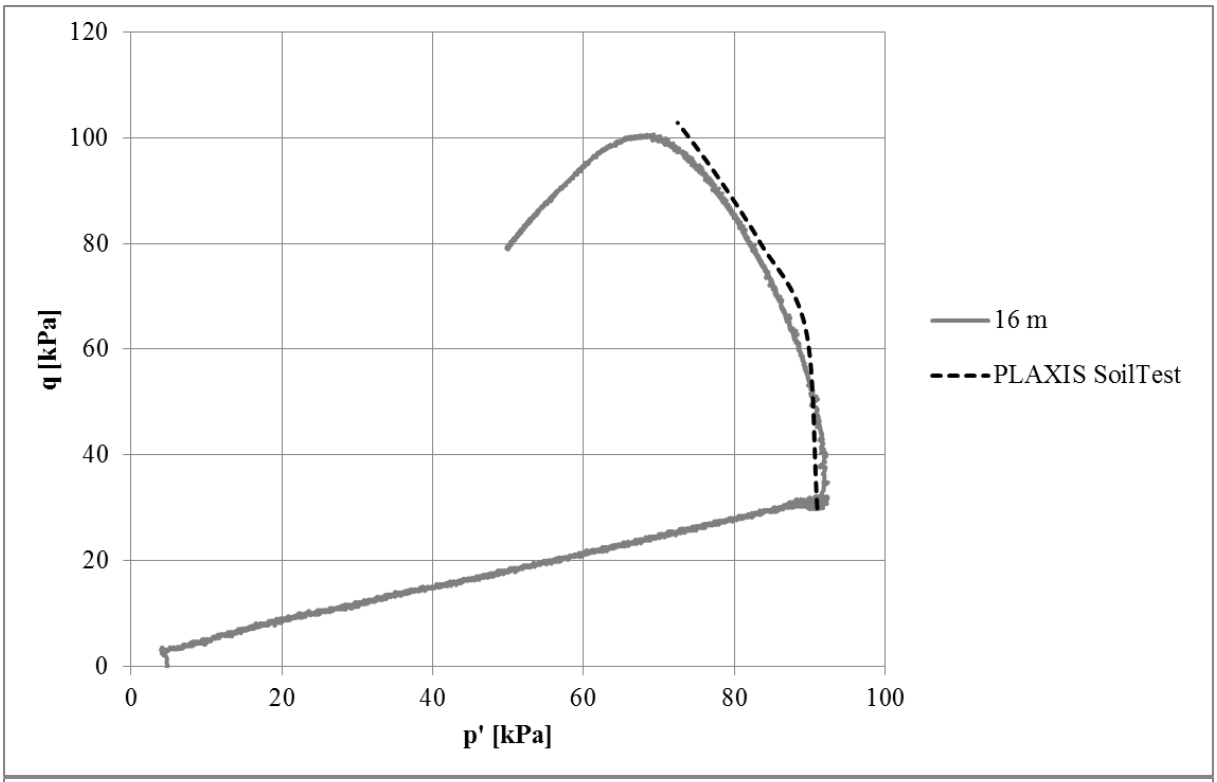

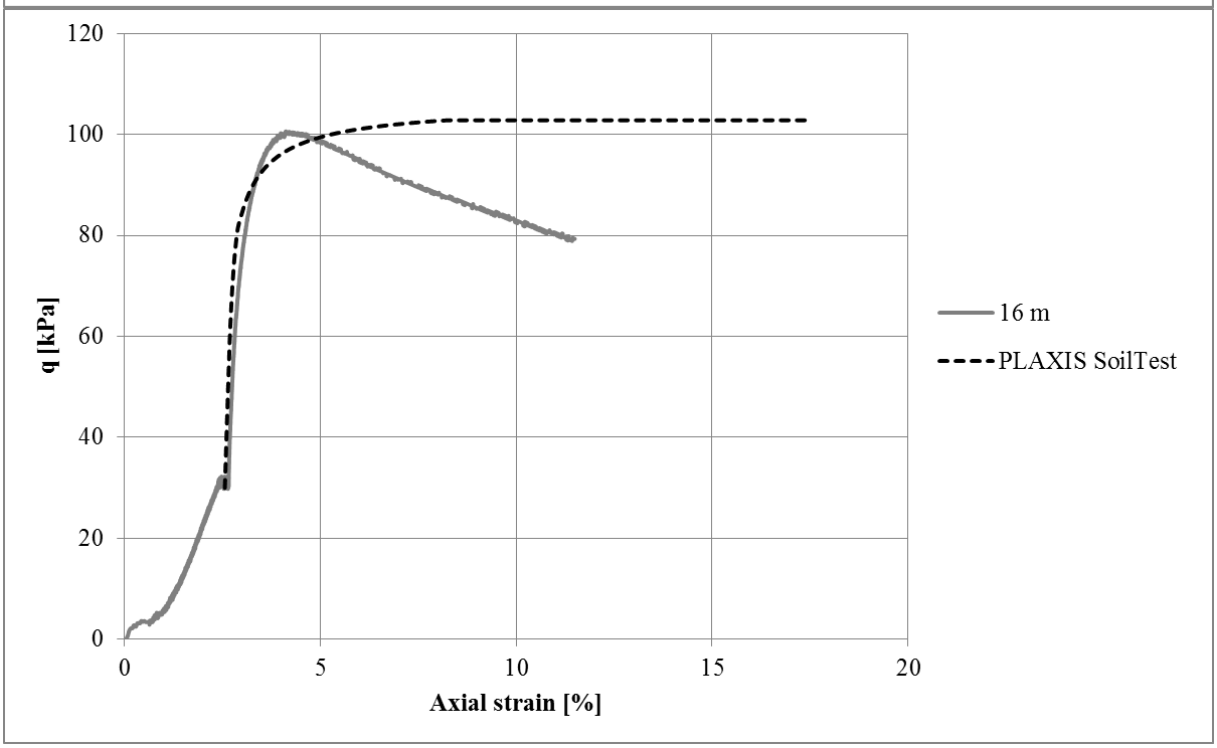

Appendix 3:1

- Blueprints from Götatunneln

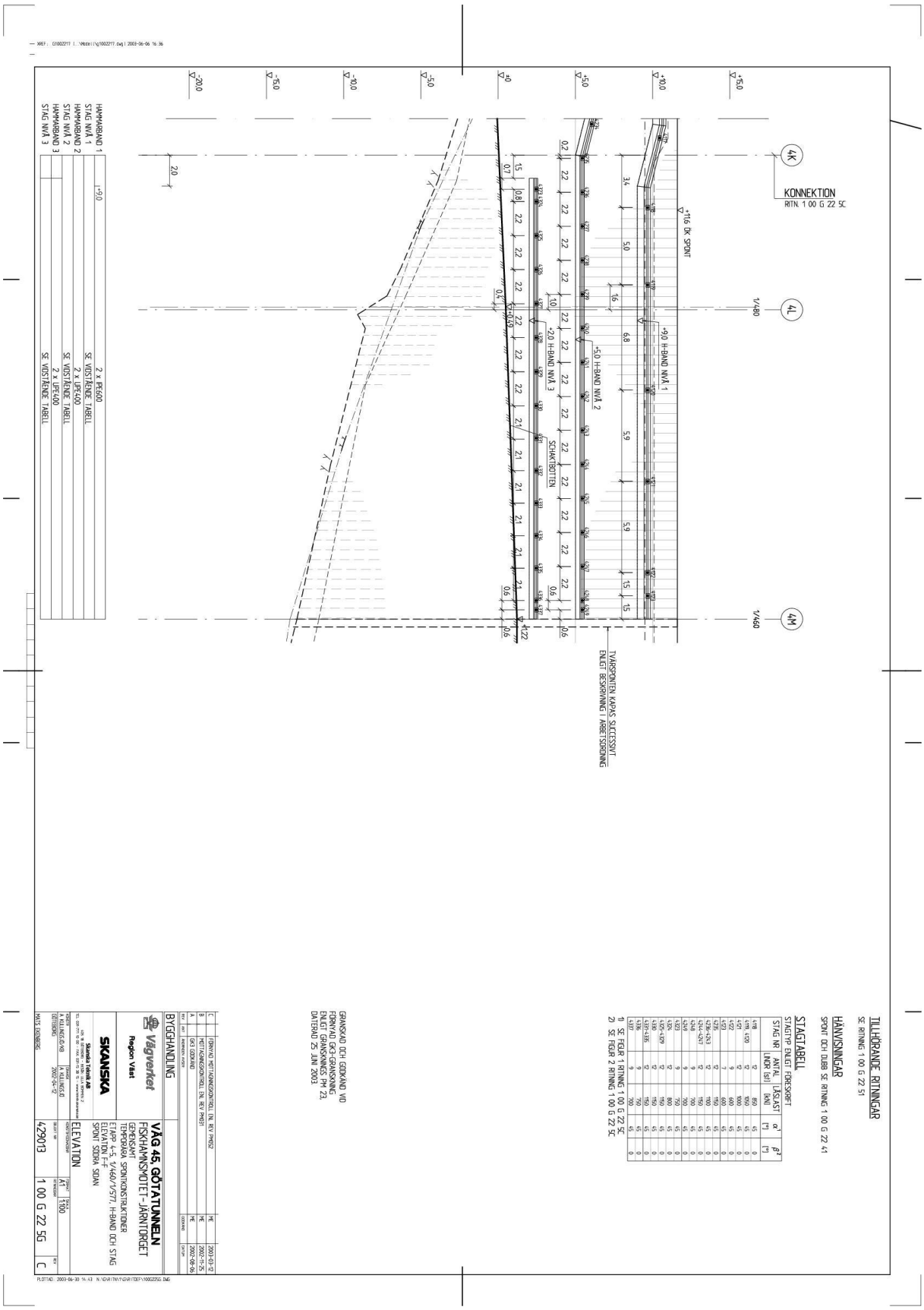

Appendix 3:2

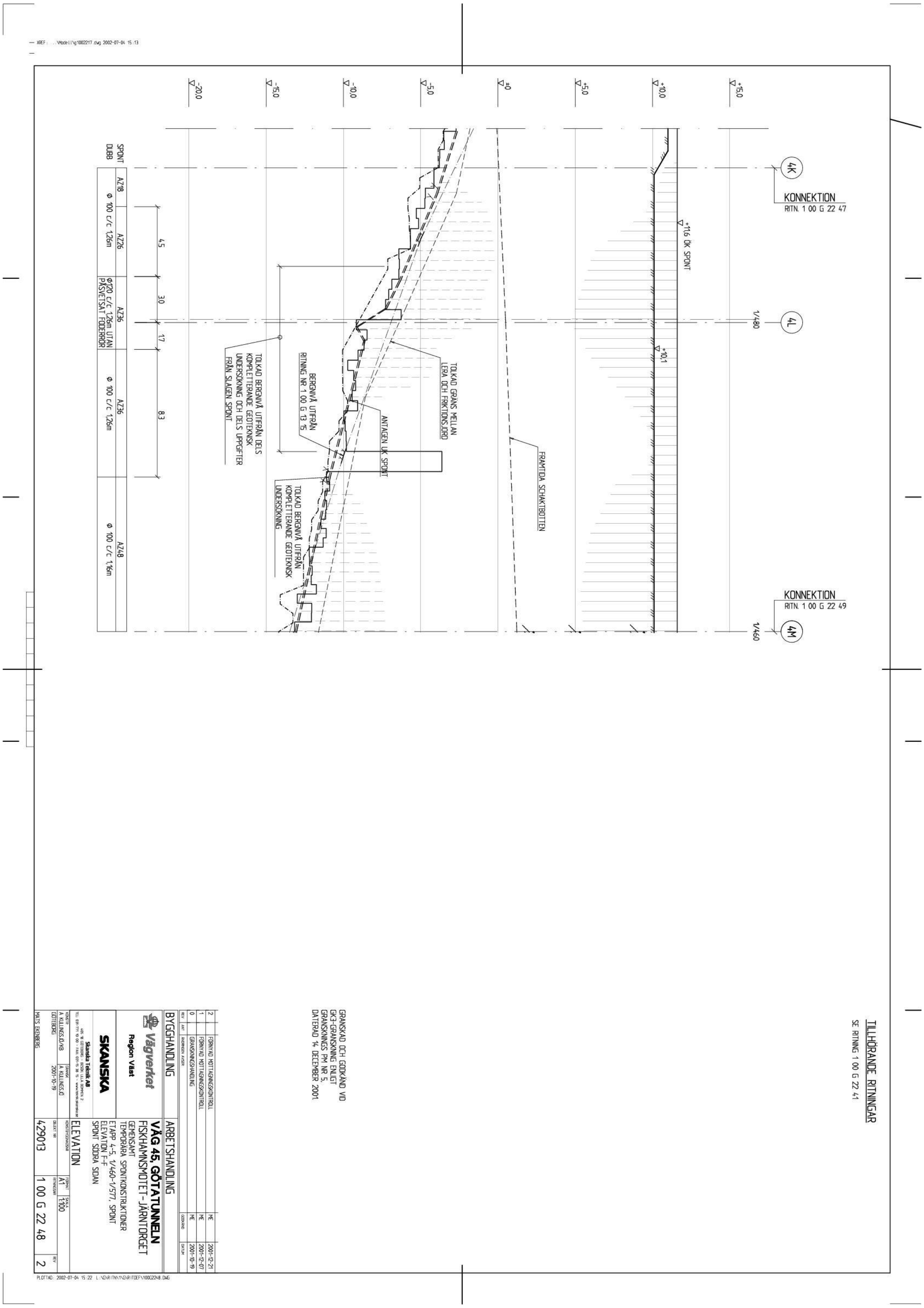

KONNEKTION
RITN. 1 00 G 22 47
KONNEKTION
RITN. 1 00 G 22 49
+11,6 ÖK SPONT
+10,1
FRAMTIDA SCHAKTBOTTEN
TOLKAD GRÄNS MELLAN LERA OCH FRIKTIONSJORD
ANTAGEN UK SPONT
BERGNIVÅ UTIFRÅN RITNING NR 1 00 G 13 15
TOLKAD BERGNIVÅ UTIFRÅN DELS KOMPLETTERANDE GEOTEKNISK UNDERSÖKNING OCH DELS UPPGIFTER FRÅN SLAGEN SPONT
TOLKAD BERGNIVÅ UTIFRÅN KOMPLETTERANDE GEOTEKNISK UNDERSÖKNING
SPONT
DUBB
AZ18
AZ26
AZ36
AZ36
AZ48
Φ 100 c/c 1,26m
Φ120 c/c 1,26m UTAN PÅSVETSAT FODERRÖR
Φ 100 c/c 1,26m
Φ 100 c/c 1,16m
4,5
3,0
1,7
8,3
TILLHÖRANDE RITNINGAR
SE RITNING 1 00 G 22 41
GRANSKAD OCH GODKÄND VID GK3-GRANSKNING ENLIGT GRANSKNINGS PM NR 5, DATERAD 14 DECEMBER 2001
2 FÖRNYAD MOTTAGNINGSKONTROLL ME 2001-12-21
1 FÖRNYAD MOTTAGNINGSKONTROLL ME 2001-12-07
0 GRANSKNINGSHANDLING ME 2001-10-19
BYGGHANDLING
ARBETSHANDLING
Vägverket Region Väst
SKANSKA
Skanska Teknik AB
VÄG 45, GÖTATUNNELN
FISKHAMNSMOTET-JÄRNTORGET
GEMENSAMT
TEMPORÄRA SPONTKONSTRUKTIONER
ETAPP 4-5, 1/460-1/577, SPONT
ELEVATION F-F
SPONT SÖDRA SIDAN
ELEVATION
A KULLINGSJÖ/KB
A KULLINGSJÖ
GÖTEBORG 2001-10-19
MATS EKENBERG
A1 1:100
429013
1 00 G 22 48
2
PLOTTAD: 2002-07-04 15:22 L:\G\RITN\1\G\RITDEF\100G2248.DWG

FÖRESKRIFTER

DIMENSIONERANDE LASTER
TRAFIKLAST: TRAFIKLAST, INOM YTOR FÖR ALLMÄN TRAFIK, ENLIGT VÄG 94.
UTBREDD LAST: INOM ÖVRIGA YTOR UTANFÖR SPONT GÄLLER MAX 5 kN/m2, DÄR EJ ANNAT ANGES.

VATTENTRYCK:
SPONTEN ÄR UNDER NEDSCHAKTNINGSSKEDEN DIMENSIONERAD FÖR ETT VATTENTRYCK MOTSVARANDE NIVÅ FÖR MEDELVATTEN (MW), +10,1 SÅVÄL I FYLLNINGEN SOM I FRIKTIONSJORDEN OVAN BERG.

FÖR SKEDEN EFTER DET ATT GROVBETONGEN ÄR FRAMGJUTEN MOT SPONTEN ÄR DIMENSIONERINGEN UTFÖRD MED ETT VATTENTRYCK MOTSVARANDE NIVÅ FÖR HÖGSTA HÖGVATTEN (HHW), +11,6 I DEN ÖVRE FYLLNINGEN.

SPONTERNA I ROSENLUNDSKANALEN ÄR DIMENSIONERADE FÖR HÖGSTA HÖGVATTEN MED UNDANTAG FÖR ARBETSMOMENT A6-A11, B2-B9, C3-C9, D2-D9, F11-F15, I2-I7 OCH J13. UNDER DESSA ARBETSMOMENT ÄR SPONTERNA I KANALEN DIMENSIONERADE FÖR MEDELVATTEN. ARBETSMOMENTEN FRAMGÅR PÅ RITNING 1 00 G 22 53.

LEDNINGAR OCH ANDRA HINDER I MARK
FÖRE SPONTSLAGNING SKALL EVENTUELLA LEDNINGAR LOKALISERAS OCH OM SÅ ERFORDRAS UTFÖRS ERFORDERLIGA SKYDDSÅTGÄRDER.

FÖRE SPONTSLAGNING SKALL EVENTUELLA HINDER I MARK SÅSOM PÅLAR, KAJKONSTRUKTIONER ETC LOKALISERAS OCH OM SÅ ERFORDRAS UTFÖRS ERFORDERLIGA ÅTGÄRDER.

SPONT, AVSER TVÄRSPONT VID 1/530 OCH INRE SPONTER
SPONT: SPONTPROFIL ENLIGT ELEVATIONS-RITNINGAR ELLER LIKVÄRDIG.

STÅLKVALITET: EN 10 248 S355GP

SPONT SOM SKARVAS SKALL STUMSVETSAS.
SPONT SLÅS I LÅS.
ÖK SPONT ENLIGT ELEVATIONSRITNINGAR.

SPONT SLÅS TILL NIVÅ ANGIVEN PÅ ELEVATIONS-RITNINGAR. INOM DE PARTIER DÄR SPONTENS UNDERKANT SAMMANFALLER MED BERGETS NIVÅ SKALL SPONT STOPPSLÅS MOT BERG.

FÖRSES SPONT MED EXTRA FODERRÖR FÖR INJEKTERINGSARBETE ANSVARAR ENTREPRENÖREN FÖR. ATT PLACERING OCH INFÄSTNING SKER I SAMRÅD MED ANSVARIG GEOKONSTRUKTÖR.

SLAGEN SPONTLÄNGD SKALL MÄTAS IN OCH INRAPPORTERAS TILL ANSVARIG GEOKONSTRUKTÖR. KLARTECKEN / ANVISNINGAR SKALL ERHÅLLAS FRÅN ANSVARIG GEOKONSTRUKTÖR INNAN SCHAKT FRAMFÖR SPONT FÅR PÅBÖRJAS.

I SAMBAND MED NEDSCHAKTNING SKALL KONTROLL AV SPONTENS TÄTHET UTFÖRAS. HAR SPONTEN GÄTT UR LÅS ELLER ÄR ÖTÄT AV ANNAN ORSAK SKALL SPONTEN TÄTAS MED PLÅT SOM SVETSAS TILL SPONTEN. ARBETET UTFÖRS EFTER SAMRÅD MED ANSVARIG GEOKONSTRUKTÖR.

HAMMARBAND
HAMMARBAND. ENL. ELEVATIONSRITNINGAR
STÅLKVALITET: SS EN 10 025 S355J0
HAMMARBANDSVINKEL: 45° DÄR EJ ANNAT ANGES.

VID HORISONTELLA HAMMARBAND SKALL NOGGRANN KILNING UTFÖRAS MELLAN SPONT OCH HAMMARBAND DÄR SÅ ERFORDRAS.

SKARVNING AV HAMMARBAND SKALL UTFÖRAS MOMENTSTYVT OCH SÅ ATT KONTINUITET ERHÅLLS. SKARVNING BÖR I MÖJLIGASTE MÅN SKE MITT EMELLAN STAGEN. INFÄSTNING AV VINKLADE HAMMARBAND MOT SPONT UTFORMAS MED KONSOLPLÅTAR SAMT TILLHÖRANDE LIVAVSTYVNINGSPLÅTAR ENLIGT DETALJER PÅ DETALJRITNINGAR.

STÄMP
STÄMP ENLIGT ELEVATIONSRITNINGAR
STÅLKVALITET: SS EN 10 210S355J2H
GOD ANLIGGNING SKALL ANORDNAS MELLAN STÄMP OCH HAMMARBAND MEDELST KILNING.

BERGSTAG
BERGSTAG: SUPALINA Ø15,7 mm
BROTTSPÄNNING 1770 N/mm2
DYFORM Ø15,2 mm
BROTTSPÄNNING 1820 N/mm2

ANTAL LINOR PER STAG OCH STAGVINKLAR ENLIGT TABELL PÅ RESPEKTIVE ELEVATIONSRITNING.

ANKARPLATTA OCH ANKARSTYCKE ENLIGT VSL STANDARD.

SUPALINORNA MED EN NYTTJANDETID ÖVER 2 ÅR SKALL INVID HAMMARBAND OCH SPONT KORROSIONSSKYDDAS VIA TILL EXEMPEL INFETTNING ELLER INKAPSLING FÖR ATT SÄKERSTÄLLA FULLGOD KAPACITET UNDER HELA NYTTJANDETIDEN. EFTER 2 ÅRS NYTTJANDETID SKALL DESSUTOM UTÖKAD KONTROLL AV STAG UTFÖRAS ENLIGT KONTROLLPROGRAM GEO.

MONTERING AV STAG I BERG UTFÖRS ENLIGT TILLHÖRANDE ARBETSBESKRIVNING FÖR TEMPORÄRA VSL BERGSTAG, UPPRÄTTADE AV INTERNORDISK SPÄNNARMERING AB, DATERAD 1996-12-16.

BERGSTAGEN SKALL FÖRANKRAS I FRISKT BERG, MED EN MINSTA FÖRANKRINGSLÄNGD ENLIGT TABELL NEDAN.

FÖRANKRINGSLÄNGD OCH FRI STAGLÄNGD DOKUMENTERAS AV ENTREPRENÖREN.

PROVDRAGNING AV STAG I BERG UTFÖRS I STEG OCH ENLIGT FÖRANKRINGSSYSTEMETS SPECIFIKA FÖRESKRIFTER. ANSVARIG GEOKONSTRUKTÖR SKALL KONTAKTAS INNAN PROVDRAGNING PÅBÖRJAS. ANSVARIG GEOKONSTRUKTÖR SKALL FINNAS TILLGÄNGLIG VID PROVDRAGNING.

PROVDRAGNINGSLAST ENLIGT TABELL NEDAN.
PROVDRAGNINGSLASTEN KAN KOMMA ATT FÖRANDRAS MED HÄNSYN TILL VID UPPSPÄNNINGEN UPPKOMMANDE HORISONTALRÖRELSER.

Antal linor	Förankrings längd	Provdragnings last	
(st)	(m)	(kN)	
5	6,0/6,0	995/1125	SUPA/DYFORM
7	6,5/7,0	1393/1575	SUPA/DYFORM
9	7,0/7,5	1791/2025	SUPA/DYFORM
12	7,5/8,5	2388/2700	SUPA/DYFORM
15	8,0/9,0	2985/3375	SUPA/DYFORM
17	9,0/10,0	3383/3825	SUPA/DYFORM
19	10,0/11,0	3781/4275	SUPA/DYFORM
20-28	11,0	9	DYFORM
29-31	12,0	9	DYFORM
32-33	12,5	9	DYFORM
34-35	13,0	9	DYFORM

9 PROVDRAGNINGSLAST FÖR FLER ÄN 19 DYFORMLINOR SE RITNING 100G225D

LÅSLAST ENLIGT TABELL PÅ RESPEKTIVE ELEVATIONSRITNING.

PROVDRAGNING AV STAG UTFÖRS I LASTSTEG MED AVLÄSNING AV RÖRELSE ENLIGT FÖLJANDE:

Steg	Last	Avläsning av rörelser
0	ca 100 kN	Uppsträckning stag, nollavläsning
1	1,0 x Plås	1, 2, 3 och 5 minuter
2	1,5 x Plås	1, 2, 3 och 5 minuter
3	1,0 x Pprov	1, 2, 3 och 5 minuter

FÖRLÄNGD OBSERVATION UTFÖRS OM RÖRELSEN I SISTA TIDSINTERVALLET FÖR LASTSTEG 1-3 ÖVERSTIGER 0,5mm.

UPPMÄTT STAGFÖRLÄNGNING SKALL KONTROLLERAS MOT TEORETISK FRAMRÄKNAD STAGFÖRLÄNGNING.

OM PROVDRAGNINGSRESULTATET AVSEENDE RÖRELSER, STAGFÖRLÄNGNING OCH KRAFT EJ AVVIKER FRÅN STÄLLDA KRAV KAN STAGET LÅSAS VID FÖRESKRIVEN LÅSLAST.
VID DE FALL DÅ PROVDRAGNINGSRESULTATET AVVIKER FRÅN STÄLLDA KRAV SKALL ANSVARIG GEOKONSTRUKTÖR KONTAKTAS FÖR ANVISNINGAR/ KLARTECKEN INNAN STAG KAN LÅSAS.

PROVDRAGNINGSPROTOKOLL MED UPPGIFTER OM FÖRANKRINGSLÄNGD, FRI STAGLÄNGD, PROVDRAGNINGSLAST OCH LÅSLAST JÄMTE TILLHÖRANDE STAGFÖRLÄNGNING UPPRÄTTAS OCH INRAPPORTERAS TILL ANSVARIG GEOKONSTRUKTÖR.

INJEKTERINGSBRUK
BYGGCEMENT vct=0,45 TILLSATS 0,5% INTRAPLAST A

GROVBETONG
BETONG: BTG K30 II
I= ENL. RITNING 100G225A
ARMERING: Nps500,
TÄCKANDE BETONGSKIKT (TB) I VOT 20 mm

GROVBETONG SKALL UTFÖRAS PÅ SCHAKTBOTTEN FÖRUTOM DÄR BERGSPRÄNGNING ERFORDRAS ELLER TRYCKBANK KVARLÄMNAS.

GROVBETONG SKALL UTFÖRAS MED JÄMN LUTNING MELLAN SPONTERNA.

GROVBETONG I KANALSPONT SKALL GJUTAS UNDER VATTEN.

NOGGRANN RENSNING SKALL UTFÖRAS UTMED SPONT OCH I SPONTBUKAR INNAN GJUTNING.

GROVBETONGEN SKALL GJUTAS IN MOT SPONT OCH IN I SPONTBUKAR.

GOD ANLIGGNING SKALL ANORDNAS MELLAN GROVBETONG OCH SPONT ELLER BERG. DÄR SÅ ERFORDRAS UTFÖRS KOMPLETTERANDE GJUTNING.

GROVBETONGEN SKALL MINST HA UPPNÅTT EN KARAKTERISTISK TRYCKHÅLLFASTHET, fcck, AV 14 Mpa INNAN
- LÄNSNING INOM KANALSPONT FÅR SKE
- NÄSTA GJUTETAPP INOM KANALSPONT FÅR PÅBÖRJAS
- VATTENTRYCKET MOT SPONTEN FÅR ÖVERSKRIDA +10,1 (MW)
- DEN FÅR TRAFIKERAS.

KANTBALK
BETONG: BTG K30 II
ARMERING: BS500, TÄCKANDE BETONGSKIKT 35mm
STAG: Ø25 BS500 STAGVINKEL 30°

FÖRANKRINGSLÄNGD I FRISKT BERG ENLIGT DETALJ. STAGPLACERING ENLIGT DETALJ.

KANTBALKENS UTBREDNING ENLIGT ELEVATIONS-RITNINGAR

PÅ DE STÄLLEN DÄR AVSTÅNDET MELLAN UNDERSTA HAMMARBANDET OCH BERGNIVÅN ÄR MINDRE ÄN 2,0m ANPASSAS STAG-c/c SÅ ATT DE INTE SÄTTS RAKT UNDER UNDERSTA HAMMARBANDETS STAG. STAGEN FÅR INTE HELLER SÄTTAS SÅ ATT DE KOLLIDERAR MED DUBBEN.

GJUTNING AV KANTBALK UTFÖRS SUCCESSIVT I ETAPPER ENLIGT FÖRESKRIFTER UNDER SCHAKT NEDAN.

BETONGBALKEN UTFÖRS SÅ ATT KONTINUITET ERHÅLLS ÖVER GJUTSKARVARNA. NÄSTA ETAPP PÅBÖRJAS EFTER SAMRÅD MED ANSVARIG GEOTEKNIKER

BETONGEN I KANTBALKEN SKALL MINST HA UPPNÅTT EN KARAKTERISTISK TRYCKHÅLLFASTHET, fcck, AV 21 MPa INNAN NÄSTFÖLJANDE ETAPP FÅR PÅBÖRJAS.

STÅL
DÄR EJ ANNAT ANGES GÄLLER STÅLKVALITET SS EN 10 025 S355J0

SVETSKLASS: WC ENLIGT BSK99, KAP. 8:14
SVETSELEKTRODER: SS EN 499-E 42 2B

ELEKTRODMATERIALETS MINSTA BROTTHÅLLFASTHET Rm=500 MPa.

VID METALLBÅGSVETSNING SKA BASISKA ELEKTRODER MED BETECKNING H10 ANVÄNDAS. VID ANNAN TYP AV SVETSNING GÄLLER MOTSVARANDE KRAV PÅ TILLSATSMATERIALET.

ALL REDOVISAD SVETS SKA UTFÖRAS AV CERTIFIERADE SVETSARE ENLIGT SS-EN 287-1 ELLER SS 06 52 01.

SCHAKT
SCHAKT FÅR EJ BEDRIVAS SÅ ATT NIVÅSKILLNADEN LOKALT ÖVERSTIGER 3,0 M. SLÄNTLUTNING FÅR EJ UTFÖRAS BRANTARE ÄN 1:1 VID LERA SAMT 1:1,5 VID FYLLNADSMATERIAL. VID STÖRRE NIVÅSKILLNAD OCH / ELLER BRANTARE LUTNING ERFORDRAS SEPARAT UTREDNING.

AVLASTNINGSSCHAKT TILL NIVÅ +11,0 RESPEKTIVE +10,1 SKALL UTFÖRAS INNAN SCHAKT TILL DJUPARE NIVÅ PÅBÖRJAS.

INOM PARTIER DÄR SPONTFOT FRAMSCHAKTAS SKALL SISTA SCHAKTETAPPEN NED TILL BERG OMFATTA EN PALLHÖJD PÅ MINST 2m
SPONTFOT FRAMSCHAKTAS FÖRSIKTIGT OCH SUCCESSIVT MED PÅFÖLJANDE BESIKTNING AV SPONTFOT, DUBB OCH BERG. BEDÖMNING AV TILLÅTEN ETAPPLÄNGD (GJUTNING AV KANTBALK) UTFÖRS I SAMRÅD MED ANSVARIG GEOKONSTRUKTÖR.

INOM DE PARTIER DÄR SPRÄNGNING ERFORDRAS SKALL SAKKUNNIG BESIKTIGA BERGET, SAMT I SAMRÅD MED ANSVARIG GEOKONSTRUKTÖR, FÖRESLÅ FÖRESKRIFTER OCH EVENTUELLA FÖRSTÄRKNINGSÅTGÄRDER FÖR SPRÄNGNINGSARBETET.

ANGIVNA LÄGSTA TILLÅTNA SCHAKTNIVÅ AVSER LÄGSTA SCHAKTNIVÅ MED HÄNSYN TILL DE TEMPORÄRA STÖDKONSTRUKTIONERNA.
INNAN SISTA SCHAKTPALLEN TAS UT SKALL DOCK SLUTLIG SCHAKTNIVÅ BESTÄMMAS I SAMRÅD MED ANSVARIG KONSTRUKTÖR. DETTA FÖR ATT OPTIMERA SCHAKTEN MED HÄNSYN TILL TUNNELKONSTRUKTIONEN OCH TILL GROVBETONGENS TJOCKLEK.

SCHAKT INOM KANALSPONT I ETAPP 5 (MELLAN HUVUDSPONT OCH INRE SPONT) SKALL UTFÖRAS ETAPPVIS ENLIGT ANVISNINGAR I ARBETSORDNING.

ÖVRIGT
UNDER SCHAKTSTADIER SKALL KONTROLL UTFÖRAS AV ATT GRUNDVATTENNIVÅN I ÖVRE MAGASINET ELLER FRITT STÅENDE VATTEN EJ ÖVERSTIGER NIVÅN +10,1 MOT SPONT MED UNDANTAG FÖR SPONTERNA I ROSENLUNDSKANALEN. (FÖRUTOM VID OVAN NÄMNDA ARBETSMOMENT).

NÄR SÅ ERFORDRAS SKALL PÅLNINGSARBETE AVBRYTAS, ÅTERFYLLNING UTFÖRAS I UPPSCHAKTADE DIKEN, LÄNSHÅLLNING UTFÖRAS, SPONTGROP FYLLES MED VATTEN. ÅTGÄRDER SAMORDNAS MED ANSVARIG GEOTEKNIKER.

KONTROLL ENLIGT KONTROLLPROGRAM GEO SKALL UTFÖRAS VID SPONT- OCH SCHAKTARBETENA.

GRUNDVATTENNIVÅN INOM SPONT I FRIKTIONSJORDEN OVAN BERG SKALL KONTROLLERAS OCH AVSÄNKAS I TAKT MED ATT SCHAKT BEDRIVS NEDÅT.
GRUNDVATTENNIVÅN SÄNKS SUCCESSIVT TILL NIVÅ MED AKTUELL SCHAKTNIVÅ.

FÖRESKRIFTER, ARBETSUTFÖRANDE OCH ARBETSORDNING KAN KOMMA ATT FÖRANDRAS MED HÄNSYN TILL DE SUCCESSIVT ERHÅLLNA RESULTATEN FRÅN KONTROLLPROGRAM GEO.

ANSVARIG GEOKONSTRUKTÖR KAN ERSÄTTAS MED EN AV DENNE UTSEDD STÄLLFÖRETRÄDARE

HAMMARBAND OCH STÄMP SKALL UTFORMAS SÅ ATT DET EJ KAN UPPSTÅ VATTENSAMLINGAR MED HÄNSYN TILL RISK FÖR DÖNSKAT ISTRYCK OCH ÖKAD VIKT.

HAMMARBAND OCH STÄMP SKALL HÅLLAS RENA FRÅN BELASTNING AV LERMASSOR OCH DYLIKT.

ENTREPRENÖREN ANSVARAR FÖR ATT SPONTKONSTRUKTIONEN SKYDDAS MOT BRANDBELASTNING SAMT MOT LASTER FRÅN TJÄLE OCH ISBILDNING BAKOM SPONTEN.

FIX OCH KOORDINATSYSTEM
HÖJDSYSTEM: GÖTEBORGS LOKALA HÖJDSYSTEM (GH88) =RH70+10,07m.

KOORDINATER ENLIGT GÖTEBORGS KOORDINATSYSTEM.

FIX NUMMER 92 814 DUBB I BERG +14,192.

TILLHÖRANDE RITNINGAR

SE RITNING 1 00 G 22 51

GRANSKAD OCH GODKÄND VID FÖRNYAD GK3-GRANSKNING ENLIGT GRANSKNINGS PM 23, DATERAD 25 JUNI 2003.

REV	ÄNT	ANDRINGEN AVSER	GODKÄND	DATUM
D		FÖRNYAD MOTTAGNINGSKONTROLL ENL REV PM064	ME	2003-05-27
C		FÖRNYAD MOTTAGNINGSKONTROLL ENL REV PM052	ME	2003-03-12
B		MOTTAGNINGSKONTROLL ENL REV PM031	ME	2002-11-25
A		GK3 GODKÄND	ME	2002-08-06

BYGGHANDLING

Vägverket
Region Väst

SKANSKA
Skanska Teknik AB
405 18 GÖTEBORG – BESÖK: LILLA BOMMEN 2
TEL: 031-777 10 00 – FAX: 031-15 38 15 – www.skanskateknik.se

VÄG 45, GÖTATUNNELN
FISKHAMNSMOTET-JÄRNTORGET
GEMENSAMT
TEMPORÄRA SPONTKONSTRUKTIONER
ETAPP 4-5, 1/460-1/577 H-BAND o STAG
FÖRESKRIFTER

TEXT

RITAD/KONTR	GRANSK	KONSTRUKTÖRSANSVAR	FORMAT	SKALA
A KULLINGS.Ø/T.J	A KULLINGS.Ø		A1	1:1
GÖTEBORG	2002-04-12	OBJEKT NR	RITNINGSNR	REV
MATS EKENBERG		429013	1 00 G 22 52	D

Appendix 4:1
- Hand calculations

Earth pressure calculation

Input

Layer	Maximum depth, zmax [m]	Soil weight, γ [kN/m^3]	Undrained shear strength, cu	Increase in undrained shear strength with depth, cu,inc [kPa/m]	Friction angle, ϕ [°]
Fill 1	1	18	0	0	30
Fill 2	3	18	0	0	30
Clay	23	16.5	29	1	0

Equations

Active pressure

Friction material $\sigma_a = (\sigma_v - u) * \tan^2\left(45 - \frac{\varphi}{2}\right) + u$

Cohesion material $\sigma_a = \sigma_v - 2 * c_u$

Passive pressure

Cohesion material $\sigma_p = \sigma_v + 2 * c_u$

Net pressure

Cohesion material $\sigma_{pnetto} = N_{cb} * c_u - (\gamma * H)$

Appendix 4:2

Depth, z [m]	Active side vertical pressure, σv,a [kPa]	Active pressure, σa,a [kPa]	Passive side vertical pressure, σv,p [kPa]	Passive pressure, σp,p [kPa]	Net earth pressure, σ_{pnetto} [kPa]
0	0	0	0	0	0
1	20	4	0	0	4
1	20	4	0	0	4
2	38	8	0	0	8
3	56	19	0	0	19
3	56	0	0	0	0
4	73	13	0	0	13
5	89	27	0	0	27
6	106	42	0	0	42
7	122	56	0	0	56
8	139	71	0	0	71
9	155	85	0	0	85
10	172	100	0	0	100
11	188	114	0	0	114
12	205	129	0	0	129
12	205	129	0	76	-12
13	221	143	17	95	-18
14	238	158	33	113	-24
15	254	172	50	132	-29
16	271	187	66	150	-35
17	287	201	83	169	-41
18	304	216	99	187	-46
19	320	230	116	206	-52
20	337	245	132	224	-58
21	353	259	149	243	-63
22	370	274	165	261	-69
23	386	288	166	264	-75
23.5	403	304	167	266	-78

Appendix 4:3

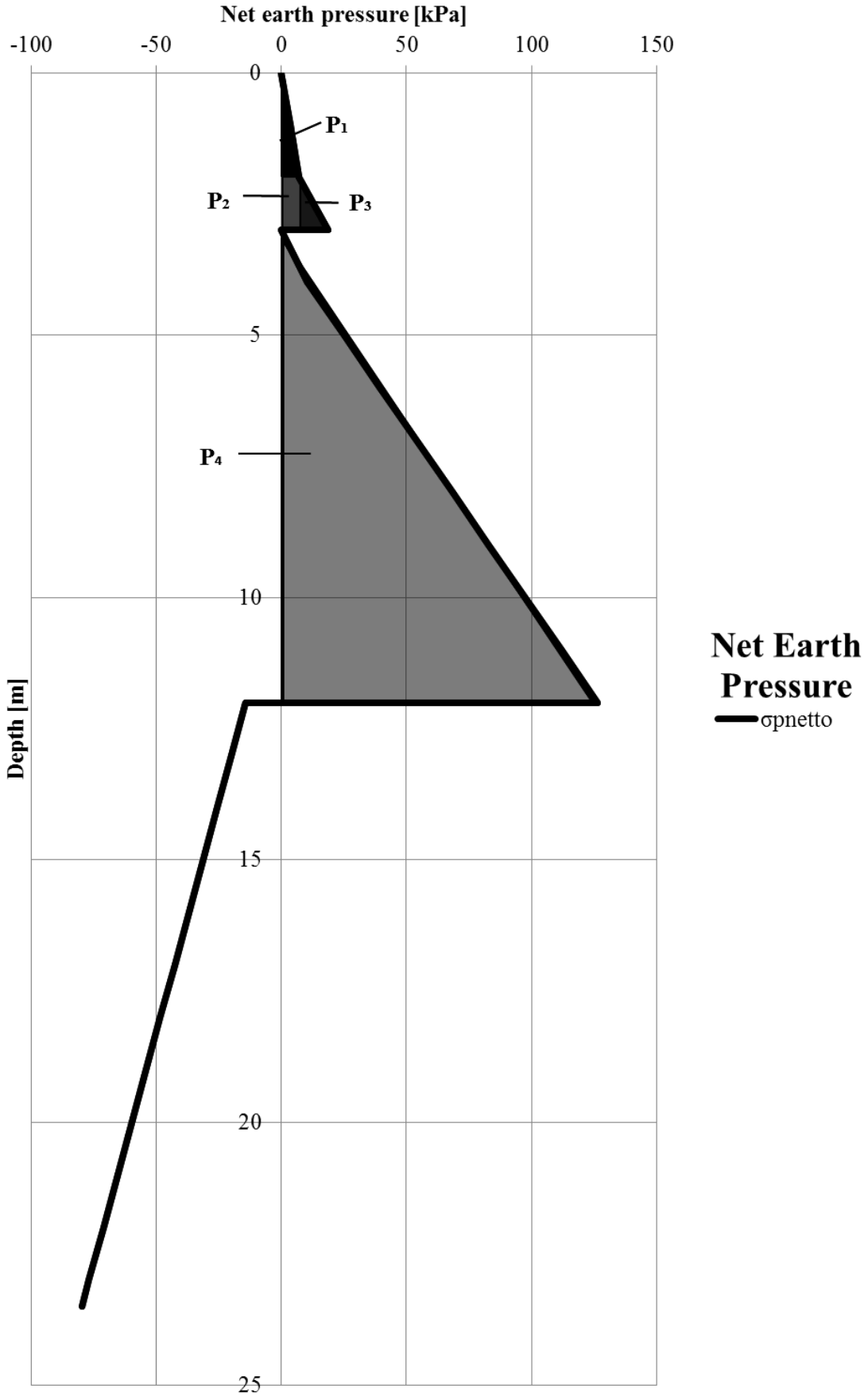
Net earth pressure [kPa]
-100
-50
0
50
100
150
0
5
10
15
20
25
Depth [m]
P1
P2
P3
P4
Net Earth Pressure
σpnetto

Appendix 4:4

Total force acting on the SPW

P1	2	kN
P2	8	kN
P3	38	kN
P4	578	kN
Sum P	626	kN

Load Intensity ————
σi [kPa]

where :H = 12 m, d = 0 m

σi = 58 kN/m

Appendix 4:5

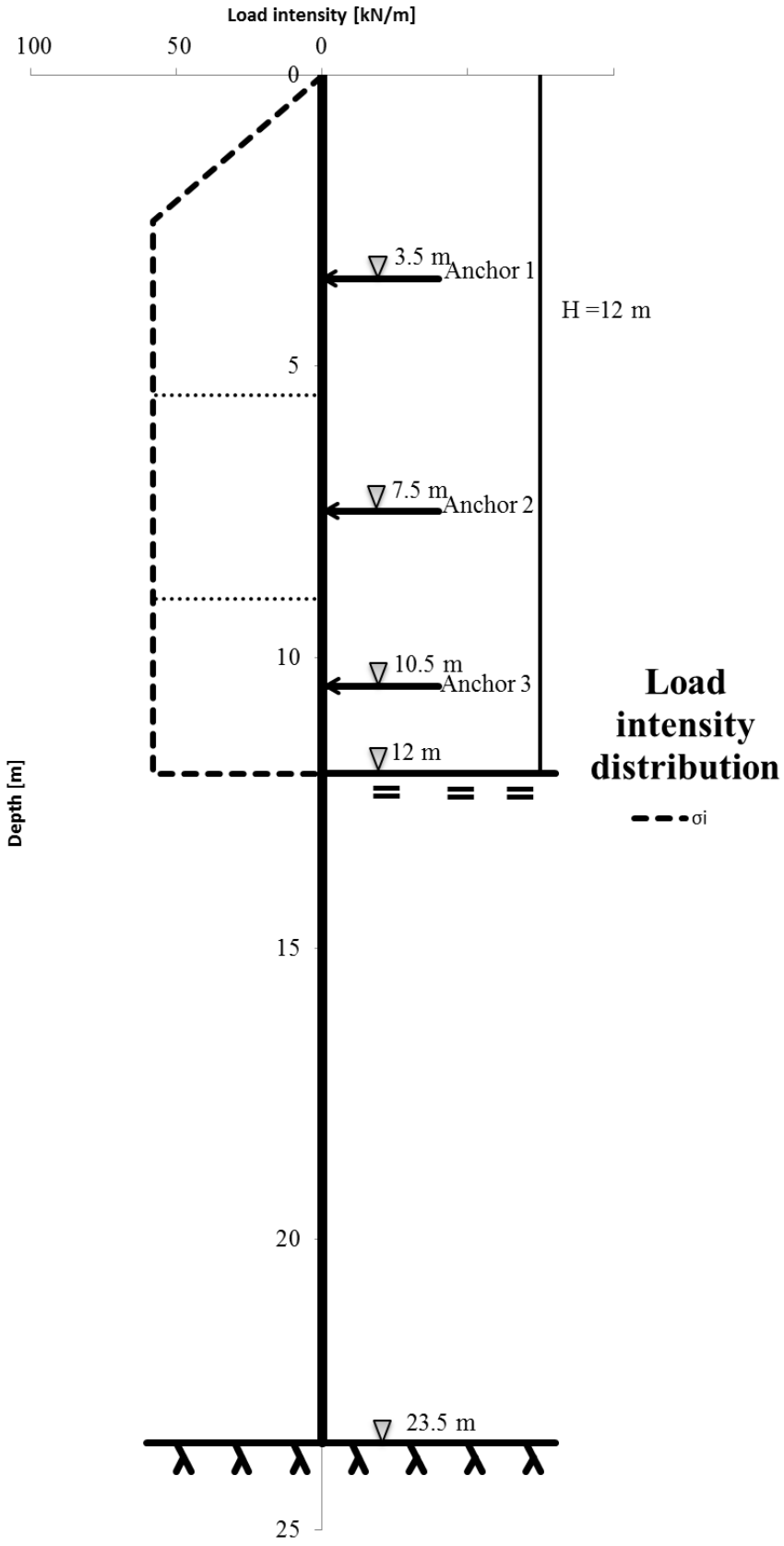
Load intensity [kN/m]
100
50
0
0
3.5 m
Anchor 1
H =12 m
5
7.5 m
Anchor 2
10
10.5 m
Anchor 3
12 m
Load intensity distribution
σi
Depth [m]
15
20
23.5 m
25

Appendix 4:6

Load interval

1	4.25 m
2	3.5 m
3	3 m

$$P_H = \sigma_i * load\ interval$$

Horisontal forces, P_H

1	247 kN/m
2	203 kN/m
3	174 kN/m

$$P = \frac{P_H}{\cos(45°)}$$

Anchor force, P

1	417 kN/m
2	343 kN/m
3	294 kN/m

$$M_{sd} = \frac{\sigma_i * l^2}{12}$$

Bending momen between anchors, Msd

87 kNm/m
59 kNm/m
44 kNm/m

Bending moment under anchor 3

16 kNm/m

$$M_{Sd} = 0.1 * H * \sigma_i \left(\frac{0.2 * H}{3} + e\right) \frac{\sigma_i * e^2}{2}$$

Bracket moment anchor 1

154 kNm/m e=1

Appendix 5:1

- Parametric studies

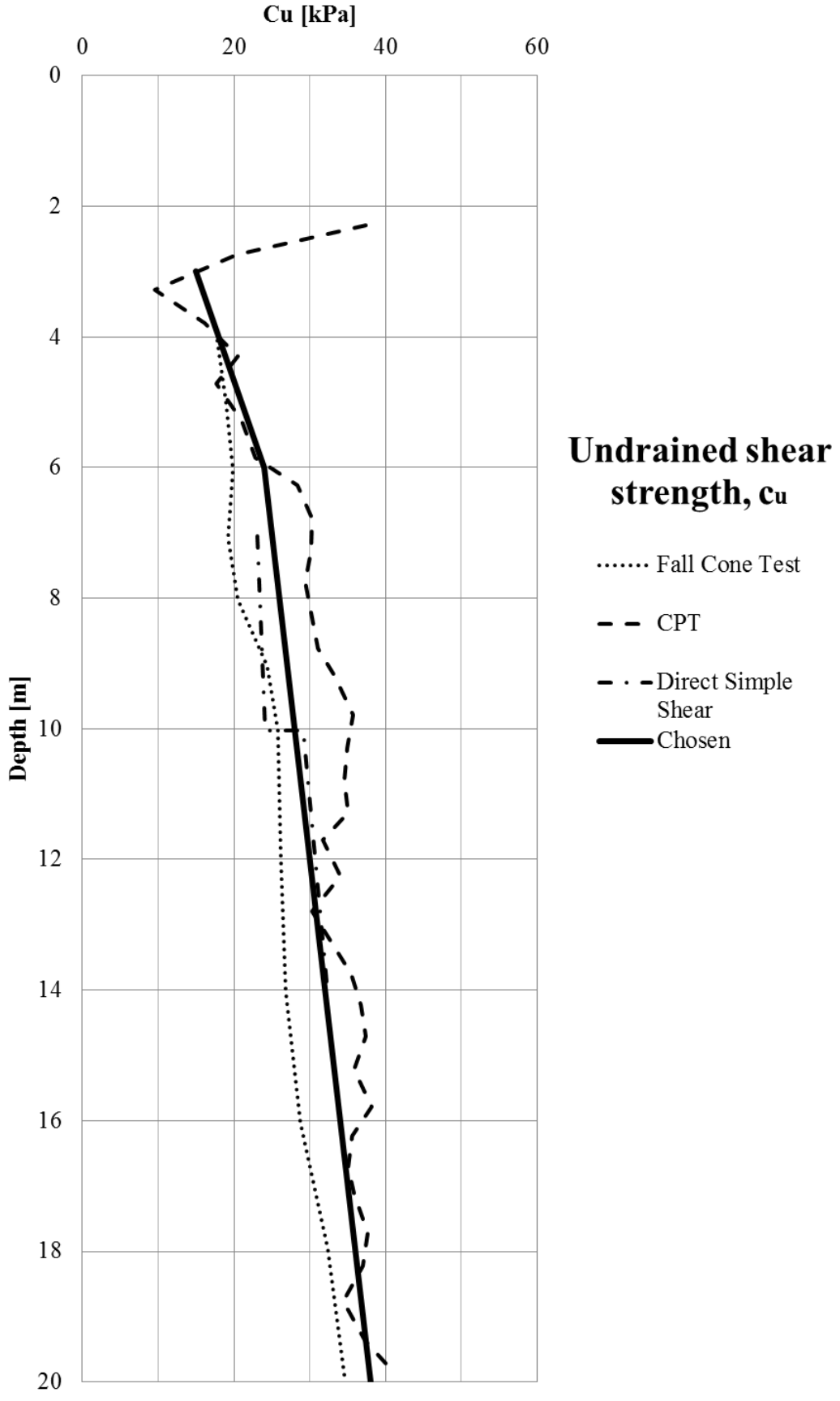

Appendix 5:2

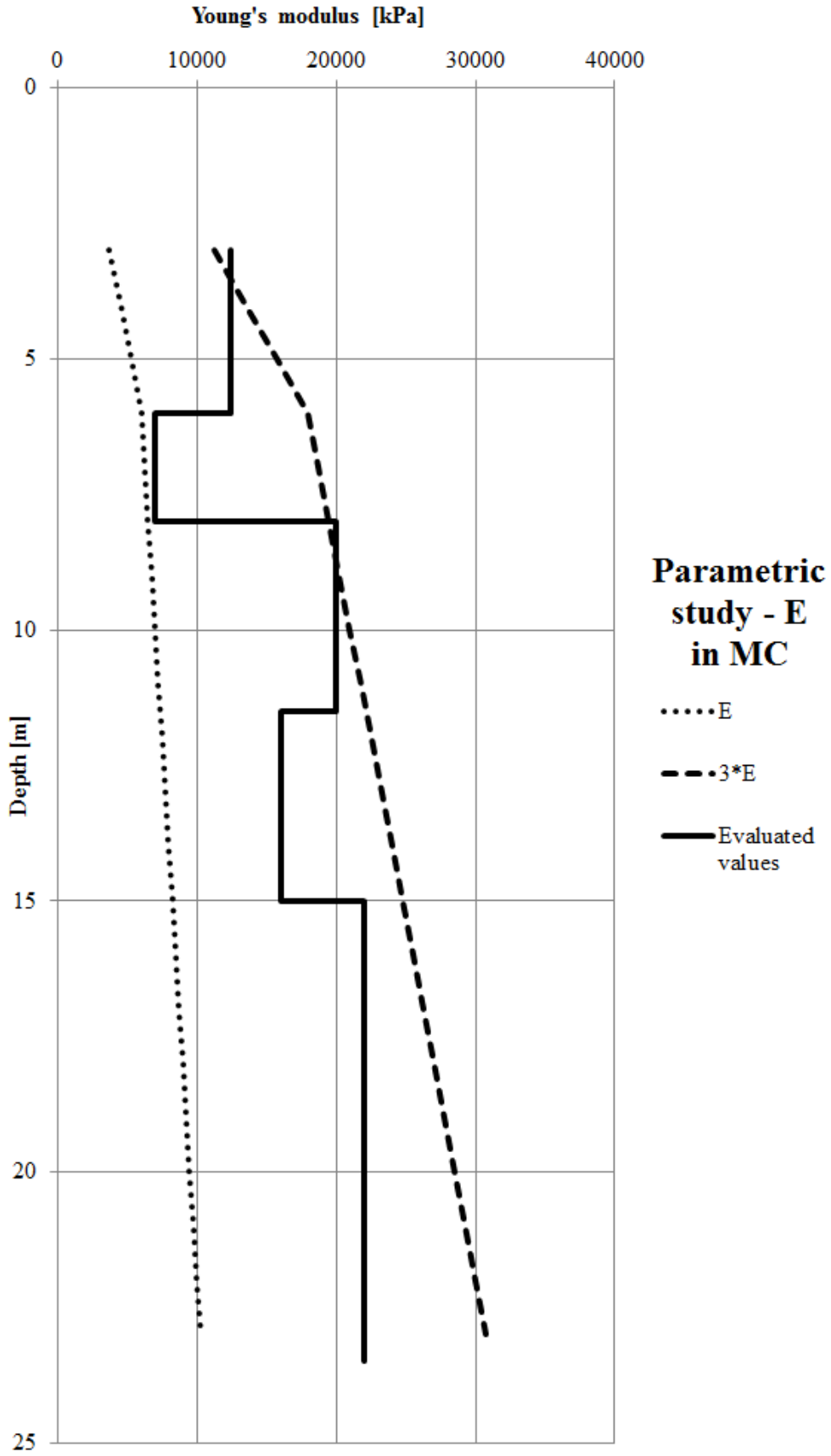
Young's modulus [kPa]
0
10000
20000
30000
40000
0
5
10
15
20
25
Depth [m]
Parametric study - E in MC
E
3*E
Evaluated values

Appendix 5:3

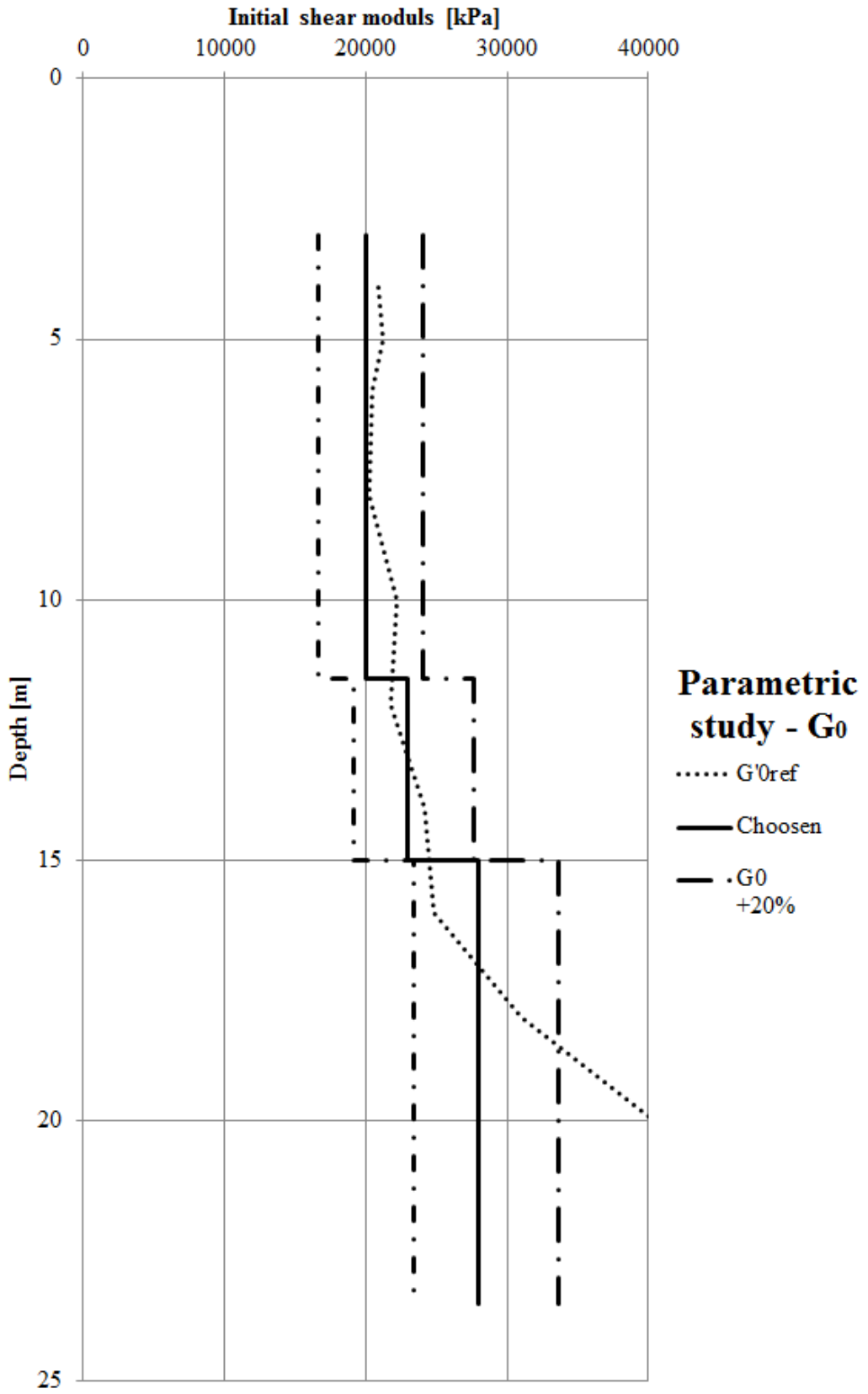
Initial shear moduls [kPa]
0
10000
20000
30000
40000
0
5
10
15
20
25
Depth [m]
Parametric study - G0
G'0ref
Choosen
G0 +20%

Appendix 5:4

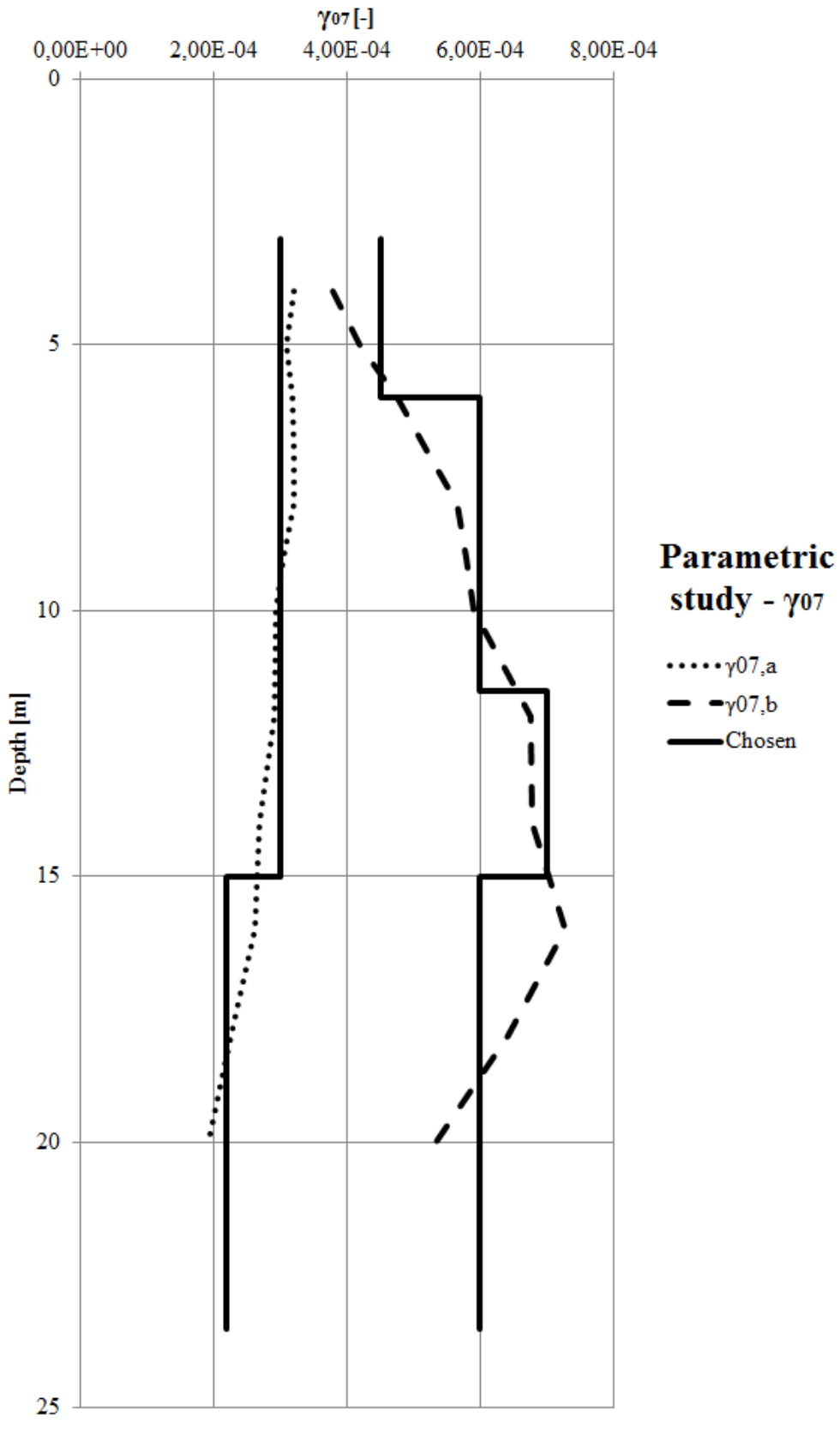
γ07 [-]
0,00E+00
2,00E-04
4,00E-04
6,00E-04
8,00E-04
0
5
10
15
20
25
Depth [m]
Parametric study - γ07
γ07,a
γ07,b
Chosen